CHAPTER-4

RESULTS AND DISCUSSION

4. RESULTS AND DISCUSSION

The results obtained for various studies have been discussed under the following heads:

A. Studies on TACE inhibitors

4.1 3D-Quantitative structure–activity relationship studies on benzothiadiazepine hydroxamates as inhibitors of TACE
4.2 Development of predictive 3D-QSAR CoMFA and CoMSIA Models for β-aminohydroxamic acid-derived TACE inhibitors
4.3 Development of predictive pharmacophore model for in silico screening and 3D-QSAR CoMFA and CoMSIA studies for lead optimization for designing of potent TACE inhibitors
4.4 Molecular modeling studies of novel 2-imidazolidinones and tetrahydropyrimidin (2*H*)-ones as potential TACE inhibitors
4.5 Molecular modeling studies of some new heterocyclic inhibitors of TACE

B. Studies on inhibitors of neuraminidase

4.6 Determining of structural requirements of influenza neuraminidase type A inhibitors and binding interaction analysis with the active Site of A/H1N1 by 3D-QSAR CoMFA and CoMSIA modeling

C. Studies on potential aromatase inhibitors

4.7 Molecular modeling studies of some novel androstanes as potential aromatase inhibitors

A. STUDIES ON TACE INHIBITORS

4.1 3D-Quantitative Structure Activity Relationship Studies on Benzothiadiazepine Hydroxamates as Inhibitors of TACE

4.1.1 Data set used

A data set consisting of 36 compounds possessing TACE inhibiting activity was selected from the published work [288]. Discarding inactive compounds and compounds with unspecified activity, a total of 29 compounds were selected. The selected compounds were divided into a training set (23 compounds) and a test set (6 compounds) in an approximate ratio of 4:1. To diversify the training and test sets, manual grouping was performed so that molecules possessing diverse functionalities and biological activity of wide range were included in both the sets. The structures of the training and test set molecules are given in **Table 4.1.1.** The mean biological activities of the chosen training and test set molecules were 6.96 and 6.97, respectively. The biological activity used in the

present study was expressed as follows:

$$pKi = -\log Ki$$

wherein, *Ki* (in M) is the absolute inhibition constant of porcine TACE.

Table 4.1.1 Structures and Biological activities of compounds used in training and test sets

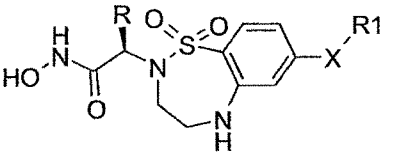

1-29

Compound	R	X	R1	*Ki* (nM)	*pKi*
1	Me	O	Me	274	6.562
2	Me	H	-	484	6.315
3*	*i*.Pr	O	Me	71	7.148
4	Me	O	H	391	6.407
5	Me	OCH_2	Phenyl	705	6.151
6	Me	OCH_2	3,5-Dimethylphenyl	229	6.640
7	Me	OCH_2	3,5-Dichlorophenyl	153	6.815
8*	Me	OCH_2	3,5-Dimethoxyphenyl	27	7.568
9	Me	OCH_2	3,5-Diethoxyphenyl	81	7.091
10*	Me	OCH_2	2,6-Dimethyl-4-pyridinyl	544	6.264
11	*i*.Bu	O	H	89	7.050
12	*i*.Bu	OCH_2	Phenyl	177	6.752
13	*i*.Bu	OCH_2	3,5-Dimethoxyphenyl	17	7.769
14*	*i*.Pr	OCH_2	3,5-Dimethoxyphenyl	10	8.00
15	*i*.Pr	OCH_2	3,5-Diethoxyphenyl	51	7.292
16	*i*.Pr	OCH_2	4,5-Dimethyl-2-thiazolyl	290	6.537
17*	$(CH_2)_2CO_2Me$	OCH_2	3,5-Dimethoxyphenyl	177	6.752
18	$(CH_2)_2CO_2Me$	OCH_2	3,5-Diethoxyphenyl	242	6.616
19	$(CH_2)_3CO_2Me$	OCH_2	3,5-Dimethoxyphenyl	10	8.00
20	$(CH_2)_3CO_2Me$	OCH_2	3,5-Diethoxyphenyl	13	7.886
21	$(CH_2)_4NHSO_2Me$	OCH_2	3,5-Dimethoxyphenyl	5	8.301
22	$(CH_2)_4NHBoc$	OCH_2	3,5-Dimethoxyphenyl	77	7.113
23	$(CH_2)_4NH_2$	OCH_2	3,5-Dimethoxyphenyl	31	7.508
24	*i*.Bu	$NHCH_2$	3,5-Dimethoxyphenyl	56	7.251
25*	Me	O	4-(Trifluoromethyl)phenyl	758	6.120
26	Me	O	4-Methoxyphenyl	621	6.206
27	Me	O	Phenyl	734	6.134
28	Me	O	3-Nitrophenyl	129	6.889
29	Me	O	4-Nitrophenyl	11	7.958

*Test set molecules

4.1.2 Alignment rules

One of the important steps in CoMFA is the derivation of active conformation and alignment of the molecules on the active conformation. The success of CoMFA depends on the relative positioning of the ligands in the fixed lattice, prior to generation of the 3D-descriptors. Thus, different alignments were performed such as atom-based (ABA), centroid/atom-based (CABA), data-based (DBA), and docked conformer-based (DCBA) alignments. The first three alignment methods are solely based on the selection of ligand atoms and the last method involves docking of the ligands with the enzyme and use of the docked conformations of the ligands for the purpose of alignment (**Figure 4.1.1**). The DCBA alignments were performed in three different ways. In one procedure,

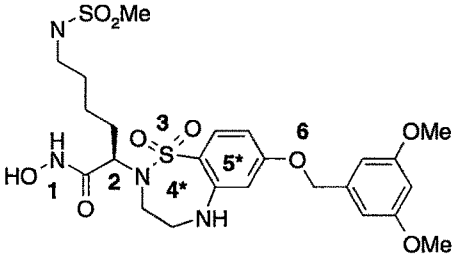

Alignment	Atoms/centroids
I	1,2,3,6
II	1,2,4*,5*,6
III	Database
IV	Docking based

Figure 4.1.1 Alignment rules

all the molecules were docked into the active site of the enzyme and the resulting conformations were used for performing 3D-QSAR analysis (DCBA-a). In the second procedure, the most active compound (i.e., compound **21**) was docked in the active site of the enzyme and rest of the other compounds were aligned (DCBA-b) on the resulting conformation of compound **21**; these aligned conformations were then used for analysis In the third procedure, the highest ranked (highest G-score) compound (i.e. compound **9**) obtained from the docking experiment was used for aligning rest of the compounds on the conformation of compound **9** (DCBA-c) for the purpose of quantitative analysis . For ABA, CABA, and DBA alignments, compound **21** was used as the template structure.

Alignment I (ABA)

In this alignment, atoms of the molecules corresponding to the atoms in the template were used for RMS fitting (**Figure 4.1.1**).

Alignment II (CABA)

Here, atoms and centroids both were selected for superimposition on the template. The atoms and centroids used for alignments are defined in **Figure 4.1.1**. These alignments were subsequently used in CoMFA/CoMSIA probe interaction energy calculations.

Alignment III (DBA)

Each analog was aligned to the template by rotation and translation so as to minimize the RMSD between atoms in the template and the corresponding atom in the analog using the DATABASE ALIGN option in SYBYL (**Figure 4.1.2**). The common fragment used for the database alignment is shown in **Figure 4.1.1**.

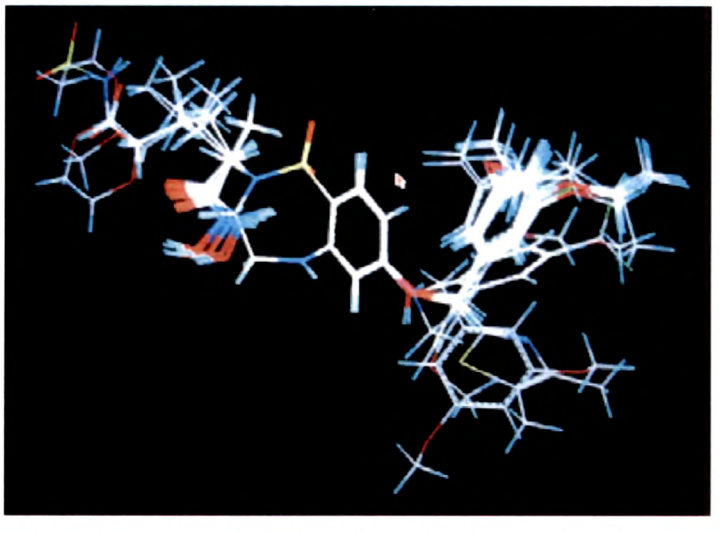

Figure 4.1.2 The alignment derived from database alignment (DBA)

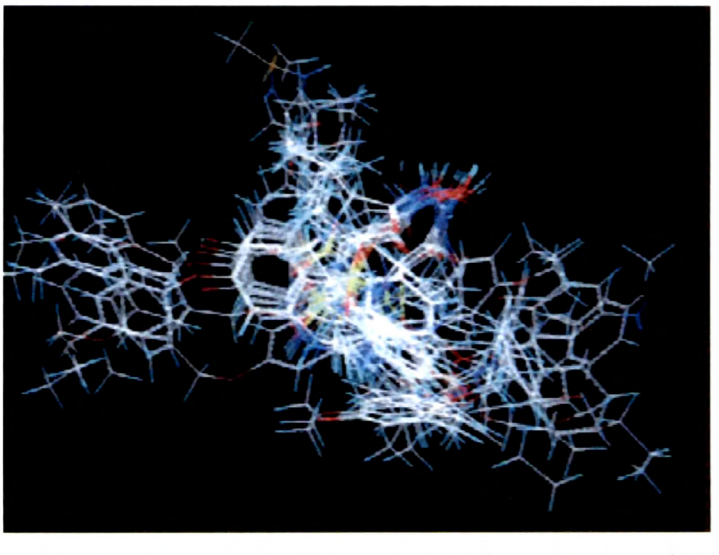

Figure 4.1.3 The alignment (DCBA-a) derived from docking of 29 TACE inhibitors to TACE

Alignment IV (DCBA-a)

To obtain docked conformations, all the molecules were subjected to docking in the active site of the enzyme. Conformations of the docked molecules were extracted and aligned on one another for performing the 3D-QSAR studies (**Figure 4.1.3**).

Alignment V (DCBA-b)

The most active compound **21** was docked in the active site and rest of the other compounds were aligned on the resulting conformation of compound **21**.

Alignment VI (DCBA-c)

The highest ranked compound (i.e., compound **9**) obtained from the docking experiments was used for aligning rest of the compounds on this conformation of compound **9**.

4.1.3 CoMFA analysis

The 3D-QSAR models for benzothiadiazepine derivatives were derived using both CoMFA as well as CoMSIA techniques. p*Ki* was used as the dependent variable in the 3D-QSAR study (**Table 4.1.1**). The lower energy conformers obtained from the MULTISEARCH option in SYBYL were used in the study. All the molecules were aligned employing atom/shape-based RMS fitting and RMSD-based database fitting techniques. Various 3D-QSAR models were generated and the best one was selected on the basis of statistics.

Table 4.1.2 Summary of CoMFA results (analysis A)

Statistical parameters	Alignments			
	I[a]	II[b]	III[c]	IV[d]
r^2_{cv} [e]	0.107	0.179	0.472	0.268
NC[f]	3	3	4	3
SEP[g]	0.512	0.532	0.443	0.468
r^2_{ncv} [h]	0.783	0.785	0.832	0.927
SEE[i]	0.487	0.445	0.107	0.190
F value	18.716	26.444	46.982	80.833
P r^2=o [j]	0	0	0	0
$r^2_{predictive}$	0.227	0.324	0.383	0.238

[a]Alignment by atom-based RMS fit; [b]Alignment by atom and shape-based RMS fit; [c]Alignment by RMSD database fit, [d]Alignment by docking based, [e]Cross-validated correlation coefficient; [f]Number of components; [g]Standard error of prediction; [h]Non cross-validated square of correlation coefficient; [i] Standard error of estimate; [j] $Pr^2 = 0$, probability that correlation coefficient r equals zero.

A preliminary study was performed to study the importance of each field individually. All further analyses were performed with steric and electrostatic fields calculated at each grid point simultaneously. Partial least square analysis was performed

using varying column filtering values. Finally, column filtering value was set to 2.0 kcal/mol. **Table 4.1.2** shows CoMFA results obtained from four different alignments using 23 molecules in the training set.

Atom-based alignment I (**Table 4.1.2**) showed cross-validated r^2 = 0.107 with three components, non-cross-validated r^2 = 0.783, F-value 18.716, and r^2_{pred} = 0.227; the steric and electrostatic contributions were 48.0% and 52.0%, respectively. The CoMFA model generated from shape-based RMS alignment II (**Table 4.1.2**) showed cross-validated r^2 = 0.179 with three components, non-cross-validated r^2 = 0.785, F-value 26.444, and r^2_{pred} = 0.324 with 37.1% steric and 62.9% electrostatic contributions. The DBA alignment III (**Table 4.1.2**) yielded cross-validated r^2 = 0.472 with four components, non-crossvalidated r^2 = 0.832, F-value 46.982, and r^2_{pred} = 0.383; the steric and electrostatic contributions were 42.7% and 57.3%, respectively. Alignment IV (docking-based) yielded a cross-validated r^2 = 0.268 with three components, non-cross-validated r^2 = 0.927, F-value 80.833, and r^2_{pred} = 0.238; the steric and electrostatic contributions were 73.9% and 26.1%, respectively. Alignments V and VI yielded poorer statistics than the one given by alignment IV hence, these models are not discussed further.

As CoMFA technique is alignment-sensitive, differences in statistical values are observed with different alignments (**Table 4.1.2**). All the CoMFA models obtained from analysis A demonstrated lower internal and external predictivity. Thus, to increase the predictive power of derived models, further experiments were performed. Based on the results of these QSAR studies, two molecules (**28** and **29**) of the training set with high residual values were omitted from the PLS analysis. Probably, the nitro group present in these compounds is adversely affecting some distant electrostatic field in the molecule leading to poor correlation.

Analysis B (**Table 4.1.3**) shows the CoMFA results obtained from four different alignments using a training set involving 21 molecules (**Table 4.1.3**); the models derived showed a better confidence level of statistical significance. Atom-based alignment I (**Table 4.1.3**) showed improved cross-validated r^2 value from 0.107 to 0.229 with three components, non-cross validated r^2 from 0.783 to 0.821, F-value from 18.716 to 23.022, and r^2_{pred} from 0.227 to 0.328. The steric and electrostatic contributions were found to be 46.1% and 53.9%, respectively. The same trend was observed in the remaining

alignments (**Table 4.1.3**). Shape-based RMS alignment II showed cross-validated r^2 = 0.421 with four components, non-crossvalidated r^2 of 0.954, F-value 82.09, and r^2_{pred} of 0.328. The DBA alignment III (**Table 4.1.3**) yielded highest cross-validated r^2 = 0.510

Table 4.1.3 Summary of CoMFA results (analysis B)

Statistical parameters	Alignments			
	I[a]	II[b]	III[c]	IV[d]
r^2_{cv} [e]	0.229	0.421	0.510	0.423
NC[f]	3	4	4	3
SEP[g]	0.412	0.513	0.421	0.437
r^2_{ncv} [h]	0.821	0.954	0.972	0.999
SEE[i]	0.457	0.445	0.098	0.023
F value	23.022	82.09	215.46	2248.70
P r^2=0[j]	0	0	0	0
$r^2_{predictive}$	0.328	0.328	0.460	0.297

[a]Alignment by atom-based RMS fit; [b]Alignment by atom and shape-based RMS fit; [c]Alignment by RMSD database fit, [d]Alignment by docking based, [e]Cross-validated correlation coefficient; [f]Number of components; [g]Standard error of prediction; [h]Non cross-validated square of correlation coefficient; [i] Standard error of estimate; [j]Pr^2 = 0, probability that correlation coefficient r equals zero.

with four components, non-crossvalidated r^2 of 0.972, F-value 215.46, and r^2_{pred} of 0.460. Alignment IV (**Table 4.1.3**) yielded cross-validated r^2 of 0.423 with three components, non-cross-validated r^2 of 0.999, F-value 2248.70, and r^2_{pred} of 0.297. It was expected that alignment IV would offer the best results, as these conformations of the molecules existed in the active site of the enzyme. Unfortunately, that was not the case; it seemed these conformations did not exist for the inhibitors prior to binding to the enzyme. This is well reported that ligand conformations could change during binding to the enzyme [289]. The enzyme as well as the ligands may show conformational changes while interacting with each other. This could be the probable reason why alignment IV did not provide better results in this case.

The model generated with alignment III with a good internal predictive ability (r^2_{cv} = 0.510) and a small standard error of estimation (SEE = 0.098) was selected as the best model to explain SAR and to carry out further analysis; all the CoMFA contours were generated using this model. The plots of actual versus predicted activities for the training and test sets of molecules are depicted in **Figures 4.1.9A** and **4.1.10A**, respectively. The field values generated at each grid point were calculated as the scalar product of the associated QSAR coefficient and the standard deviation of all values in the corresponding column of the data table (STD*COEFF) plotted as the percentage

contributions to QSAR equation. The CoMFA steric and electrostatic contour maps are shown in **Figures 4.1.4 and 4.1.5**, respectively. The green colored regions indicate areas where steric bulk enhances TACE inhibitory activity, and the yellow contours indicate regions where steric bulk is detrimental for biological activity. Blue colored regions show areas where electropositively charged groups enhance TACE inhibitory activity, while red regions represent where electronegatively charged groups improve the activity. The results of PLS analysis are summarized from CoMFA studies in **Table 4.1.3.**

4.1.4 CoMSIA analysis

The CoMSIA analysis was performed using steric, electrostatic, hydrophobic, hydrogen bond donor and acceptor fields. Presently, CoMSIA offers five different fields;

Table 4.1.4 Summary of CoMSIA results

Descriptors	r^2_{cv}	NC	SEP	r^2_{ncv}	SEE	F-value	P $r^2 = 0$	r^2_{pred}
H[a]	0.435	1	0.544	0.607	0.418	29.396	0	-0.172
D[b]	0.201	4	0.652	0.654	0.427	07.565	0	-0.244
A[c]	0.398	1	0.550	0.533	0.446	23.498	0	-0.189
D+A	0.386	3	0.552	0.824	0.305	56.126	0	-0.715
H+D	0.245	3	0.612	0.718	0.364	18.668	0	0.131
H+A	0.403	1	0.514	0.615	0.394	22.926	0	- 0.583
H+D+A	0.417	3	0.564	0.876	0.249	39.903	0	- 0.394
S[d]+E[e]+D	0.416	3	0.513	0.951	0.084	109.811	0	0.323
H+S+E	0.600	5	0.539	0.905	0.021	2304.546	0	0.415
S+E+A	0.496	4	0.522	0.970	0.126	128.404	0	0.409
S+E+D+A	0.522	3	0.505	0.965	0.132	156.292	0	0.341
SEDAH	0.550	3	0.511	0.956	0.148	122.619	0	0.399
SEAH	0.533	3	0.511	0.965	0.132	156.292	0	0.341
SEDH[f]	**0.556**	**3**	**0.497**	**0.946**	**0.163**	**99.785**	**0**	**0.535**

Contribution of fields (Fractions)

Descriptors	S	E	A	D	H
H[a]	-	-	-	-	
D[b]	-	-	-	-	-
A[c]	-	-	-	-	-
D+A	-	-	0.553	0.447	-
H+D	-	-	-	0.442	0.558
H+A	-	-	0.406	-	0.594
H+D+A	-	-	0.280	0.321	0.399
S[d]+E[e]+D	0.229	0.556	-	0.214	-
H+S+E	0.214	-	-	-	-
S+E+A	0.547	-	-	-	0.238
S+E+D+A	0.221	0.428	0.155	0.196	-
SEDAH	0.180	0.398	0.129	0.150	0.143
SEAH	0.215	0.458	0.140	-	0.188
SEDH[f]	**0.199**	**0.464**	-	**0.175**	**0.162**

[a]Hydrophobic field; [b]Hydrogen bond donor field; [c]Hydrogen bond acceptor field; [d]Steric field; [e]Electrostatic field; [f] Best model for CoMSIA

3D-QSAR models can be generated using the above fields in different combinations. The atom and shape-based alignment III (**Table 4.1.3)** used in CoMFA studies served as the alignment for CoMSIA and the results of the study are summarized in **Table 4.1.4.** The CoMSIA model showed considerable correlation and predictive properties.

The CoMSIA model with combination of all the fields yielded a cross-validated r^2 = 0.550 with three components, non-cross-validated r^2 = 0.956, F-value 122.619 and r^2_{pred} = 0.399. The contributions of steric, electrostatic, hydrophobic, hydrogen bond donor and acceptor fields of this model were 18.0%, 39.8%, 14.3%, 15.0%, and 12.9%, respectively. The CoMSIA model with a combination of steric, electrostatic, hydrophobic and hydrogen bond donor fields yielded the highest cross-validated r^2 = 0.556 with three components, non-cross-validated r^2 = 0.946, F-value 99.785, and r^2_{pred} of 0.535. The steric, electrostatic, hydrophobic, and hydrogen bond donor fields contributions were 19.9%, 46.4%, 16.2%, and 17.5%, respectively. Combinations of steric, electrostatic, and hydrogen bond donor fields yielded a CoMSIA model with a cross-validated r^2 = 0.416 with three components, non-cross-validated r^2 = 0.951, F- value 109.811, and r^2_{pred} = 0.323.

The steric, electrostatic, and hydrogen bond donor contributions were 22.9%, 55.6%, and 21.4%, respectively. The models generated by various combinations of CoMSIA fields (**Table 4.1.4**) showed moderate to high, internal and external predictions, in which the hydrophobic fields were observed to be predominant over the hydrogen bond donor and hydrogen bond acceptor fields. The plots of actual versus predicted activities for the training and test set molecules from the best CoMSIA model are shown in **Figures 4.1.9B and 4.1.10B**, respectively. The CoMSIA steric and electrostatic contours (not shown) were positioned similarly to those of the CoMFA model, hence are not discussed. The hydrophobic contour maps of CoMSIA (STDDEV*COEFF) is displayed in **Figure 4.1.6**. The results of CoMSIA PLS analysis are summarized in **Table 4.1.4.** The CoMSIA model generated from steric and electrostatic fields did not vary both in terms of statistical values and positions of contours as compared to its CoMFA model and hence are not included in **Table 4.1.4.**

4.1.5 CoMFA versus CoMSIA analyses

A comparison of statistical results of the two QSAR analyses is given in **Table 4.1.5.** Both CoMFA and CoMSIA models exceeded $r^2_{cv} > 0.5$ which indicated stability of

the model and reasonable predictability [290]. Comparative molecular similarity indices analysis showed higher cross-validated r^2 value (0.556) than that of CoMFA (0.510).

Table 4.1.5 Comparison of Statistical parameters for CoMFA (analysis B; alignment III) and CoMSIA

	r^2_{cv}	N	r^2_{ncv}	SEE	F-value	$r^2_{Predictive}$
CoMFA	0.510	4	0.972	0.098	215.46	0.460
CoMSIA	0.556	3	0.946	0.163	99.785	0.535

4.1.6 Graphical interpretation of the CoMFA and CoMSIA models

To visualize the information content of the derived 3D-QSAR model, CoMFA contour maps were generated by interpolating the products between the 3D-QSAR coefficients and their associated standard deviations. **Figures 4.1.4** and **4.1.5** indicate the

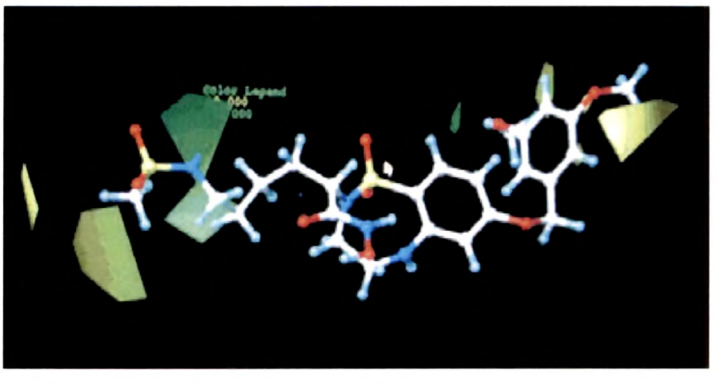

Figure 4.1.4 The CoMFA steric STDEV*COEFF contour plots of active compound **21** from analysis-B. Sterically favored areas (contribution level 80%) are represented by green polyhedra. Sterically disfavored areas (contribution level 20%) are represented by yellow polyhedra

CoMFA steric and electrostatic contour maps respectively, obtained from analysis B using compound (**21**) as a reference structure. In these figures, the green contours represent regions of high steric tolerance (80% contribution) while the yellow contours represent regions of low steric bulk tolerance (20% contribution). The increase in positive charge is favored in blue regions while increase in negative charge is favored in red regions. The green contour present in the vicinity of substituted nitrogen atom of methanesulfonyl group indicates that generally steric bulk is favored at this site. The good inhibitory potency of compounds **19** (*Ki* = 10) and **20** (*Ki* = 13) is due to orientation of bulkier groups toward the sterically favored areas. While in case of compounds **4** (*Ki* =

391), **5** (*Ki* = 705), **6** (*Ki* = 229), **7** (*Ki* = 153), **25** (*Ki* = 758), **26** (*Ki* = 621) and **27** (*Ki* = 734) there is an absence of bulky groups in this region. A yellow region near the methanesulphonamido group shows that a bulky substituent at this site decreases potency. This is in line with the SAR indicating lower activity for compound **22** (*Ki* = 77) in which an N-Boc group is introduced at this position compared to its non-Boc analog, compound **23** (*Ki* = 31). The electrostatic contours of CoMFA (**Figure 4.1.5**) show red contour near 5-methoxyphenyl group of the template molecule where high electron density is expected to increase the activity. Compound **8** (*Ki* = 27) exhibits good activity wherein the electronegative oxygen of methoxyphenyl group favorable for inhibitory activity is buried in red contour. Compound **26** has got low activity (*Ki* = 621) as there is

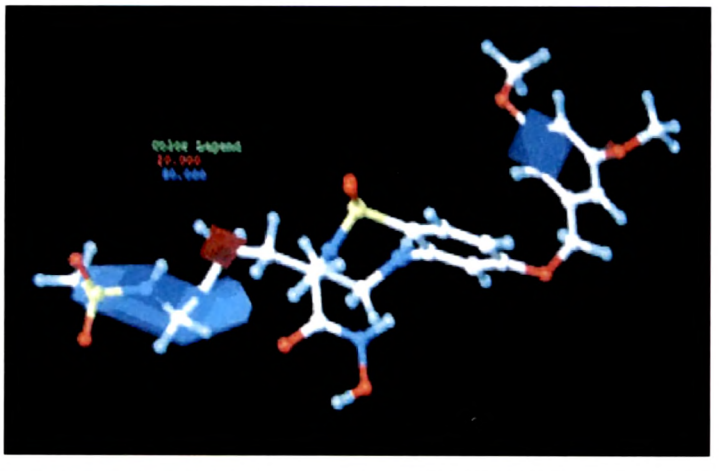

Figure 4.1.5 The CoMFA electrostatic STDEV*COEFF contour plots of active compound **21** from analysis-B. Positively charged favored areas (contribution level 80%) are represented by blue polyhedra. Negatively charged favored areas (contribution level 20%) are represented by red polyhedra.

absence of electronegative group in this region. The electrostatic contours show blue polyhedron in the vicinity of the 3-methoxyphenyl group where low electron density is expected to increase activity. Compounds which are not having N at aromatic substituted groups such as compound **13** (*Ki* = 17) and compound **19** (*Ki* = 10) show good TACE inhibitory activity. Compared to compound **19**, compound **10** possesses lesser activity (*Ki* = 544), as the favorable (blue) electropositive contour is seen embedded in pyridine ring. As the orientation of thiazolyl ring in molecule **16** is not inclined toward this contour, this could be one of the reasons compound **16** (*Ki* = 290) is having better activity than compound **10** (*Ki* = 544).

Table 4.1.6 Actual and predicted activities and residuals of the training set and test set molecules using analysis B; III[c] of COMFA and best model from COMSIA (Table 4.1.3)

Comp.	*pKi*				
		predicted			
	Experimental	CoMFA	Residual	CoMSIA	Residual
1	6.562	6.402	0.160	6.318	0.244
2	6.315	6.293	0.022	6.405	-0.090
3*	7.148	6.588	0.560	6.737	0.411
4	6.407	6.410	-0.003	6.478	-0.071
5	6.151	6.260	-0.109	6.250	-0.099
6	6.640	6.588	0.052	6.623	0.017
7	6.815	6.748	0.067	6.640	0.175
8*	7.568	7.011	0.557	7.062	0.506
9	7.091	7.117	-0.026	7.140	-0.049
10*	6.264	6.459	-0.195	6.704	-0.440
11	7.050	6.931	0.119	6.781	0.269
12	6.752	6.849	-0.097	6.928	-0.176
13	7.769	7.776	-0007	7.613	0.156
14*	8.00	7.186	0.814	7.290	0.710
15	7.292	7.216	0.076	7.390	-0.090
16	6.537	6.509	0.028	6.730	-0.193
17*	6.752	6.975	-0.223	7.128	-0.376
18	6.616	6.533	0.083	6.726	-0.110
19	8.00	8.035	-0.035	8.086	-0.086
20	7.886	7.918	0.032	7.886	0.000
21	8.301	8.209	0.092	8.108	0.193
22	7.113	7.084	0.029	7.221	-0.108
23	7.508	7.689	-0.181	7.542	-0.034
24	7.251	7.243	-0.008	7.229	0.022
25*	6.120	6.424	-0.304	6.165	-0.045
26	6.206	6.232	-0.026	6.044	0.162
27	6.134	6.177	-0.041	6.081	0.055

*Test set molecules

A white disfavored hydrophobic contour (**Figure 4.1.6**) is observed in the vicinity of 5-methoxyphenyl group where hydrophobic substituents are detrimental for TACE inhibitory activity. This is true for compounds having 2,6-dimethyl-4-pyridyl substitution, compound **10** (*Ki* = 544); 3,5-dichlorophenyl, compound **7** (*Ki* = 153), and 4-trifluoromethylphenyl, compound **25** (*Ki* = 758); having less activity as these groups lie in the hydrophobic disfavored areas. The hydrophobic contours (**Figure 4.1.6**) show presence of a cyan contour surrounding the substituted nitrogen of methanesulphonamide group, which indicate that more hydrophobic substituents may improve the biological activity in this position.

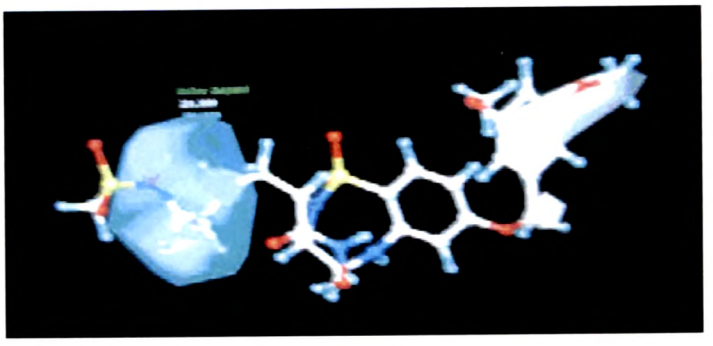

Figure 4.1.6 The CoMSIA hydrophobic fields-cyan polyhedra indicate regions where hydrophobic substituents are favored and white polyhedra indicate disfavored regions.

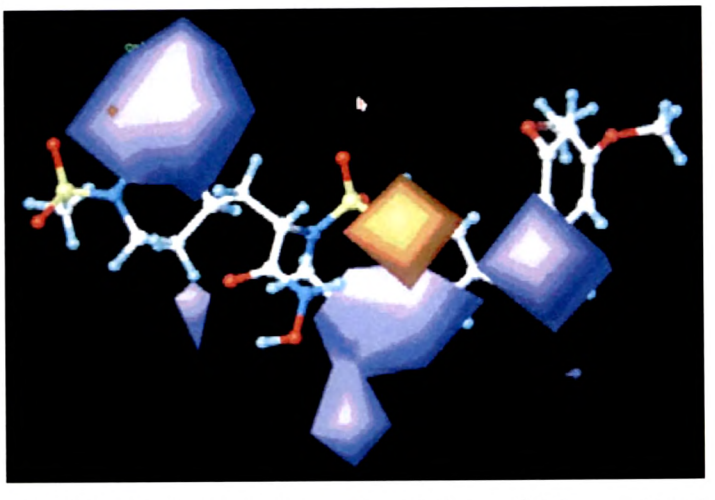

Figure 4.1.7 The CoMSIA hydrogen bond donor fields-purple polyhedra indicate regions where hydrogen bond donor substituents are favored and white polyhedra indicate disfavored regions

The purple polyhedron near the vicinity of methanesulfonamido group indicates that hydrogen bond donor groups favor for higher activity (**Figure 4.1.7**). This is in accordance with compound **22** (*Ki* = 77) and **23** (*Ki* = 31) while compounds having carbonyl group show decrease in the activity as is the case with compound **17** (*Ki* = 177) and compound **18** (*Ki* = 242). The second contour present in the vicinity of benzyloxy group indicates that hydrogen bond donors favor for higher activity. The orange contour present on the benzodiazepine ring (**Figure 4.1.7**) indicates that substitutions at this position with hydrogen bond donor groups are detrimental for the activity; hence, no substitutions have been tried in this position.

As the crystal structure of TACE is available, the interaction of compound **21** with the active site of crystal structure of TACE is shown in **Figure 4.1.8A**. Apart from bonding with the oxygen of hydroxamic acid, there is a strong bonding between oxygen

A

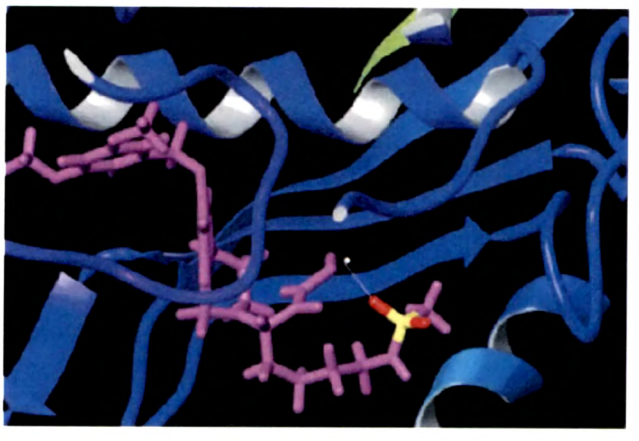

B

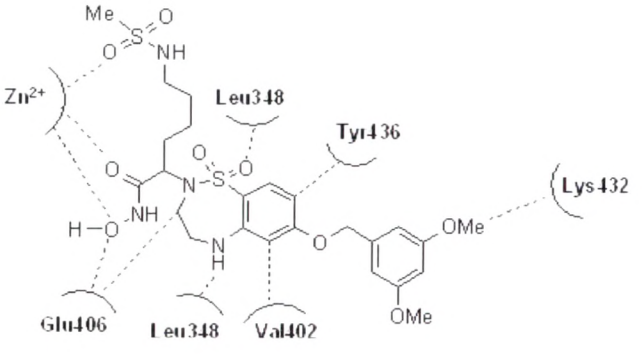

Figure 4.1.8 (**A**) Interaction of active site Zn^{2+} ion (shown in white color) with oxygen (red color) of SO_2Me group of template compound (**21**) has been shown in violet color except for oxygen (red) and sulfur (yellow). (**B**) Interaction of active site of TACE with the template compound (**21**)

of SO_2Me group present in the compound **21** and zinc ion; this could be one of the reasons why the template compound has got good inhibitory activity. Lue348, Glu406, Val402, Tyr436 and Lys432 of the active site of TACE are interacting with the scaffold as shown in **Figure 4.1.8B**.

Efforts were made to compare the contour maps with the steric, electrostatic, hydrophobic and hydrogen bond donor properties of the active site but they were not found in consonance, probably because of the reason discussed earlier i.e. the enzyme conformation changed after binding with the ligands.

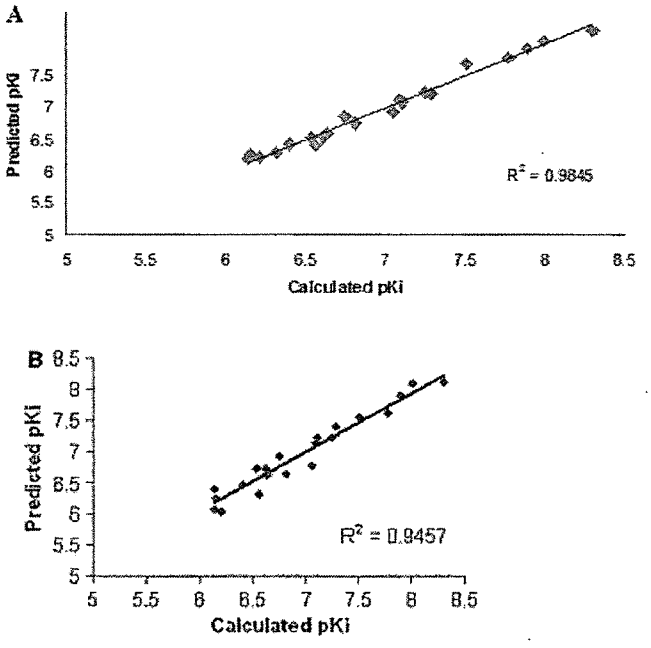

Figure 4.1.9 Plots of calculated versus predicted activities of training sets of compounds. (A) CoMFA (analysis B III[c]). (B) CoMSIA

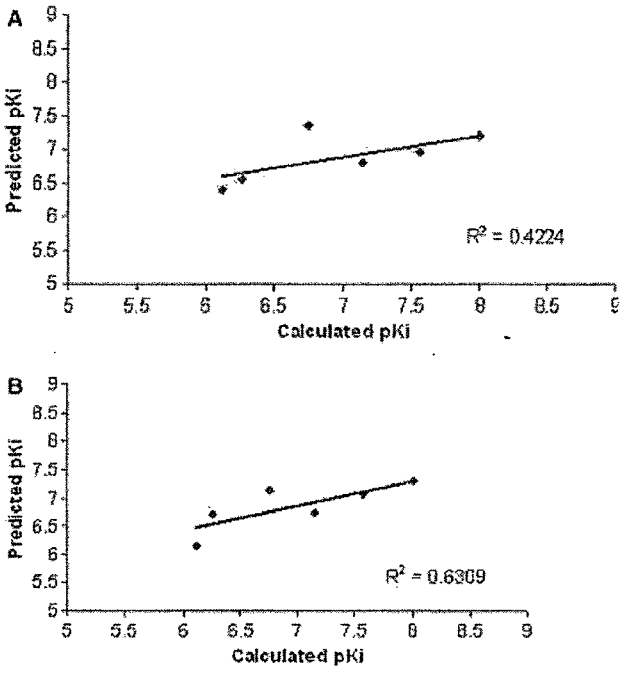

Figure 4.1.10 Plots of calculated versus predicted activities of test sets of compounds (A) CoMFA (analysis B III[c]). (B) CoMSIA (SEDH)

4.1.7 Designing of newer TACE inhibitors using the developed CoMSIA model

The external predictivity of CoMSIA model (SEDH) is better than that of CoMFA model hence, the contour maps generated with CoMSIA were used for designing of newer inhibitors. The steric contour maps indicated green and yellow color

contours as sterically favorable and unfavorable areas. Thus, it was thought logical to put more bulky groups in the carbon chain of the methanesulfonyl group of the template molecule **21**, as green contour is present in the vicinity of substituted amido group of methanesulfonyl. The predicted activities were found to increase after putting the bulky groups. It was observed that compounds with substituents like ethyl, propyl, butyl and cyclohexyl at N-substituted sulfonylmethyl and 3-methylbenzyloxy positions showed sig-

Table 4.1.7 Designed molecules with their predicted activities

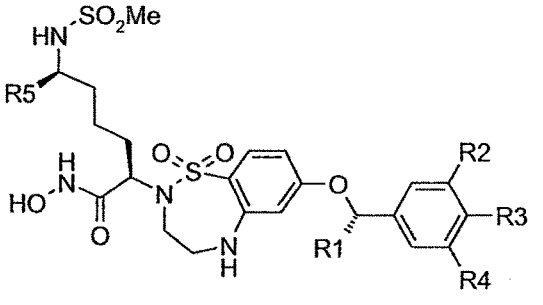

Comp.	R1	R2	R3	R4	R5	CoMSIA Predicted *pKi*
21 (Template)	H	-OMe	H	-OMe	H	8.108
D1	-	-	$-C_5H_{11}$	-	-	8.288
D2	-	-	$-C_4H_9$	-	-	8.243
D3	-	-	$-C_4H_9$	-	$-C_6H_5$ (*S*)	8.224
D4	-	$-C(CH_3)_3$	-	-	-	8.222
D5	$-NH_2$ (*R*)	-	-	-	-	8.182

nificant increase in the activity. The inhibitory activity of template molecule got decreased after decreasing/increasing chain length of substituted amido group. Substitutions were carried out on the methylsulfonyl group of the template molecule in the vicinity of blue polyhedron with electropositive groups, as blue polyhedron represents positively charged favored areas, resulting into slight increase in the inhibitory activity. Substituents with electron donating groups (through resonance) such as $-OCH_3$, -NHMe, $-N(Me)_2$, and -SMe resulted into increase in the activity when compared with the template. Hydrophobic groups (alkyl) were placed at 5-methoxy position in the vicinity of white polyhedron, resulting into decrease in inhibitory activity but substitution at 3-methoxy and 4 positions of phenyl group increased the activity. Substitutions were tried on the upper side of benzothiadiazepine in the vicinity of orange polyhedron with hydrogen

donor groups like -CH_3 and NH_2, resulting into decrease in the inhibitory activity, thus supporting the model. Based on the graphical interpretation of CoMSIA model, it was planned to design new molecules with higher TACE inhibitory activity than the template molecule. Different substituents were tried on the template structure at different positions using the contour maps for guidance. Some of the best compounds (**D1–D5**) with increased TACE inhibitory profiles are given in **Table 4.1.7.** Unfortunately, a substantial increase in biological activity could not be observed in the designed compounds.

4.2 Development of Predictive 3D-QSAR CoMFA and CoMSIA Models for β-Aminohydroxamic Acid-Derived TACE Inhibitors

4.2.1 Dataset for analysis

Sixty two molecules selected for this study were taken from the published work by Gilmore *et al.*[291] and Chen *et al.* [292]. Molecules which did not have bioactivity in exact numerical form for the inhibition and those whose biological activity was not expressed in IC_{50} were removed from the analysis. Finally, 56 molecules were considered for the study. The structures of the training and test molecules are given in **Table 4.2.1.** The biological activity used in this study was expressed as pIC_{50} = -log IC_{50} where, IC_{50} is the concentration in moles (M) of the inhibitor producing 50% inhibition of porcine TACE. For calculation of pIC_{50} values, molar concentrations (IC_{50}) only were utilized.

4.2.2 Alignment rules

Molecular conformation and orientation is one of the most sensitive input areas in 3D-QSAR studies. In the present study, superimposition of the molecules was carried out by different approaches using compound **29** (**Table 4.2.1**) as the template structure as given below:

Alignment I- Each analog was aligned to the template by rotation and translation so as to minimize the RMSD between atoms in the template and the corresponding atom in the analog using the DATABASE ALIGN option in SYBYL. Common fragment used for alignment is shown in **Figure 4.2.1.**

Alignment II- In this alignment, atoms of the molecules were used for RMS (root mean square) fitting corresponding to the atoms in the template.

Table 4.2.1 Structures and biological activities of compounds used in training and test sets

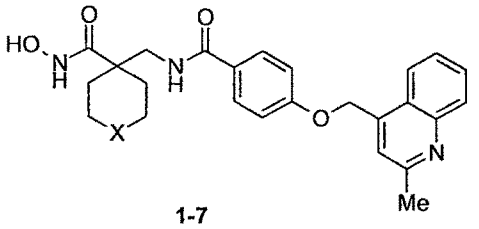

1-7

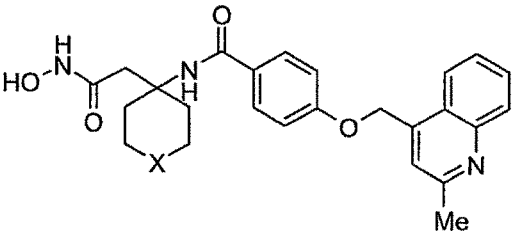

8-30

Comp.	X	IC_{50}	pIC_{50}	ClogP
1	CH_2	8.6	8.065	4.25
2	NBoc	2.4	8.619	3.52
3	NH	4.9	8.309	2.39
4	*N*-Propyl	11	7.958	3.84
5*	*N*-(CO) *t*.Butyl	2.3	8.638	3.85
6	N-SO_2Me	1.9	8.721	2.29
7	O	2.3	8.638	2.35
8*	CH_2	1.4	8.853	3.21
9*	N-Boc	7.7	8.113	2.81
10	*N*-Methyl	3.1	8.508	1.60
11	*N*-Ethyl	2.2	8.657	2.13
12*	*N*-Propyl	2.0	8.699	2.67
13	*N*-*t*.Butyl	3.7	8.431	2.83
14	*N*-CH_2- *t*Butyl	2.6	8.585	3.36
15	*N*-Dimethylpropargyl	2.3	8.638	2.68
16	*N*-Phenyl	1.9	8.721	3.39
17	*N*-$(CH_2)_2$COO*t*.Bu	1.9	8.721	3.10
18	*N*-$(CH_2)_2$COOH	3.2	8.499	1.41
19	*N*-2-(4,5-Dihydrothiazole)	1.2	8.920	2.10
20	*N*-$CH_2CH_2SO_2$Me	1.2	8.920	0.73
21*	*N*-$CH_2CH_2SO_2$Et	1.4	8.853	1.26
22	*N*-CH_2CH_2F	2.6	8.585	1.94
23*	*N*-C(O)Me	1.9	8.721	1.49
24	*N*-C(O)Et	2.7	8.568	2.02
25	*N*-C(O)-*i*.Propyl	1.2	8.920	2.36
26	*N*-C(O)-*t*.Butyl	2.1	8.677	2.71
27	*N*-C(O)CH_2-*t*.Butyl	1.9	8.721	3.24
28	*N*-C(O)-*i*.Butyl	2.2	8.657	2.90
29	*N*-SO_2Me	1.0	9.00	1.59
30*	*N*-C(O)NMe_2	2.8	8.522	1.95

(continued)

Table 4.2.1 (continued)

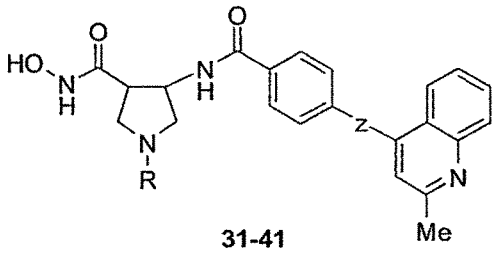

31-41

Comp.	R	Z	IC_{50}	pIC_{50}	ClogP
31	H	OCH_2	6.3	8.200	1.15
32	$-CO_2$-*t*.Butyl	O	1.3	8.886	3.95
33	H	O	3.5	8.455	1.57
34		CH_2	2.5	8.602	1.47
35	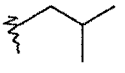	CH_2	1.6	8.795	2.88
36	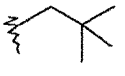	CH_2	1.6	8.795	3.23
37	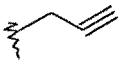	CH_2	4.3	8.366	1.76
38	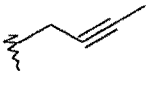	CH_2	1.0	9.00	1.92
39	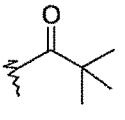	CH_2	1.5	8.823	2.35
40	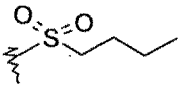	CH_2	1.1	8.958	2.81
41	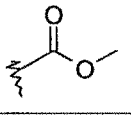	CH_2	3.3	8.481	1.22

(continued)

Table 4.2.1 (continued)

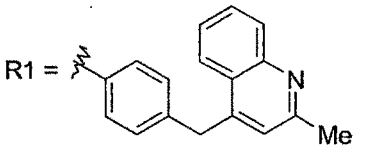

42-45

Comp.	Structure	IC_{50}	pIC_{50}	CLogP
42*	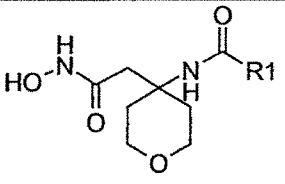	97	7.013	1.81
43	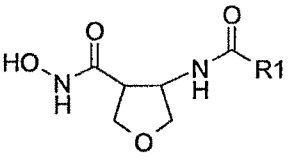	2.0	8.698	1.28
44*	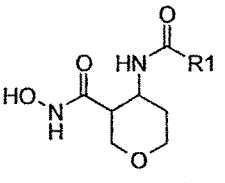	1.0	9.00	1.54
45	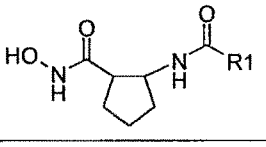	1.8	8.744	2.23

(continued)

Table 4.2.1 (continued)

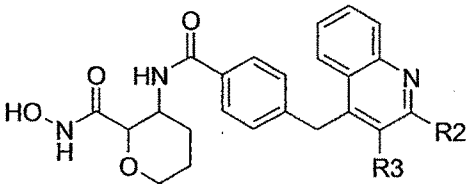

46-56

Comp.	R2	R3	IC_{50}	pIC_{50}	CLogP
46	CF_3	H	2.2	8.657	1.65
47	Et	H	1.7	8.769	2.07
48*	Morpholinyl	H	1.6	8.795	-0.10
49	NMe_2	H	1.2	8.920	1.80
50	Cyclopropyl	H	1.3	8.886	2.13
51	H	Me	1.5	8.823	1.54
52*	Me	Me	1.2	8.920	2.00
53	Me	Et	7.8	8.107	2.53
54			1.0	9.000	2.20
55			2.6	8.585	0.74
56			1.3	8.886	1.00

*Test set molecules

Alignment III – Here, centroids, rather than the exact superimposition of atoms of the rings were used for RMS fitting to the template.

Alignment IV – Here, both centroids and atoms were selected for superimposition on the template. The centroids and atoms used for alignments are defined in **Figure 4.2.1.**

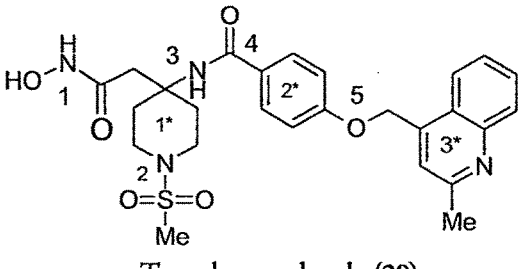

Template molecule (29)

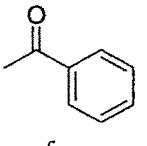

Common fragment used for database alignment

Alignment	
I	Database alignment
II	1,2,4,5
III	1*,2*,3*
IV	2*,3*,3,5
V	Docked conformer-based

Figure 4.2.1 Alignment rules adopted for the CoMFA studies

These alignments were subsequently used in CoMFA/CoMSIA probe interaction energy calculations.

Alignment V – Template structure was docked in the active site of TACE enzyme (pdb code: 2fv5) and the resulting conformer was used for the database alignment as per Alignment I.

4.2.3 CoMFA analysis

This study was aimed at elucidating the structural features required for TACE inhibition and to obtain predictive 3D-QSAR model, which could provide a guide for rational synthesis of potent novel compounds. It would have been difficult to perform the QSAR study at two dimensional level, as the series under investigation contains structurally diverse compounds with variations at different positions (**Figure 4.2.2**).

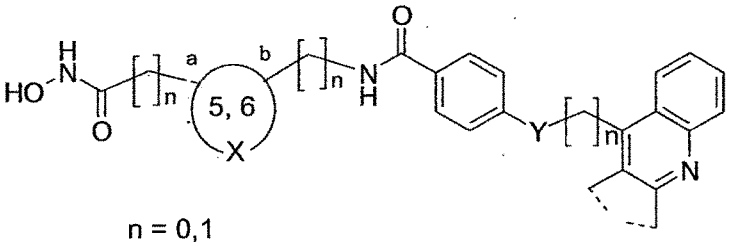

n = 0,1
Five membered ring, X = N-R
Six membered ring, X = CH_2,O,NH,N-R
Y = CH_2,O,NH
a,b = vicinal/geminal locations

Figure 4.2.2 General structure for the five series of compounds under study

The 3D-QSAR models for β-aminohydroxamic acid derivatives were derived using both CoMFA as well as CoMSIA techniques. The negative logarithm of the IC_{50} (pIC_{50}) was used as dependent variable in the 3D-QSAR study (**Table 4.2.1**). Selection of the training set and test set molecules was done by considering the fact that the test set molecules represents a range of biological activity similar to that of the training set. The selected compounds were divided into a training set (45 compounds) and a test set (11 compounds) in an approximate ratio of 4:1 (**Table 4.2.2**). To diversify the training set and test set, they were grouped manually so that molecules possessing diverse functionalities and biological activity of wide range were included in both the sets. The mean biological activities (pIC_{50}) of the chosen training and test set molecules were 8.65 and 8.55, respectively. Thus, it could be considered that the test set is the true representative of the training set. All the molecules were aligned employing atom/shape based RMS fitting and RMSD-based database fitting techniques. Various 3D-QSAR

Table 4.2.2 Observed and predicted activities and residuals of the training and test sets using best COMFA and COMSIA models

Comp.	pIC_{50}				
	observed	predicted			
		CoMFA	(Residual)	CoMSIA	(Residual)
1	8.065	8.217	(- 0.152)	8.291	(-0.226)
2	8.619	8.709	(-0.090)	8.746	(-0.127)
3	8.309	8.319	(-0.010)	8.300	(0.009)
4	7.958	7.838	(0.120)	8.163	(-0.205)
5*	8.638	8.666	(-0.028)	8.336	(0.302)
6	8.721	8.531	(0.190)	8.506	(0.215)
7	8.638	8.546	(0.092)	8.307	(0.338)
8*	8.853	8.831	(0.022)	8.813	(0.040)
9*	8.113	7.951	(0.162)	7.885	(0.228)
10	8.508	8.698	(-0.190)	8.808	(-0.300)
11	8.657	8.696	(-0.039)	8.787	(-0.130)
12*	8.699	8.626	(0.073)	8.776	(-0.077)
13	8.431	8.421	(0.010)	8.445	(-0.014)
14	8.585	8.676	(-0.091)	8.783	(-0.198)
15	8.638	8.744	(-0.106)	8.798	(-0.161)
16	8.721	8.788	(-0.067)	8.810	(-0.089)
17	8.721	8.621	(0.100)	8.789	(-0.068)
18	8.499	8.552	(-0.053)	8.785	(-0.286)
19	8.920	8.980	(-0.060)	8.781	(0.139)
20	8.920	8.670	(0.250)	8.824	(0.096)
21*	8.853	8.757	(0.096)	8.804	(0.049)
22	8.585	8.651	(-0.066)	8.801	(-0.216)
23*	8.721	8.711	(0.010)	8.814	(0.204)
24	8.568	8.573	(-0.005)	8.929	(0.246)
25	8.920	8.977	(-0.057)	8.938	(0.168)
26	8.677	9.006	(-0.329)	8.890	(-0.009)
27	8.721	8.931	(-0.210)	8.828	(0.261)
28	8.657	8.658	(-0.001)	8.928	(-0.169)
29	9.000	8.919	(0.081)	8.335	(-0.171)
30*	8.552	8.230	(0.322)	8.525	(0.072)
31	8.200	8.267	(-0.067)	8.837	(-0.217)
32	8.886	8.781	(0.105)	8.608	(-0.325)
33	8.455	8.485	(-0.030)	8.694	(0.049)
34	8.602	8.572	(0.030)	8.754	(-0.153)
35	8.795	8.740	(0.055)	8.766	(-0.092)
36	8.795	8.674	(-0.121)	8.731	(0.041)
37	8.366	8.633	(-0.267)	8.731	(-0.365)
38	9.00	8.993	(0.007)	8.736	(0.264)

(continued)

Table 4.2.2 (continued)

Comp.	pIC_{50}				
	Observed	predicted			
		CoMFA (Residual)		CoMSIA (Residual)	
39	8.823	8.663	(0.160)	8.755	(0.068)
40	8.958	8.938	(0.020)	8.851	(0.075)
41	8.481	8.559	(-0.078)	8.787	(-0.306)
42*	7.013	7.381	(-0.368)	7.300	(-0.287)
43	8.698	8.556	(0.142)	8.788	(-0.090)
44*	9.000	8.807	(0.193)	8.739	(0.261)
45	8.744	8.590	(0.154)	8.669	(0.075)
46	8.657	8.673	(-0.016)	8.735	(-0.078)
47	8.769	8.826	(-0.057)	8.708	(0.061)
48*	8.795	8.870	(-0.075)	8.800	(0.005)
49	8.920	8.881	(0.039)	8.718	(0.202)
50	8.886	8.902	(-0.016)	8.719	(0.167)
51	8.823	8.828	(-0.005)	8.694	(0.129)
52*	8.920	8.915	(0.005)	8.709	(0.211)
53	8.107	8.016	(0.091)	8.012	(0.095)
54	9.000	8.867	(0.133)	8.704	(0.296)
55	8.585	8.599	(-0.014)	8.707	(-0.122)
56	8.886	8.890	(-0.004)	8.716	(0.170)

* Test set molecules

models were generated and the best model was chosen on the basis of statistics obtained for each model.

A preliminary study was performed to study the importance of each field individually. All further analyses were performed with steric and electrostatic fields calculated at each grid point simultaneously. Partial least square analysis was performed using varying column filtering values. Finally, column filtering was set to 2.0 kcal/mol. Different alignments such as data-based (alignment I), atom-based (alignment II), centroid-based (alignment III), centroid and atom-based (alignment IV) and docked conformer-based (alignment V) alignments (**Figure 4.2.1**) were used for developing various CoMFA models.

Database alignment I showed cross-validated r^2 = 0.137 with nine components, non-cross-validated r^2 = 0.871, F-value 159.071[$F_{05}(10, 30)$ = 2.16 (Tab)], predictive r^2 = 0.234; the steric and electrostatic contributions were 70.1 and 29.9%, respectively. The CoMFA model generated from atom-based RMS alignment II showed cross-validated r^2 = 0.112 with seven components, non-cross-validated r^2 = 0.858, F-value 65.250 [F_{05}(07,

30) = 2.33 (Tab)], predictive r^2 = 0.216 with 60.2 % steric and 39.8% electrostatic contributions. The centroid-based alignment III yielded cross-validated r^2 = 0.139 with six components, non-cross-validated r^2 = 0.864, F-value 30.00 [F_{05}(06, 40) = 2.34 (Tab)]

Table 4.2.3 Summary of CoMFA results

Parameters	Alignment V	
	V^a	V^b
r^2_{cv} [c]	0.673	0.662
NC[d]	2	2
SEP[e]	0.394	0.374
r^2_{ncv} [f]	0.860	0.741
SEE[g]	0.243	0.327
F-value	86.073	61.451
P r^2=o[h]	0	0
Contribution steric (fraction)	0.594	0.590
Contribution electrostatic (fraction)	0.406	0.375
Contribution ClogP (fraction)	-	0.035
r^2_{pred} [i]	0.642	0.381
SD	0.011	0.013

[a]Alignment by docked conformation based RMSD database. [b]Alignment by docked conformation based RMSD database with ClogP as an. additional descriptor. [c]Cross-validated correlation coefficient. [d]Number of components. [e]Standard error of prediction. [f] Non cross-validated square of correlation coefficient. [g]Standard error of estimate. [h]Pr^2 = 0, probability that correlation coefficient r equals zero. [i]Predicitve r^2.

and predictive r^2 = 0.267. The steric and electrostatic contributions were 68.3% and 31.7%, respectively. Alignment IV (centroid and atom-based) yielded a cross-validated r^2 = 0.153 with seven components, non-cross-validated r^2 = 0.912, F-value 72.60 [F_{05}(07, 30) = 2.33 (Tab)] and predictive r^2 = 0.303. The steric and electrostatic contributions were 64.3% and 35.7%, respectively. Alignment V (**Table 4.2.3; V^a**) yielded the highest cross-validated r^2 of 0.673 with two components, non-cross-validated r^2 of 0.860, F-value 86.073 [F_{05}(02, 40) = 3.22 (Tab)] and predictive r^2 of 0.642.

The biological activity of compounds may have contributions from other physico-chemical factors than just steric and electrostatic interactions. One such parameter is hydrophobicity. To represent hydrophobicity, CLogP could be a suitable parameter. Hence, to study the effects of hydrophobic/lipophilic properties of molecules on TACE inhibitory activity, CLogP as an additional descriptor in the CoMFA analysis was included. Inclusion of CLogP in the CoMFA models with all of the five alignments did not increase internal or external predictivity and exhibited low to moderate lipophilic

contributions as compared to CoMFA models utilizing steric and electrostatic fields only (**Table 4.2.3; V**[b]). In the *in vitro* binding studies, log P may not play a direct role in cont-

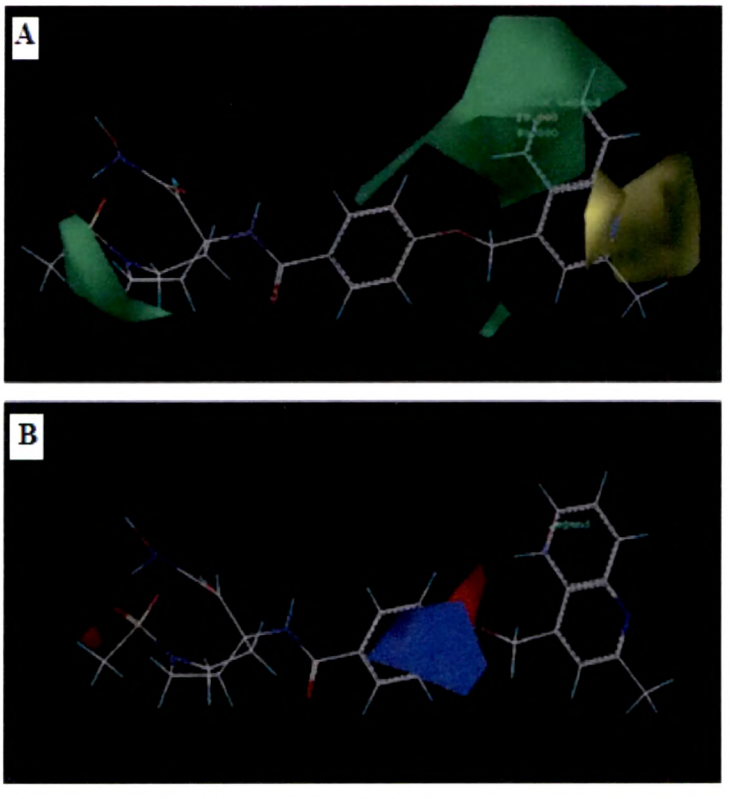

Figure 4.2.3 (**A**) The CoMFA steric STDEV*COEFF contour plots of active compound (**29**). Sterically favored areas (contribution level 80%) are represented by green polyhedra. Sterically disfavored areas (contribution level 20%) are represented by yellow polyhedra. (**B**) The CoMFA electrostatic STDEV*COEFF contour plots of active compound (**29**). Positively charged favored areas (contribution level 80%) are represented by blue polyhedron. Negatively charged favored areas (contribution level 20%) are represented by red polyhedra.

rolling the biological activity as the drug molecules are not required to cross the membrane barriers inclusion of log P clearly indicated that hydrophobic interactions are not dominant ones in the binding of the inhibitors with the enzyme. The model generated with alignment V[a] with a good internal predictive ability (r^2_{cv} = 0.673) and a small standard error of estimation (SEE = 0.243) was selected as the best model to explain SAR and to carry out further analysis, and all the CoMFA contours were generated using this model. The field values generated at each grid point were calculated as the scalar product of the associated QSAR coefficient and the standard deviation of all values in the corresponding column of the data table (STD*COEFF) plotted as the percentage contributions to QSAR equation. The CoMFA steric and electrostatic contour

maps are shown in **Figure 4.2.3 A and B** respectively. The green colored regions indicate areas where steric bulk enhances TACE inhibitory activity, while the yellow contours indicate regions where steric bulk is detrimental for biological activity. Blue-colored regions show areas where electropositively-charged groups enhanced TACE inhibitory activity, while red regions represent where electronegatively-charged groups improved the activity. The plots of observed versus predicted activities for the training and test sets of molecules are depicted in **Figures 4.2.4** and **4.2.5**, respectively.

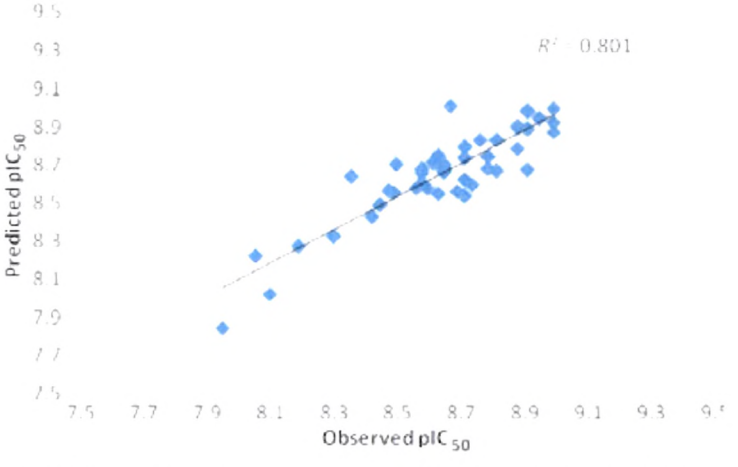

Figure 4.2.4 Plot of observed versus predicted activity of training set of compounds using CoMFA

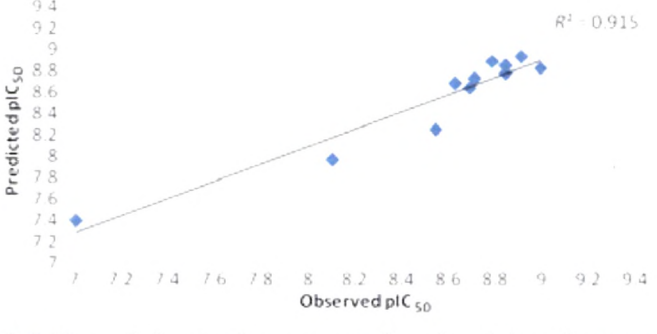

Figure 4.2.5 Plot of observed versus predicted activity of test set of compounds using CoMFA

4.2.4 CoMSIA analysis

The CoMSIA analysis was performed using steric, electrostatic, hydrophobic, and hydrogen bond donor and acceptor fields. Presently, CoMSIA offers five different fields; 3D-QSAR models could be generated using the above fields in different combinations. The docked conformer-based alignment V (**Table 4.2.3; V**[a]) used in CoMFA studies served as the alignment for CoMSIA and the results of the study are summarized in

Table 4.2.4. The CoMSIA model showed considerable correlation and predictive properties.

The CoMSIA model with combination of all the fields yielded a cross-validated r^2 = 0.566 with three components, non-cross-validated r^2 = 0.834, F-value 70.243 [F_{05}(03, 40) = 2.84 (Tab)] and predictive r^2 = 0.351. The contributions of steric, electrostatic, hydrophobic, hydrogen bond donor and acceptor fields of this model were 11.3, 18.3, 20.7, 29.0 and 20.7% respectively. The CoMSIA model with a combination of steric, electrostatic and hydrophobic fields yielded the highest cross-validated r^2 = 0.635 with three components, non-cross-validated r^2 = 0.858, F-value 84.451[F_{05}(03, 40) = 2.84 (Tab)] and predictive r^2 of 0.441. The steric, electrostatic and hydrophobic field contributions were 24.4, 27.1 and 48.4%, respectively. Combinations of steric, electrostatic and hydrogen bond donor fields yielded a CoMSIA model with a cross-validated r^2 = 0.599 with two components, non-crossvalidated r^2 = 0.861, F-value 86.929 [F_{05}(02, 40) = 3.22 (Tab)] and predicted r^2 = 0.341. The steric, electrostatic and hydrogen bond donor contributions were 22.0, 26.5 and 51.5%, respectively. The models generated by various combinations of CoMSIA fields (**Table 4.2.4**) showed moderate to high, internal and external predictivity, in which the hydrophobic fields were observed to be dominant over the hydrogen bond donor and hydrogen bond acceptor fields. The CoMSIA steric and electrostatic contours (not shown) were positioned similarly to those

Table 4.2.4 Summary of CoMSIA analysis

Field(s)	r^2_{cv}	NC	SEP	r^2_{ncv}	SEE	F-value	P r^2 = 0	r^2_{pred}
H[a]	0.562	3	0.429	0.732	0.324	52.252	0	0.289
D[b]	0.532	2	0.412	0.697	0.354	49.474	0	0.363
A[c]	0.581	3	0.421	0.752	0.324	51.562	0	0.284
D+A	0.543	2	0.435	0.703	0.351	50.813	0	0.294
H+D	0.590	3	0.417	0.779	0.306	49.344	0	0.318
H+A	0.562	3	0.427	0.758	0.320	66.532	0	0.241
H+D+A	0.556	3	0.429	0.704	0.350	68.932	0	0.312
S[d]+E[e]+D	0.599	2	0.412	0.861	0.242	86.929	0	0.341
H+S+E[f]	**0.635**	**3**	**0.393**	**0.858**	**0.245**	**84.451**	**0**	**0.441**
S+E+A	0.633	3	0.394	0.825	0.273	65.784	0	0.319
S+E+D+A	0.609	3	0.393	0.858	0.268	68.712	0	0.118
SEDAH	0.566	3	0.429	0.834	0.265	70.243	0	0.351
SEAH	0.596	3	0.414	0.818	0.278	62.713	0	0.364
SEDH	0.617	3	0.403	0.855	0.248	82.519	0	0.356

[a] Hydrophobic field; [b] Hydrogen bond donor field; [c] Hydrogen bond acceptor field; [d] Steric field; [e] Electrostatic field; [f] Best model for CoMSIA (shown in bold values)

of the CoMFA model, hence are not discussed. The hydrophobic contour maps of CoMSIA (STDDEV*COEFF) is displayed in **Figure 4.2.6**. The results of CoMSIA PLS analysis are summarized in **Table 4.2.4**. The bold values in **Table 4.2.4** indicate best

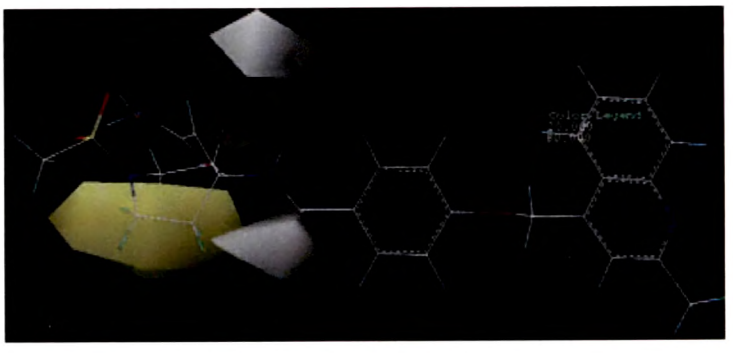

Figure 4.2.6 The CoMSIA hydrophobic fields- yellow polyhedra indicate regions where hydrophobic substituents are favored and white polyhedra indicate disfavored regions.

model (HSE) for CoMSIA. The CoMSIA model generated from steric and electrostatic fields did not show much differentiation both in terms of statistical values and positions of contours as compared to the best CoMFA model (alignment V^a) and hence are not included in the table.

4.2.5 CoMFA vs. CoMSIA

A comparison of the statistical results of the two QSAR analyses is listed in **Table 4.2.5**. Both CoMFA and CoMSIA models exceeded $r^2_{cv} > 0.5$ which indicated stability of the model and reasonable predictability [290]. Comparative molecular field analysis showed higher cross-validated r^2 value of 0.673 than 0.635 for CoMSIA.

Table 4.2.5 Comparison of Statistical parameters for CoMFA and CoMSIA

Analysis type	r^2_{cv}	SEP	N	r^2_{ncv}	SEE	F-value	r^2_{pred}
CoMFA	0.673	0.394	2	0.860	0.243	86.073	0.642
CoMSIA	0.635	0.393	3	0.858	0.245	84.451	0.441

4.2.6 Graphical interpretation of the CoMFA and CoMSIA models

To visualize the information contents of the derived 3D-QSAR model, CoMFA contour maps were generated by interpolating the products between the 3D-QSAR coefficients and their associated standard deviations. **Figures 4.2.3A and B** indicate the CoMFA steric and electrostatic contour maps respectively, obtained from the best model

(alignment V^a) using compound **29**, as the reference. In this figure, the green contours represent regions of high steric tolerance (80% contribution), while the yellow contours represent regions of low steric tolerance (20% contribution). Increase in positive charge is favored in blue regions while increase in negative charge is favored in red regions. The steric contour map of CoMFA (**Figure 4.2.3A**) shows a green contour enclosing the quinoline ring of the template structure. This indicates that bulky groups here would enhance the TACE inhibitory activity. Good inhibitory activity of **54** (IC_{50} 1.00), **49** (IC_{50} 1.2), **50** (IC_{50} 1.3) and **56** (IC_{50} 1.30), is because of orientation of bulkier groups towards sterically favored green contour. The steric contour map of CoMFA also shows a large contour enclosing the piperidine ring of the template molecule where more bulky substitutions are expected to increase the activity. High potency of compounds **27** (IC_{50} 1.90), **32** (IC_{50} 1.3), **38** (IC_{50} 1.0) and **40** (IC_{50} 1.1) is because of orientation of bulkier groups towards this sterically favored green contour. Molecules **31** (IC_{50} 6.30) and **33** (IC_{50} 3.5) lacking bulky groups at first position of the pyrrolidine were less active. The steric contour map also shows yellow contour near quinoline ring. Here, bulky substituents are not tolerated hence molecule **53** (IC_{50} 7.8) exhibited low inhibitory activity as quinoline ring of this compound lies in the yellow region.

The electrostatic contour map of CoMFA (**Figure 4.2.3B**) shows red contour surrounding the central benzamide ring of the template molecule where high electron density is expected to increase the activity. Compound **32** (IC_{50} 1.3) exhibits good activity wherein the electronegative oxygen of the ether linkage between phenyl and quinoline groups, favorable for inhibitory activity, is buried in red contour. The electrostatic contours show blue polyhedron in the vicinity of central phenyl ring where low electron density is expected to increase activity. The hydrophobic contour map (**Figure 4.2.6**) shows presence of a yellow contour surrounding the piperidine ring, indicating that more hydrophobic substituents may improve the biological activity (as seen in compounds **34–36, 38**). This may be the reason why compound **31** shows poor inhibitory profile. The white disfavored hydrophobic contour is observed in the vicinity of benzene ring where hydrophobic substituents are detrimental for TACE inhibitory activity. This is in agreement with the fact that no synthetic efforts have been made to add substituents on the benzene ring.

4.2.7 External validation of the developed CoMFA model

A good model should be able to predict correctly activities of those external compounds which are not part of the studied data. On survey of literature, we could find one such compound which is a hydroxamate and has been evaluated quantitatively as porcine TACE inhibitor. External validation of CoMFA model was performed by predicting the activity of this reported TACE inhibitor IK682 (**Figure 4.2.7**), a well-known hydroxamate derivative. The predicted activity (pIC_{50} = 8.991) was found to be very close to the experimentally determined value (pIC_{50} = 9.00) [240]. This observation validates our model developed through alignment V[a].

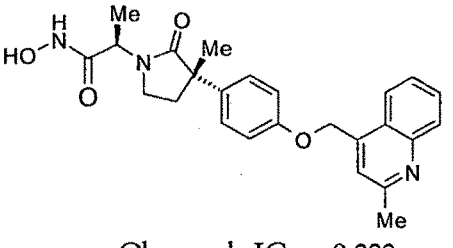

Observed pIC_{50} = 9.000
Predicted pIC_{50} = 8.991

Figure 4.2.7 Structure of IK-682

4.3 Development of Predictive Pharmacophore Model for *In Silico* Screening, 3D QSAR CoMFA and CoMSIA Models for Lead Optimization, and Designing of Newer Potent TACE Inhibitors

4.3.1 Data set for analysis

Over the last few years, a number of classes of TACE inhibitors have been identified. A set of 486 molecules having TACE inhibitory activity was collected from the literature [240,242,291,293-301]. Compounds with defined stereochemistry and discrete quantum of biological activity only were selected, excluding the recemates and those compounds which were reported to have biological activity less than or more than a particular value. Although porcine TACE and human TACE both have quite high homology [295,296] but due to higher abundance of biological data on pTACE over hTACE and for the purpose of uniformity, compounds evaluated on pTACE only were included in the study. On the above described basis, a set of 220 compounds were considered for the pharmacophore generation. The *in vitro* bioactivities of the inhibitors so selected, were reported to be expressed as the concentration of the test compounds that inhibited pTACE by 50% (IC_{50}). To avoid redundancy of information, the data set was further refined by removing

compounds with similar biological activity and chemical structures. On the basis of structural variations and differences in the biological activity, ultimately 80 compounds (**Figure 4.3.1; Table 4.3.1**) with IC_{50} values ranging from 0.066 to 17,000 nM were used in the study [240,242,291,293-301]. The IC_{50} values (in moles/litre) were converted into negative logarithm of IC_{50} (pIC_{50}). For carrying out pharmacophore modeling and CoMFA/CoMSIA 3D-QSAR studies, these 80 compounds were divided into training (61) and test (19) compounds adopting the following two rules: (a) both training and test set compounds were represented from each class of compounds to ensure structural diversity [if one class had only one compound, it was assigned to the training set (e.g., compound 80)]; (b) both, training and test sets covered the bioactivities (IC_{50}) as wide as possible. If there was only one compound with maximum or minimum order of bioactivity in a class, such a compound was assigned to the training set.

4.3.2 Pharmacophore model generation, validation and *in silico* screening of data base

4.3.2.1 Generation of common pharmacophore hypothesis

The development of common pharmacophore hypothesis (CPH) and alignment based on it were carried out using PHASE [38], version 2.5 (Schrödinger, LLC, New York) installed on an SGI workstation. Structures of the 61 compounds of the training set were imported from the project table in the "Develop Pharmacophore Model" panel and refined (cleaned) geometrically using Ligprep module available with Schrodinger. Conformations were generated by the mixed MCMM/LMOD method using a maximum of 2,000 steps with a distance-dependent dielectric solvent model and an OPLS-2005 force field. All the conformers were subsequently minimised using truncated Newton conjugate gradient minimisation up to 500 iterations. For each molecule, a set of conformers with a maximum energy difference of 15 kcal/mol relative to the global energy minimum conformer were retained. A redundancy check of 2 Å in the heavy atom positions was applied to remove duplicate conformers. Pharmacophore features-hydrogen bond acceptor (A), hydrogen bond donor (D), hydrophobic group (H), negatively charged group (N), positively charged group (P) and aromatic ring (R) were

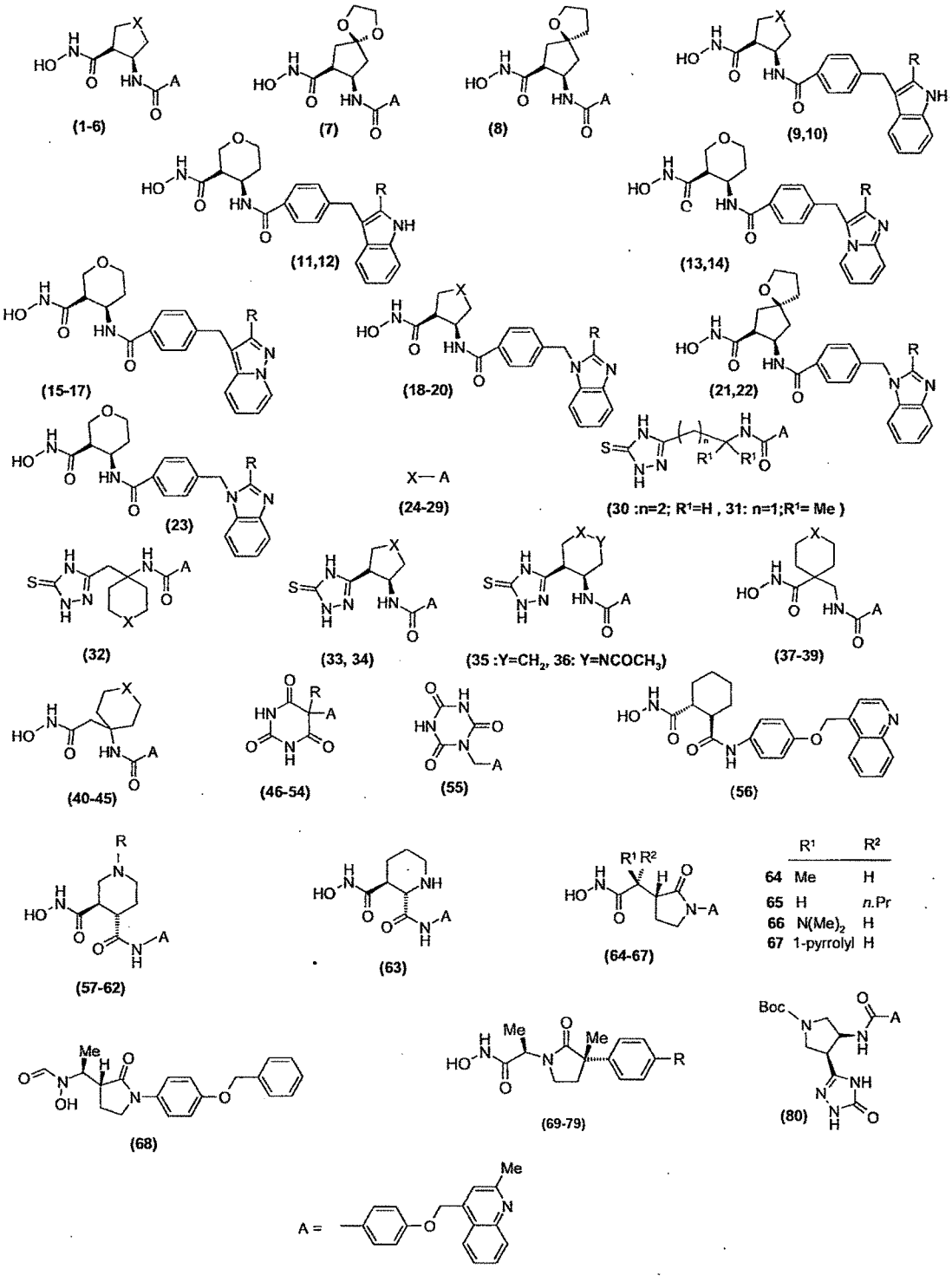

Figure 4.3.1 Compounds used to derive pharmacophore hypotheses and CoMFA/CoMSIA models (substituents X and R are defined in Table 4.3.1)

Table 4.3.1 Compounds used in the study and their IC_{50} values

Comp.	X	R	Biological activity				
			Observed		Predicted (pIC_{50})		
			IC_{50} (nM)	pIC_{50}	Phase (CPH1)	CoMFA	CoMSIA
1*	CH_2	-	1.00	9.000	9.08	9.495	9.213
2	CF_2	-	6.30	8.200	8.26	8.171	8.023
3*	N-C(O)OCH_3	-	1.00	9.000	9.03	9.357	9.321
4*	N-*i*Pr	-	0.40	9.392	9.42	8.857	9.013
5 *(T)	N-Allyl	-	0.94	9.026	8.95	8.834	8.974
6*	N-2-Propynyl	-	0.14	9.853	9.77	9.372	9.387
7*	O	-	1.00	9.000	9.07	8.823	8.875
8* (T)	CH_2	-	1.00	9.000	7.91	7.892	7.928
09	NH	Me	2.2	8.656	8.64	8.715	8.654
10* (T)	$NCH_2C{\equiv}CH$	Me	1.0	9.000	8.36	8.354	8.378
11	-	Me	6.0	8.221	8.17	8.425	8.314
12*	-	Et	1.0	9.000	9.03	8.871	8.912
13 (T)	-	*i*Pr	3.2	8.494	7.48	7.42	7.899
14*	-	Cyclopropyl	1.0	9.000	8.98	8.885	8.912
15	-	Et	2.0	8.698	8.74	8.849	9.012
16	-	*t*Bu	2.8	8.552	8.57	8.848	8.124
17*	-	CF_3	1.0	9.000	8.89	9.026	9.127
18*	N-BOC	Me	1.0	9.000	9.01	9.060	8.951
19	NH	Me	2.6	8.585	8.59	8.716	8.613
20*	O	CF_3	1.0	9.000	8.98	9.343	9.214
21	-	*i*Pr	1.1	8.958	8.91	8.895	8.913
22 (T)	-	*t*Bu	2.0	8.696	8.95	8.983	8.876
23	-	CF_2CH_3	2.6	8.585	8.59	8.576	8.736

(continued)

Table 4.3.1 (continued)

Comp.	X	R	Biological activity				
			Observed		Predicted (pIC_{50})		
			IC_{50} (nM)	pIC_{50}	Phase (CPH1)	CoMFA	CoMSIA
24#	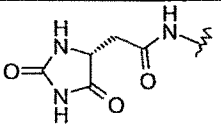	-	170	6.769	6.75	6.528	6.635
25# (T)	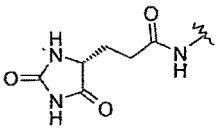	-	150	6.823	8.01	7.985	7.845
26	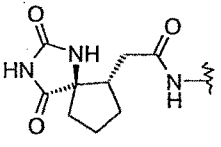	-	11	7.958	7.89	8.111	7.824
27	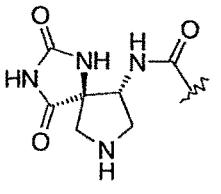	-	25	7.602	7.62	7.625	7.618
28	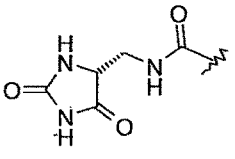	-	98	7.008	7.11	7.417	7.297
29#	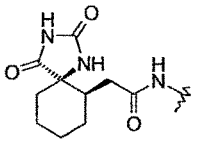	-	900	6.045	6.12	6.135	6.126
30#	-	-	294	6.531	6.52	6.765	6.523
31 (T)	-		55	7.239	7.86	7.913	7.896
32	*N*-Boc	-	36	7.443	7.61	7.336	7.397
33	NH	-	92	7.036	7.01	6.943	7.098
34	*N*-Propyl	-	9.9	8.004	7.96	7.816	7.934
35	NH	-	43	7.366	7.32	7.392	7.386
36 (T)	CH_2	-	2.5	8.602	7.78	7.83	7.941

(continued)

Table 4.3.1 (continued)

Comp.	X	R	Biological activity				
			Observed		Predicted (pIC_{50})		
			IC_{50} (nM)	pIC_{50}	Phase (CPH1)	CoMFA	CoMSIA
37	CH_2	-	8.6	8.065	8.05	8.183	8.179
38 (T)	NH	-	4.9	8.309	9.05	9.153	9.107
39	*N*-Propyl	-	11	7.958	7.94	8.125	8.109
40	*N*-Methyl	-	3.1	8.508	8.39	8.352	8.369
41	*N*-*t*.Bu	-	3.7	8.431	8.40	8.425	8.429
42	*N*-$(CH_2)_2COOH$	-	3.2	8.494	8.51	8.682	8.610
43	N-CH_2CH_2F	-	2.6	8.585	8.71	8.624	8.513
44	*N*-$C(O)CH_2$*t*.Bu	-	1.9	8.721	8.81	8.706	8.714
45 (T)	N-$C(O)NMe_2$	-	2.8	8.552	8.20	8.195	8.267
46#	-	Me	1030	5.987	6.78	6.729	6.534
47 (T)	-	4-*n*Hex-piperazin-1-yl	81	7.091	7.35	7.365	7.342
48#	-	Piperazin-1-yl	1100	5.958	6.34	6.459	6.437
49	-	4-Me-piperazin-1-yl	91	7.040	6.62	6.508	6.497
50#	-	4-Bn-piperazin-1-yl	195	6.709	6.66	6.530	6.541
51	-	4[$Ph(CH_2)_2$]-piperazin-1-yl	84	7.075	7.13	7.170	6.953
52#	-	4-(4-NO_2-Ph)-piperazin-1-yl	2800	5.552	5.68	5.532	5.536
53#	-	4-Ac-piperazin-1-yl	620	6.202	6.23	6.354	6.349
54 # (T)	-	4-Boc-piperazin-1-yl	160	6.795	6.78	6.984	6.864
55#	-	-	7300	5.136	5.01	5.168	5.163
56	-	-	8.00	8.096	8.15	7.512	7.834
57* (T)	-	Cyclopropancarbonyl	1.00	9.00	9.08	9.324	9.124
58*	-	2-Furoyl	.066	10.180	10.000	10.181	10.184

(continued)

Table 4.3.1 (continued)

Comp.	X	R	Biological activity				
			Observed			Predicted (pIC_{50})	
			IC_{50} (nM)	pIC_{50}	Phase (CPH1)	CoMFA	CoMSIA
59*	-	Cyclopropanecabonyl	0.45	9.346	9.56	9.685	9.679
60*	-	Methanesulfonyl	0.48	9.318	9.37	9.013	9.125
61*(T)	-	Methoxycarbonyl	0.28	9.552	9.47	9.489	9.493
62	-	Cyclobutyl	1.60	8.795	8.78	7.822	7.633
63*	-	-	1.00	9.00	9.09	8.632	8.798
64*	-	-	1.00	9.00	9.47	7.762	7.782
65#	-	-	140	6.853	6.84	6.913	6.901
66(T)	-	-	7.00	8.154	8.18	8.143	8.103
67(T)	-	-	26	7.858	7.79	7.697	7.703
68#	-	-	111	6.954	6.87	6.882	6.893
69#	-	Methoxy	887	6.052	6.47	6.459	6.323
70	-	Allyloxy	97	7.013	6.70	6.693	6.698
71	-	Benzyloxy	4	8.397	8.37	8.145	8.213
72# (T)	-	Phenyl	13000	4.886	6.87	6.832	6.793
73	-	3-Nitrobenzyloxy	6	8.221	8.41	8.826	8.712
74 (T)	-	3,5-di-MeO-benzyloxy	7	8.154	8.23	8.234	8.241
75	-	3,5-Bis-CF_3-benzyloxy	2	8.698	8.65	8.831	8.856
76	-	(Pyridine-4-yl)methoxy	21	7.677	7.72	7.216	7.318
77	-	(Quinolin-4-yl)methoxy	1.8	8.744	8.73	8.565	8.569
78*(T)	-	(2-Me-quinolin-4-yl)methoxy	1	9.00	8.05	8.154	8.132
79#	-	H	2200	5.657	5.75	5.972	5.875
80#	-	-	162	6.790	6.75	7.003	6.875

*: Active compound ; # : Inactive compound; T: Test set

defined by a set of chemical structure patterns as SMARTS queries and assigned one of the three possible geometries that defined the physical characteristics of the site:

Point : The site is located on a single atom in the SMARTS query.

Vector : The site is located on a single atom in the SMARTS query, and assigned directionality according to one or more vectors originating from the atom.

Group : The site is located at the centre of a group of atoms in the SMARTS query. For aromatic rings, the site is assigned directionality, defined by a vector that is normal to the plane of the ring.

Active and inactive thresholds of pIC_{50} of 9.00 and 7.00 respectively, were applied to the dataset of the above obtained 80 compounds to yield 21 actives and 17 inactives **(Tables 4.3.1)** that were used for pharmacophore generation and subsequent scoring. Compounds having activity ≥ 9.00 were considered as active compounds and those having ≤7.00 were considered as inactive. Common pharmacophoric features were then identified from a set of variants - a set of feature types that define a possible pharmacophore - using a tree-based partitioning algorithm with maximum tree depth of four with the requirement that all 21 actives must match. The final size of the pharmacophore box was fixed at 1 Å to optimize the number of final CPHs. CPHs were examined using a scoring function to yield the best alignment of the active ligands using an overall maximum root mean square deviation (RMSD) value of 1.2 Å with default options for distance tolerance. The quality of alignment was measured by a survival score (S), defined as:

$$S = W_{site} S_{site} + W_{vec} S_{vec} + W_{vol} S_{vol} + W_{sel} S_{sel} + W^{m}_{rew} - W_{E}\Delta E + W_{act}A$$

Where, W's are weights and S's are scores; S_{site} represents alignment score, the RMSD in the site point position; S_{vec} represents vector score, and averages the cosine of the angles formed by corresponding pairs of vector features in aligned structures; S_{vol} represents volume score based on overlap of van der Waals models of nonhydrogen atoms in each pair of structures; and S_{sel} represents selectivity score, and accounts for what fraction of molecules are likely to match the hypothesis regardless of their activity towards the receptor. W_{site}, W_{vec}, W_{vol} have default values of 1.0, while W_{sel} has a default value of 0.0. In hypothesis generation, default values have been used. The reward comes in the form of W^{m}_{rew}, where W_{rew} is user-adjustable (1.0 by default) and m is the number of actives that match the hypothesis minus one. $W_{E}\Delta E$ represents penalty included for high-energy structures by subtracting a multiple of the relative energy from the final score and penalize hypothesis for which the reference ligand activity is lower than the highest activity, by adding a multiple of the reference ligand activity to the score represented by $W_{act}A$, where A is the activity.

4.3.2.2 Assessment of CPH using Partial Least Square Analysis

A training set of 61 molecules were selected as described earlier incorporating biological and chemical diversity in the data set. This training set was used to generate atom-based QSAR models for all of the generated hypotheses using a grid spacing of 1.0 Å. Models containing six or more partial least squares (PLS) factors tended to fit the pIC_{50} values beyond their experimental uncertainty, therefore only one to five factor models were considered. Each of these models was validated using an external test set of 19 molecules that were not considered during model generation. The CPH with best predictive value and satisfactory statistics (i.e. CPH1) was chosen for alignment of molecules and used for further 3D-QSAR studies.

Pharmacophore models containing three, four and five sites were generated using a terminal box size of 1 Å with 21 highly active molecules, belonging to different chemical classes, using a tree based partition algorithm. The three- and four-featured Common Pharmacophore Hypotheses (CPHs) were rejected, as they were unable to define the complete binding space of the selected molecules. A total of 699 probable five-featured CPHs belonging to 14 types (AAADD, AAADH, AAADR, AAAHR, AAARR,

Table 4.3.2 Summary of PLS analyses results for the best five common pharmacophore hypotheses (CPHs) with survival scores

CPH	Survival Score	SD	r^2_{ncv}	F	RMSE	r^2_{cv}
1	**2.831**	**0.1363**	**0.9926**	**1243.7**	**0.7681**	**0.5925**
2	2.543	0.0796	0.9958	2264.2	0.8325	0.4797
3	2.597	0.1388	0.9872	738.3	0.802	0.5171
4	2.627	0.1308	0.9886	832.8	0.880	0.4186
5	2.543	0.1864	0.9771	383.2	0.8896	0.4085

Bold values indicate the model having the best statistical figures when compared to other developed models. SD: standard deviation of the regression; r^2_{ncv}: r-squared non-cross validated; F: variance ratio; RMSE: root- mean-squared error; r^2_{cv}: r-squared cross validated.

AADDH, AADDR, AADHR, AADRR, AAHRR, ADDHR, ADDRR, ADHRR and DDHRR) were subjected to stringent scoring function analysis with respect to actives using default parameters for site, vector and volume. Reference relative conformational energy (kJ/mol) was included in the score with a weight of 0.01 and ligand activity,

expressed as pIC_{50}, with a weight of 1.0. Hypotheses emerging from this process were subsequently scored with respect to the 17 inactives, using a weight of 1.0. The hypotheses that survived the scoring process were used to build an atom-based QSAR model in PHASE. Training set molecules were aligned on these CPH and analyzed by PLS analysis described in PHASE with 5 PLS components. Over-fitting of results was observed when more than 5 PLS components were analyzed. The predictivity of each hypothesis was analyzed by test set molecules. A summary of statistical data of the best five CPHs, labeled CPH1 to CPH5, with their survival scores is listed in **Table 4.3.2.** More consistent external predictivity was observed for CPH1 for each combination as compared to the others.

4.3.2.3 Superimposition of pharmacophore features on the active site of TACE

Since crystal structure of pTACE is not available in PDB, hTACE (pdb code: 2fv5) was used for performing superimposition studies. The hTACE structure (pdb code: 2fv5, chain B) obtained from Protein Data Bank (PDB, USA) was used for the superimposition of the pharmacophore features because after performing BLAST-2 search [302] with pTACE, it was observed that sequence of human TACE has high degree of homology with that of pTACE (highest identity/BLAST Score). The sequence of the 839 amino acids of the pTACE was retrieved from the Swiss-Port Database [303].

4.3.2.4 Use and validation of the generated pharmacophore model for *in silico* screening

The generated pharmacophore model was used to carry out a search for potential TACE inhibitors of the ASINEX (http://zinc.docking.org/vendor0/asin/index.html asin_p0.0.sdf) database version 2006.3, # in catalog: 372187, made up of 45,533 molecules. Four highly active molecules (**78, 81-83**) and two inactives (**84, 85**) as shown in **Figure 4.3.2** for TACE inhibitory activity were planted from outside in the database. The minimum criteria for retrieval of hits was that all the five out of five pharmacophoric features must match, with default tolerance on matching the pharmacophore features to each of the five inter-feature distances. The molecules were minimized using Ligprep module and a maximum of 100 conformers were generated for each molecule using the ligand torsional search method.

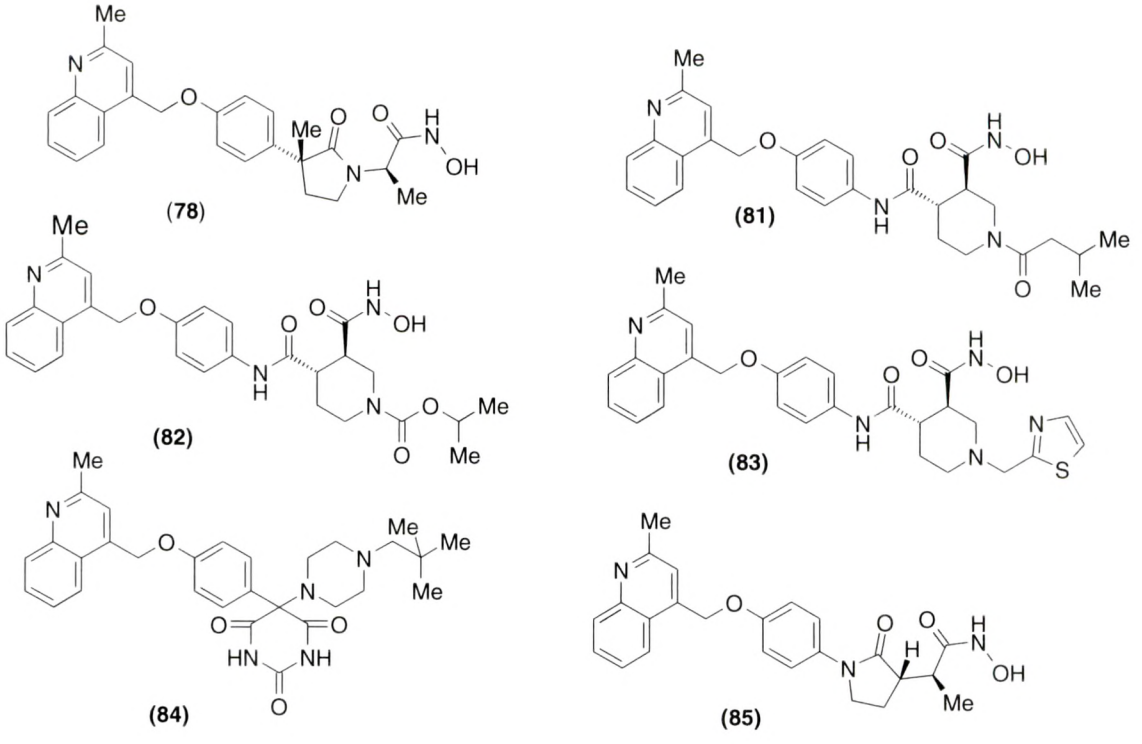

Figure 4.3.2 Chemical structures of four active (**78, 81-83**) and two inactive (**84, 85**) TACE inhibitors used for validation of *in silico* screening method

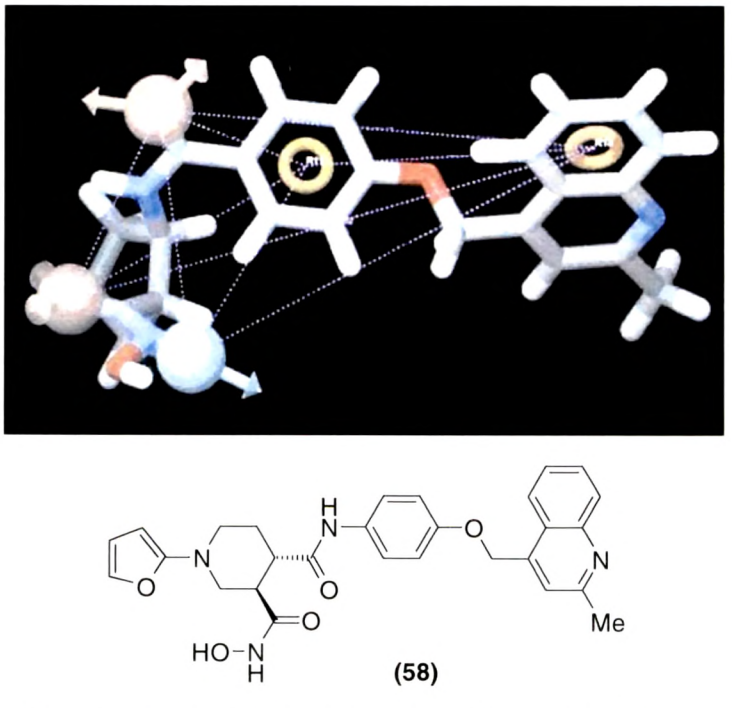

Figure 4.3.3 Mapping of active compound (**58**) on the pharmacophore features (CPH1)

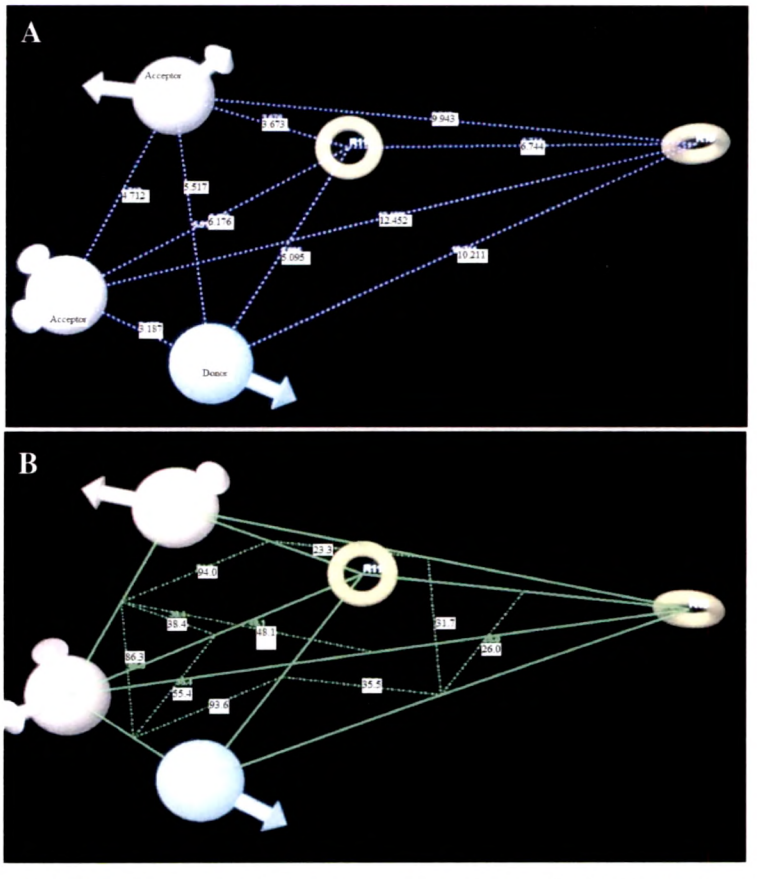

Figure 4.3.4 Geometry of the pharmacophore (CPH1). Red spheres with vectors- acceptor features, orange torus- aromatic ring features, blue sphere- donor features **A**) distances **B**) angles

Out of the five pharmacophore models developed using PHASE, CPH1 showed excellent r^2 value for the training set (0.9926) and good predictive power with r^2_{cv} of 0.5925. Observed and predicted values of the training and test set molecules are given in the **Table 4.3.1**.

The pharmacophore contains two aromatic ring features, one mapping on the central phenyl ring and the other on the phenyl part of the quinoline ring, as shown in **Figure 4.3.3**, two acceptor features, one mapping on the lone pair of oxygen of central carbonyl of the amide group and the other mapping on oxygen of the carbonyl group of the hydroxamate, and one hydrogen donor, NH of the hydroxamate moiety **(Figure 4.3.3)**. The distances and angles among the pharmacophoric features are depicted in **Figure 4.3.4** (**A)** and **(B)** respectively.

As crystal structure of hTACE is available, the superimposition of pharmacophore features on the active site has been carried out to further assess the

compatibility of generated pharmacophore features (two aromatic rings, two acceptors and one donor) with the active site as shown in **Figure 4.3.5**. The first aromatic ring P1'

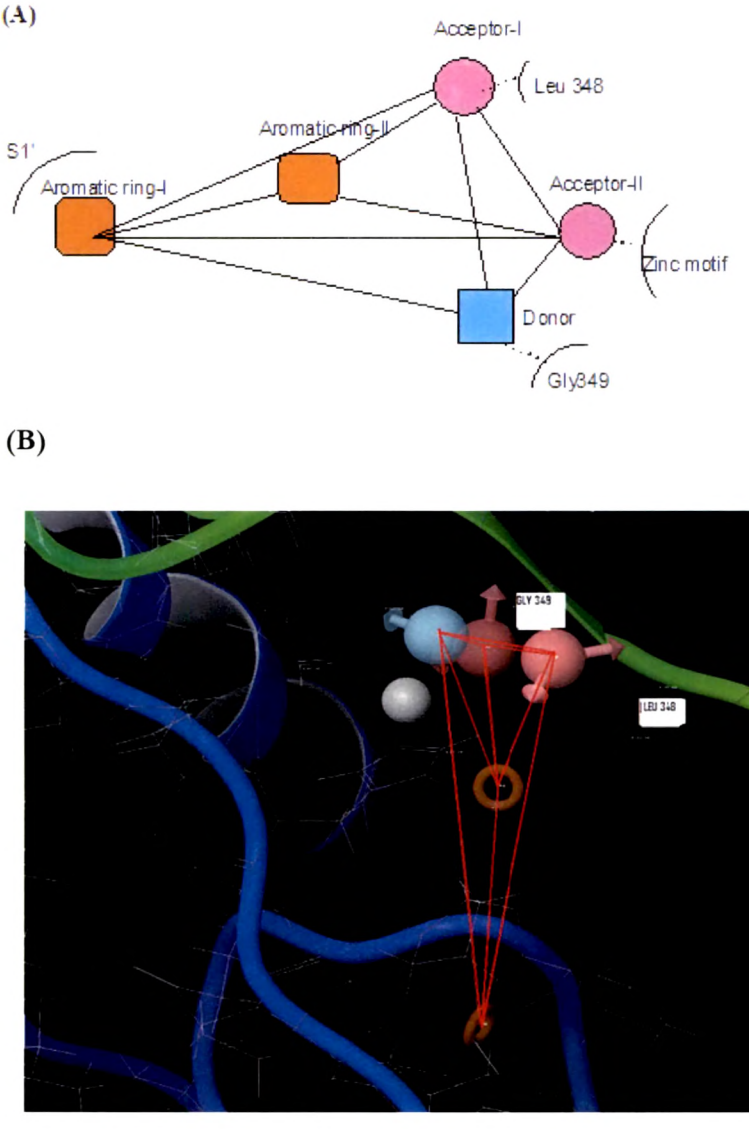

Figure 4.3.5 Mapping of the Pharmacophore features (CPH1) in the active site of TACE. (**A**) 2D Representation of pharmacophoric features interacting with TACE. (**B**) Interaction of Pharmacophoric features with TACE (Chain-B of 2fv5 pdb).

side chain and the third and fourth acceptor and donor features lie in the vicinity of Leu348 and Gly349 residues respectively, confirming further that this acceptor and donor region is important to have a bonding with the NH group of Leu348 and CO of Gly349. The fifth pharmacophore feature i.e. acceptor is aligned towards the zinc motif (**Figure**

4.3.5A, B). Thus, the identified pharmacophore features are in perfect consonance with the active site of hTACE.

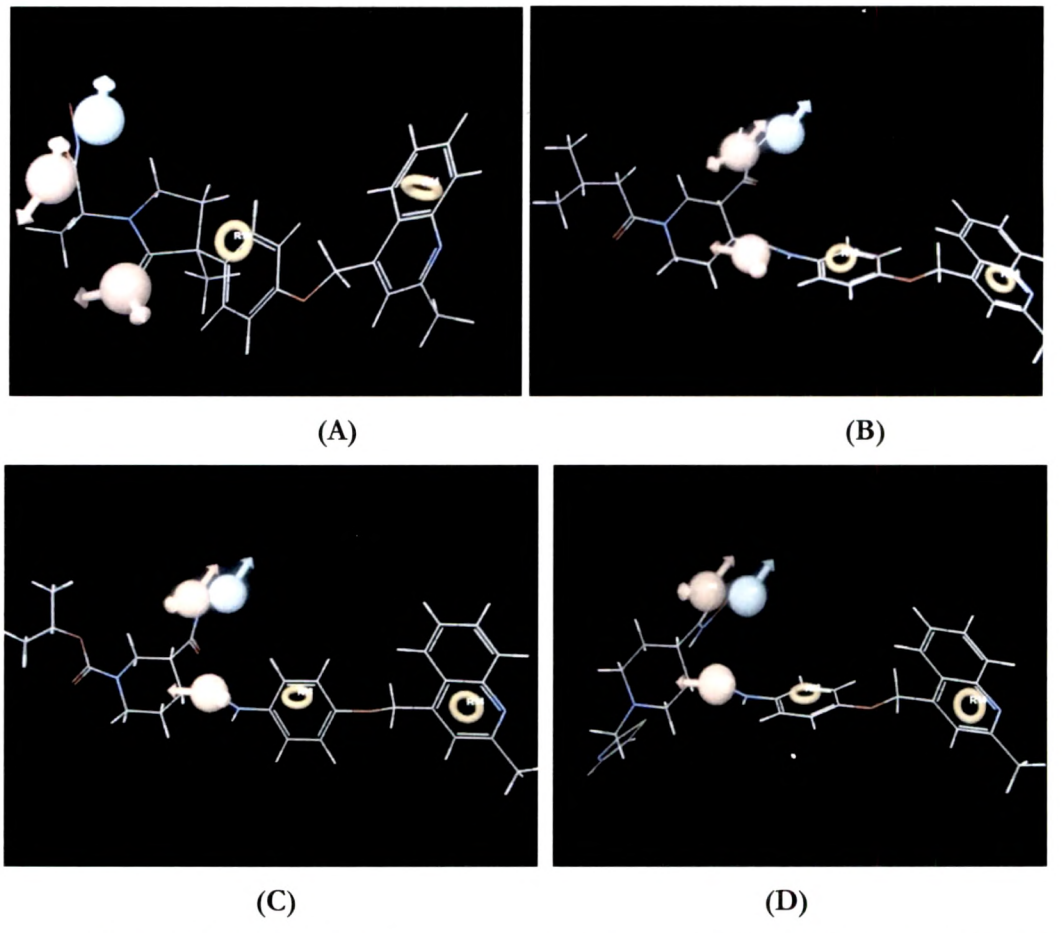

Figure 4.3.6 Mapping of active compounds on CPH1, (**A**) Compound **78**, (**B**) Compound **81**, (**C**) Compound **82**, (**D**) Compound **83**

The developed pharmacophore model (CPH1) was used for *in silico* screening of ASINEX data base for potential compounds possessing TACE inhibitory activity. In order to validate the screening protocol, four active and two inactive molecules were grafted into the data base. The four active molecules **78** (IK682), **81**, **82** and **83** having TACE inhibitory activity and two inactives, **84** and **85** were taken from the literature [240,293,294]. **Figure 4.3.1** shows the chemical structures of these compounds. The *in silico* screening process retrieved 453 positive hits along with the above said four grafted active molecules and filtered out the two grafted inactives. This clearly proved the reliability of the developed pharmacophore model (CPH1). **Figure 4.3.6A-D** shows mapping of all four active compounds on CPH1. For IK682 (**78**), the two acceptors mapped on the two carbonyl groups, one present on pyrrolidine ring and the other as a part of hydroxamate

group (**Figure 4.3.6A**). The two aromatic ring features of the pharmacophore, mapped on the central phenyl ring and on the phenyl part of the quinoline ring. The donor feature mapped on the NH of hydroxamate group. Compound **81** (pIC_{50} = 9.657) reported by Xue *et al.* [294] is a selective and potent TACE inhibitor. One acceptor feature of the pharmacophore mapped on the carbonyl group of anilido group, and the other acceptor on the carbonyl of hydroxamate group. The aromatic ring features mapped on the central phenyl ring and on the pyridine ring of the quinoline moiety (**Figure 4.3.6B**). **Figures 4.3.6C** and **4.3.6D** show the mapping of compound **82** and compound **83** on CPH1. These studies provide confidence in the reliability of the model and the pharmacophore model (CPH1) so developed could be utilized for *in silico* screening of any data base for TACE inhibitory activity.

The hypothesis CPH1 with two hydrogen bond acceptors (A), one donor group (D), and two aromatic rings (R) as pharmacophoric features was further subjected to CoMFA and CoMSIA studies. **Figure 4.3.7** shows the alignment of the molecules under study along with CPH1. Efforts were also made to develop a model based on the alignment employing atom/shape-based RMS fitting and RMSD-based database fitting techniques for the lower energy conformers obtained from MULTUSEARCH option in SYBYL. However, models derived by using alignment based on lower energy conformers resulted into poor statistics hence, are not discussed in detail. CPH1-based alignments were considered for further analysis. CoMFA generated a good internal predictive ability (r^2_{cv} = 0.594), a small standard error of estimation (SEE = 0.213) and having predictive r^2 in acceptable range (predictive r^2 > 0.300). This model was used to explain SAR and to carry out further analysis, and all the values generated at each grid point were calculated as the scalar product of the associated QSAR coefficient and the standard deviation of all values in the corresponding column of the data table (STD*COEFF) plotted as the percentage contributions to QSAR equation. The CoMFA steric and electrostatic contour maps are shown in **Figures 4.3.8** and **4.3.9**, respectively. The green colored regions indicate areas where steric bulk enhances TACE inhibitory activity, while the yellow contours indicate regions where steric bulk is detrimental for biological activity. Blue colored regions show areas where electropositively charged groups enhance TACE inhibitory activity, while red regions represent where electronegatively charged groups improve the activity. The results of PLS analyses from CoMFA studies are summarized in **Table 4.3.3.**

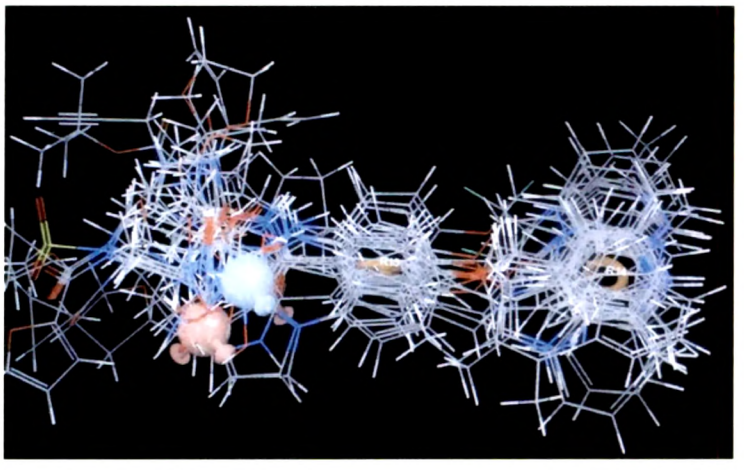

Figure 4.3.7 Common pharmacophore hypothesis 1 (CPH1)-based alignment of TACE inhibitors

The CoMSIA analysis was performed using steric, electrostatic, hydrophobic, hydrogen bond donor and acceptor fields. Results of this study are summarized in **Table 4.3.3**. The CoMSIA models showed good correlation and predictive properties. The CoMSIA model with combination of all the fields yielded a cross-validated r^2 = 0.456 with six components, non-cross-validated r^2 = 0.875, F-value 130.089 [F_{05} (06, 60) = 2.254 (Tab)] and predictive r^2 = 0.421. The contributions of steric, electrostatic, hydrophobic, hydrogen bond donor and acceptor fields of this model were 20.0, 22.6, 18.2, 22.3 and 17.0% respectively. The CoMSIA model with a combination of steric, electrostatic and hydrophobic fields yielded the highest cross-validated r^2 = 0.598 with six components, non-cross-validated r^2 = 0.943, F-value 232.34 [F_{05} (06, 54) = 2.254 (Tab)] but having poor predictive r^2 i.e. 0.312. The steric, electrostatic and hydrophobic field contributions were 29.7, 29.1 and 41.2%, respectively. A combination of steric, electrostatic and hydrogen bond donor fields yielded a CoMSIA model with a crossvalidated r^2 = 0.475 with five components, non-crossvalidated r^2 = 0.912, F-value 123.23 [F_{05} (05, 55) = 2.368 (Tab)] and predictive r^2 = 0.338. The steric, electrostatic and hydrogen bond donor contributions were 29.5, 28.2 and 42.3 %, respectively. CoMSIA model generated with combination of steric, electrostatic, hydrogen bond acceptor and hydrophobic fields yielded a cross-validated r^2 = 0.572 with five components, non-crossvalidated r^2 = 0.974, F-value 341.79 [F_{05}(05, 55) = 2.368 (Tab)] and excellent predictive r^2 = 0.529. The steric, electrostatic and hydrogen bond acceptor and hydrophobic fields of this model were 25.4, 29.2, 20.0 and 25.4%, respectively. The CoMSIA model with this combination (SEAH; **Table 4.3.3**) was considered to be the

best model as it has got the best internal as well as external predictive ability. The models generated by various combinations of CoMSIA fields (**Table 4.3.3**) showed moderate to high, internal and external predictions, in which the hydrogen bond donor fields were observed to be dominant over the hydrophobic fields and hydrogen bond acceptor fields.

Table 4.3.3 Summary of CoMFA and CoMSIA results

	Descriptors	r^2_{cv}	NC	r^2_{ncv}	SEE	F-value	r^2_{pred}	Contribution (Fraction) S	E	A	D	H
CoMFA	SE	**0.594**	**5**	**0.936**	**0.213**	**285.868**	**0.419**	**55.7**	**44.3**	-	-	-
COMSIA	H[a]	0.498	6	0.960	0.241	220.529	0.150	-	-	-	-	-
	D[b]	0.457	3	0.786	0.543	70.981	0.108	-	-	-	-	-
	A[c]	0.213	5	0.829	0.512	56.13	0.173	-	-	-	-	-
	DA	0.402	2	0.713	0.624	73.201	0.168	-	-	44.4	55.6	-
	HD	0.404	5	0.915	0.349	160.053	0.512	-	-	-	51.5	48.5
	HA	0.374	5	0.927	0.320	180.724	0.324	-	-	44.0	-	56.0
	HDA	0.434	2	0.823	0.572	92.976	0.321	-	-	28.3	35.8	35.9
	S[d]ED	0.475	5	0.912	0.412	123.23	0.338	29.5	28.2	-	42.3	-
	HSE[e]	0.598	6	0.943	0.242	232.34	0.312	29.7	29.1	-	-	41.2
	SEA	0.467	5	0.920	0.370	110.798	0.496	35.5	31.3	33.2	-	-
	SEDA	0.545	6	0.975	0.191	356.147	0.354	26.3	27.5	17.0	29.1	-
	SEDAH	0.456	6	0.875	0.422	130.089	0.421	20.0	22.6	17.0	22.3	18.2
	SEAH[f]	**0.572**	**5**	**0.974**	**0.195**	**341.790**	**0.529**	**25.4**	**29.2**	**20.0**	-	**25.4**
	SEDH	0.509	5	0.921	0.336	173.477	0.429	21.0	20.9	-	29.1	29.0

[a]Hydrophobic field, [b]Hydrogen bond donor field, [c]Hydrogen bond acceptor field, [d]Steric field, [e]Electrostatic field, [f]Best model for CoMSIA.

The CoMSIA steric and electrostatic contours (not shown) were positioned similarly to those of the CoMFA model, hence are not discussed. The results of CoMSIA PLS analysis are summarized in **Table 4.3.3**. The CoMSIA model generated from steric and electrostatic fields did not vary both in terms of statistical values and positions of contours, as compared to CoMFA model hence not included in the table. The

hydrophobic contour maps of CoMSIA (STDDEV*COEFF) is displayed in **Figure 4.3.11.**

4.3.3 Graphical Interpretation of 3D CoMFA and CoMSIA models

Additional insight into the structural requirements for TACE inhibitory activity could be gained by visualizing the 3D-QSAR contour maps. This information can then be used to design new more potent analoges. A pictorial representation of the generated contours is given in **Figures 4.3.8–4.3.11. Figures 4.3.8** and **4.3.9** indicate the CoMFA steric and electrostatic contour maps, respectively, using **(i)** compound **58** (most active compound) and **(ii)** compound **72** (least active), as reference structures. In these figures, the green contours represent regions of high steric tolerance (80% contribution), while the yellow contours represent regions of low steric tolerance (20% contribution). Increase in positive charge is favored in blue regions while increase in negative charge is favored in red regions. The steric contour map of CoMFA (**Figure 4.3.8**) shows a green contour enclosing the quinoline ring of the template structure. This indicates that bulky groups here would enhance the TACE inhibitory activity. Good inhibitory potency of **6** (IC_{50} 0.14), **61** (IC_{50} 0.28), **4** (IC_{50} 0.40), **59** (IC_{50} 0.45), **60** (IC_{50} 0.48) and **5** (IC_{50} 0.94) is because of orientation of bulkier groups toward sterically favored green contour. Absence of the bulkier group at this position leads to decrease in the activity, as this could be observed with compounds **72** (IC_{50} 13000), **79** (IC_{50} 2200), **69** (IC_{50} 887), **68** (IC_{50} 111) and **70** (IC_{50} 97) which have got poor TACE inhibitory activity. The steric contour map of CoMFA also shows a large contour enclosing the piperidine ring of the template molecule where more bulky substitutions are expected to increase the activity. High potency of compounds **6** (IC_{50} 0.14), **61** (IC_{50} 0.28), **59** (IC_{50} 0.45), **10** (IC_{50} 1.0) and **62** (IC_{50} 1.60) is because of orientation of bulkier groups toward the sterically favored green contour. The steric contour map also shows yellow contour near quinoline ring. Here, bulky substituents are not tolerated hence compound **47** (IC_{50} 81), **48** (IC_{50} 1110), **29** (IC_{50} 900), **30** (IC_{50} 294), **24** (IC_{50} 170) and **25** (IC_{50} 150) exhibited low inhibitory activity as quinoline ring of these compounds lie in the yellow region. Compound **72** has got the least activity in the series as it occupies the region in the sterically disfavored area which is clearly evident from **Figure 4.3.9b.**

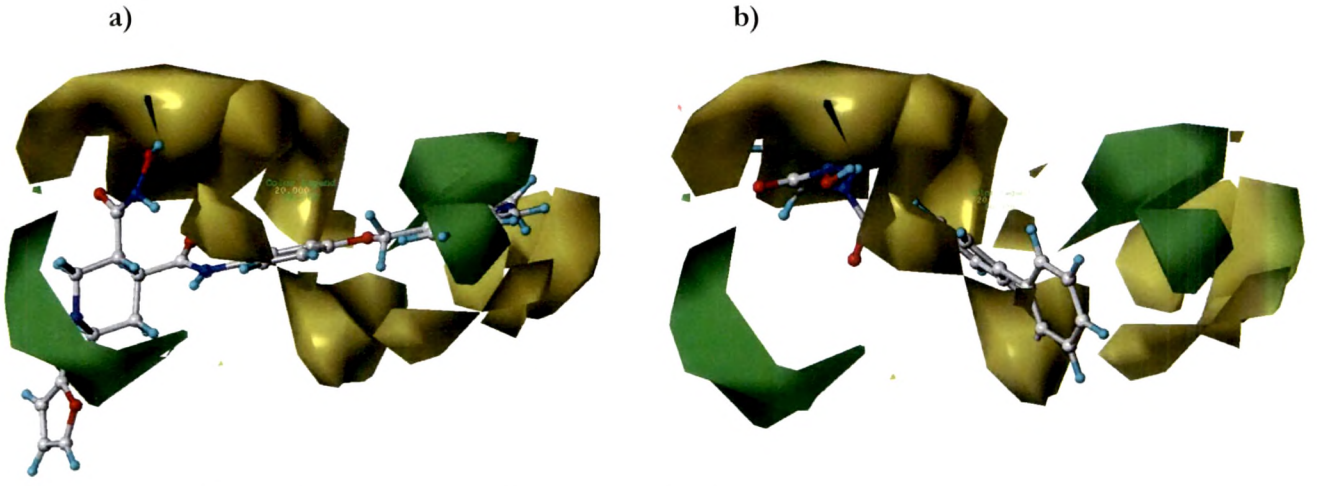

Figure 4.3.8 The CoMFA steric STDEV*COEFF contour plots of (**a**) active compound **58** and (**b**) inactive compound **72**. Sterically favored areas (contribution level 80%) are represented by green polyhedra. Sterically disfavored areas (contribution level 20%) are represented by yellow polyhedra.

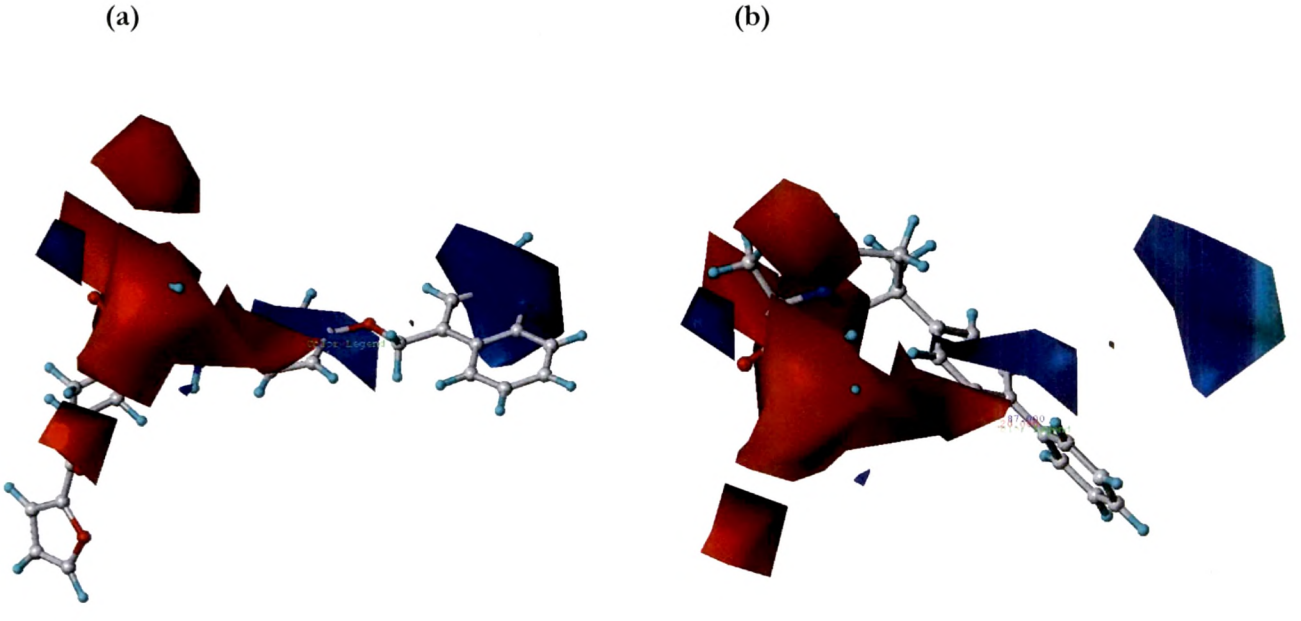

Figure 4.3.9 The CoMFA electrostatic STDEV*COEFF contour plots of (**a**) active compound **58** and (**b**) inactive compound **72**. Positively charged favored areas (contribution level 80%) are represented by blue polyhedron. Negatively charged favored areas (contribution level 20%) are represented by red polyhedra.

The electrostatic contours of CoMFA (**Figure 4.3.9a**) are clearly distributed in three regions i.e. quinoline region, central phenyl ring favoring electropositive substituent groups and red contour surrounding the piperidine ring towards the hydroxamate group of the template molecule where high electron density is expected to increase the activity.

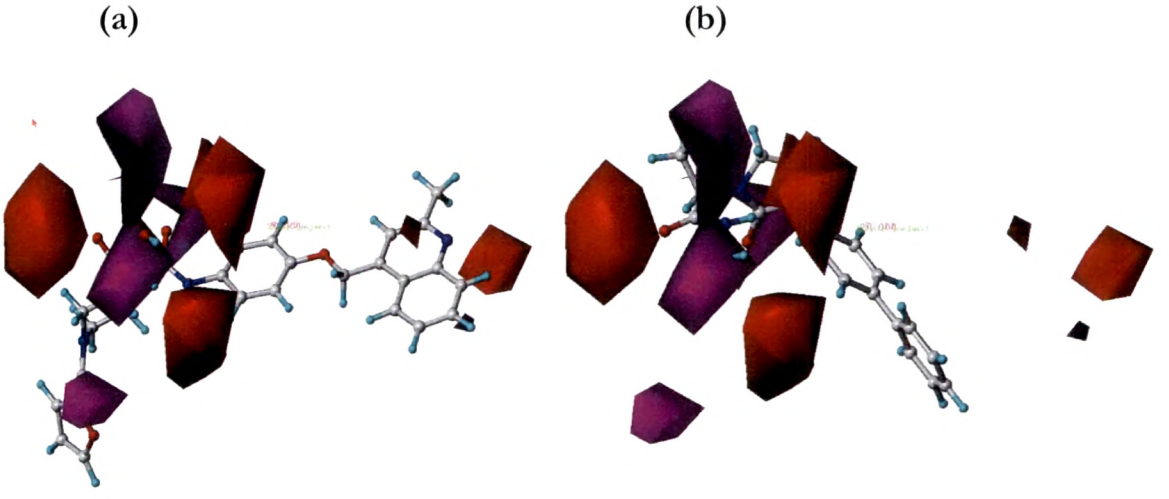

Figure 4.3.10 The CoMSIA hydrogen bond acceptor fields of (**a**) active compound **58** and (**b**) inactive compound **72**. Magenta polyhedra indicate regions where hydrogen bond acceptor substituents are favored and red polyhedra indicate disfavored regions.

The CoMSIA hydrogen bond acceptor fields (magenta polyhedral) (**Figure 4.3.10**) indicate regions where hydrogen bond acceptor substituents are favored and red polyhedra indicate disfavored regions. The magenta polyhedron, indicating hydrogen bond acceptor favorable region, is present in the surrounding of piperidine ring where carbonyl groups attached to 1, 3 or 4 positions act as hydrogen bond acceptors. Thus, hydrogen acceptor atom (an electronegative atom such as fluorine, oxygen or nitrogen is a hydrogen bond acceptor) substituted at 1, 3 or 4 positions of piperidine ring may enhance the TACE inhibitory activity. As for as compound **72** is concerned, the hydrogen bond acceptor group i.e. carbonyl group is projected towards the disfavored region (red polyhedra) (**Figure 4.3.10b)** leading to decrease in its activity.

The CoMSIA hydrophobic fields (yellow polyhedra) **(Figure 4.3.11)** indicate regions where hydrophobic substituents are favored and white polyhedra indicate disfavored regions. A white disfavored hydrophobic contour (**Figure 4.3.11**) is observed in the vicinity of hydroxamate group where hydrophobic substituents are detrimental for TACE inhibitory activity. The hydrophobic contour map (**Figure 4.3.11**) shows presence of a yellow contour surrounding the quinoline ring indicating that more hydrophobic substituent in this region may improve the biological activity. In **Figure 4.3.11a**, the quinoline ring present in compound **58** lies in the favored region whereas in **Figure 4.3.11b**, biphenyl ring present in compound **72** is not oriented towards the favored region which could be a probable reason for the difference in the activity of these two compounds.

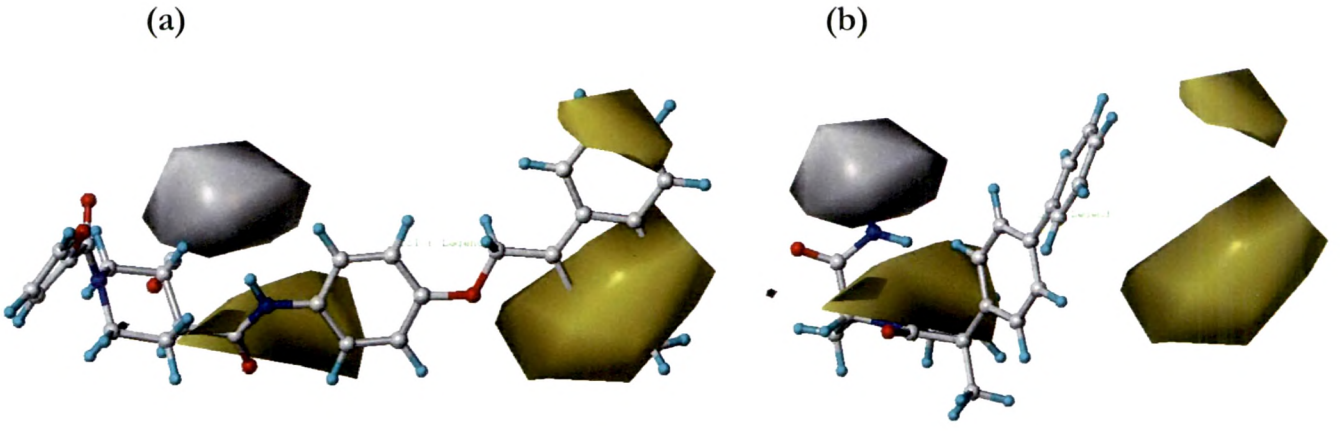

Figure 4.3.11 The CoMSIA hydrophobic fields of (**a**) active compounds **58** and (**b**) inactive compound **72**. Yellow polyhedra indicate regions where hydrophobic substituents are favored and white polyhedra indicate disfavored regions.

4.3.4 3D Database Screening

In order to discover unknown biological activities of existing compounds in corporate or public databases and subsequently to identify new structures for TACE inhibitory activity, **ASINEX** database made up of 45,533 molecules, was screened with the CPH1 hypothesis. To be retrieved as a hit, a database compound must possess appropriate functional groups, which can simultaneously reside within the respective tolerance spheres of pharmacophore features. Each feature is associated with a weight. Better the overall superimposition of functional groups of the molecule to the appropriate feature of the pharmacophore better the score of the fit. The *in silico* screening process retrieved 453 positive hits along with the above said four grafted active molecules and filtered out the two grafted inactives.

4.3.4.1 Docking of the hits in the active site of hTACE

All the positive hits which were retrived during *in silico* processing except the active compounds (**78, 81-83**), were further docked in the active site of hTACE. Based on their docking scores (G-score) these compounds were prioritized and the first fifty ranked compounds were selected for further processing.

4.3.4.2 Decreasing the Number of Hits using Lipinski's rule of five

In order to decrease the number of hits provided by 3D database query of CPH1 and hTACE docking, Lipinski's rule of five was applied. Lipinski's rule is used to indicate whether a molecule is likely to be orally bioavailable (bioactive). The "rule of five" is so

called because most of the features start with the number five. In general, an orally active drug has:

- Not more than 5 hydrogen bond donors
- Not more than 10 hydrogen bond acceptors
- A molecular weight under 500
- A logP under 5

First fifty compounds having Glide score in decreasing order were further screened on the basis of rule of five and only those compounds following this rule were further selected. The selected top twenty one hits are shown in **Table 4.3.2.1**. The best

Table 4.3.2.1 List of best hits as an output of virtual screening

Comp	Structure	G-Score	M. Wt.	CLogP	A	D	Rel. TPSA	*TPSA
1.	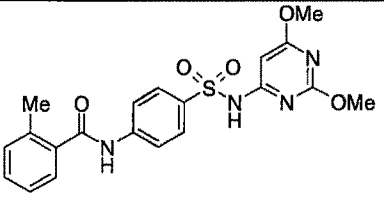	-10.44	428.47	3.700	7	2	5.12	255.79
2.	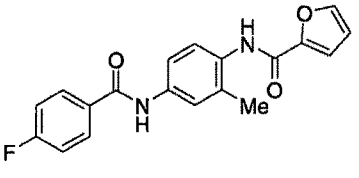	-10.33	338.34	3.770	3	2	1.78	71.34
3.	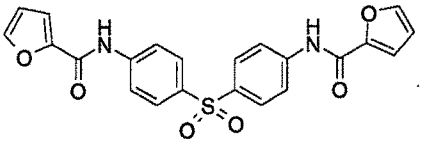	-10.24	436.45	4.830	4	2	5.42	254.90
4.	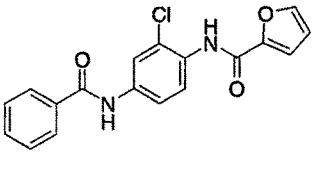	-10.14	340.77	3.970	2	2	1.93	71.34
5.	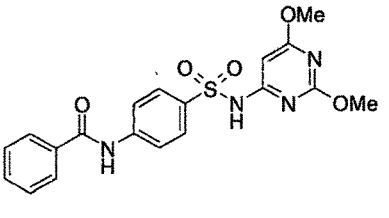	-10.14	414.44	3.400	7	2	5.44	255.79

6.	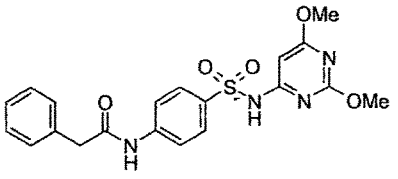	-10.10	428.47	3.560	7	2	5.12	255.79
7.	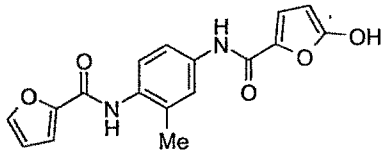	-10.00	326.31	2.930	3	3	2.76	104.71
8.	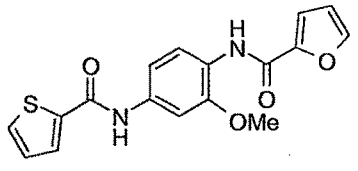	-10.00	342.38	3.390	3	2	2.86	108.81
9.	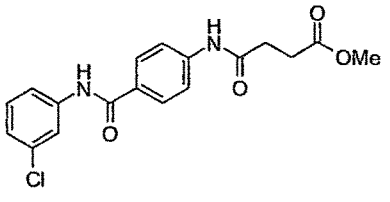	-9.84	360.80	3.250	3	2	2.01	84.50
10.	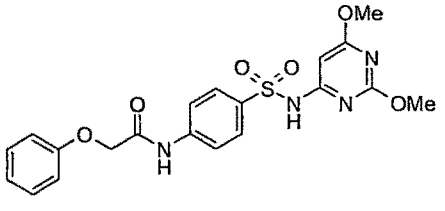	-9.81	444.47	3.390	8	2	5.20	265.02
11.	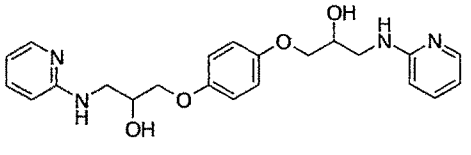	-9.81	410.48	2.180	6	4	1.94	108.76
12.	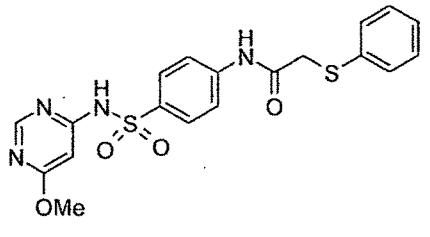	-9.79	430.51	2.090	7	2	2.56	135.58
13.	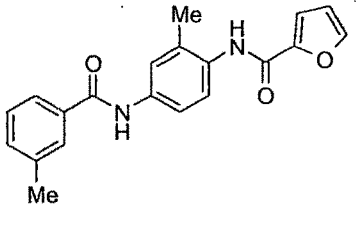	-9.74	334.38	3.940	2	2	1.66	71.34

14.	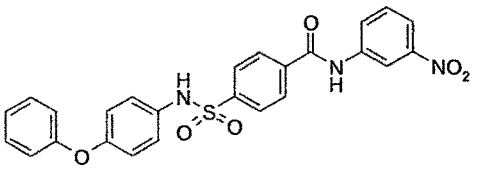	-9.59	489.51	6.150	5	2	5.39	291.32
15.	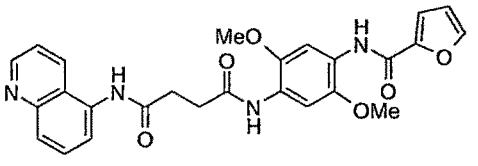	-9.57	488.50	3.730	7	3	2.00	127.88
16.	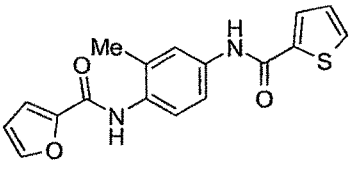	-9.57	326.38	3.690	2	2	2.69	99.58
17.	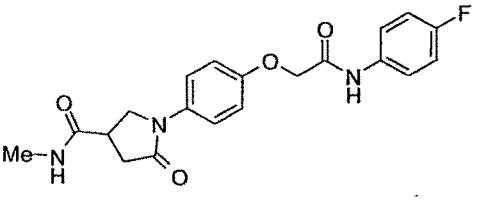	-9.38	385.40	1.940	5	2	1.83	87.74
18.	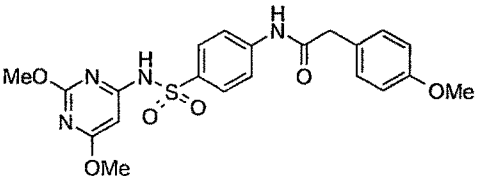	-9.33	458.50	3.570	8	2	4.91	265.02
19.	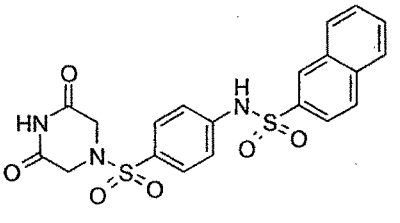	-9.30	459.50	3.450	6	2	8.38	402.28
20.	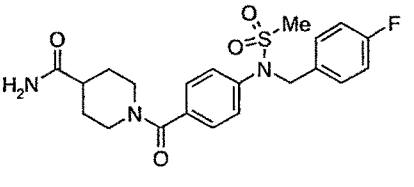	-9.27	433.51	2.690	5	1	4.39	237.06
21.	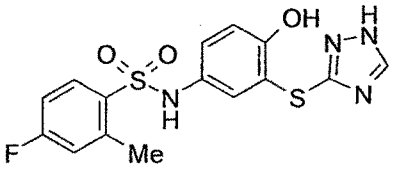	-9.27	380.42	3.990	7	3	7.43	282.44

*Total polar surface area

feature of these compounds is that none of them have hydroxamate as a zinc binding ligand. This is highly desirable as hydroxamate group generates some toxic metabolites in

the body during metabolism [295]. Further processing/development of these compounds is in progress in the laboratory.

4.4 Molecular Modeling Studies of Novel 2-Imidazolidinones and Tetrahydropyrimidin-2(1*H*)-ones as Potential TACE Inhibitors

It became evident from the survey of literature that γ-lactamhydroxamates (I) are the most potent and selective TACE inhibitors. Two compounds of the series namely, IK-682 and BMS-561392 have shown high binding for TACE in molecular modeling studies. These compounds have also shown high selectivity for TACE over a number of MMPs[240,304].

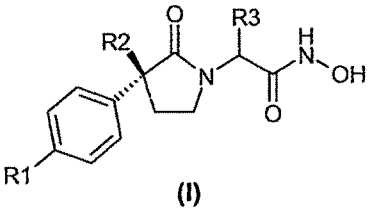

(I)

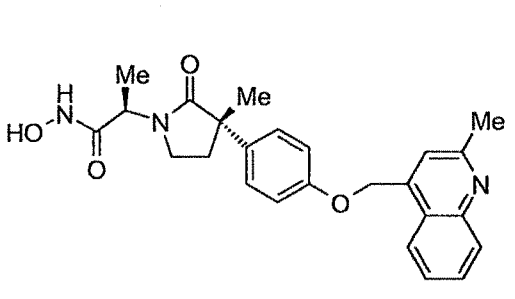

IK-682

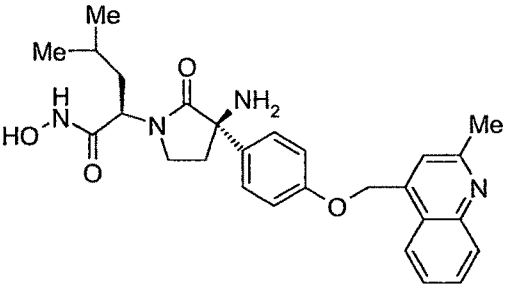

BMS-561392

In order to identify the structural requirements for γ-lactamhydroxamates as selective TACE inhibitors, molecular modeling studies have been performed. These studies revealed four binding grouping in this series of compounds [241]

- The aromatic moiety occupies the S1' site of the enzyme. The choice of aromatic moiety is of prime importance as this not only is responsible for the selectivity over MMPs but can also be modified suitably so that the compound can be active *in vivo*,
- The oxygen atom of the pyrrolidinone ring forms a hydrogen bond with Leu348 and Gly349,
- The methyl group of IK-682 and the isobutyl group of BMS-561392 occupy the small hydrophobic pocket known as S2' and

- The hydroxamic acid forms a stable five membered ring with the zinc atom, present in the catalytic site of the enzyme.

Taking the above discribed four TACE binding groups of γ-lactamhydroxamates into consideration, it was thought logical to replace the asymmetric carbon of γ-lactam with achiral nitrogen to offer imidazolidinone ring structure in the designed compounds (**II; n = 1**). This change would not only remove the asymmetric environment but would also change the overall electron density in the ring. For the aryl group it was thought of having substituted phenyl (**III**), substituted phenyl ether/thioether (**IV**), 1,3,4-thiadiazole (**V**) or 1,3-thiazole rings (**VI**).

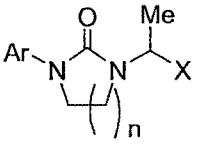

(II)

n = 1, 2

X = -CONHOH
-COOH
$-CH_2SH$

Ar

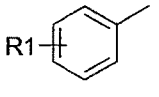

(III)

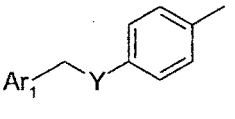

(IV)

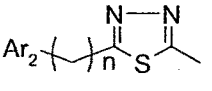

(V)

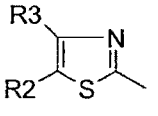

(VI)

It is known that S1' site of TACE is larger than that of MMPs and this fact has been exploited in designing of selective TACE inhibitors [239,240,305,306]. It was planned to incorporate large aromatic moieties for the group 'Ar' to increase selectivity for TACE over MMPs. The aim of this study was to find new selective TACE inhibitors.

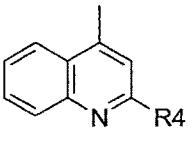

(VII)

During the development of IK-682 and BMS-561392 it was observed that inclusion of 4-quinolinyl group for the substituent 'Ar_1' not only enhanced selectivity of the compounds for TACE but also improved their potency. Hence some of the

compounds were designed to have 4-quinolinyl group **(VII)** for the 'Ar_1' grouping. The R_4 group was incorporated in the quinolinyl moiety to observe the effect of bulk size in this position.

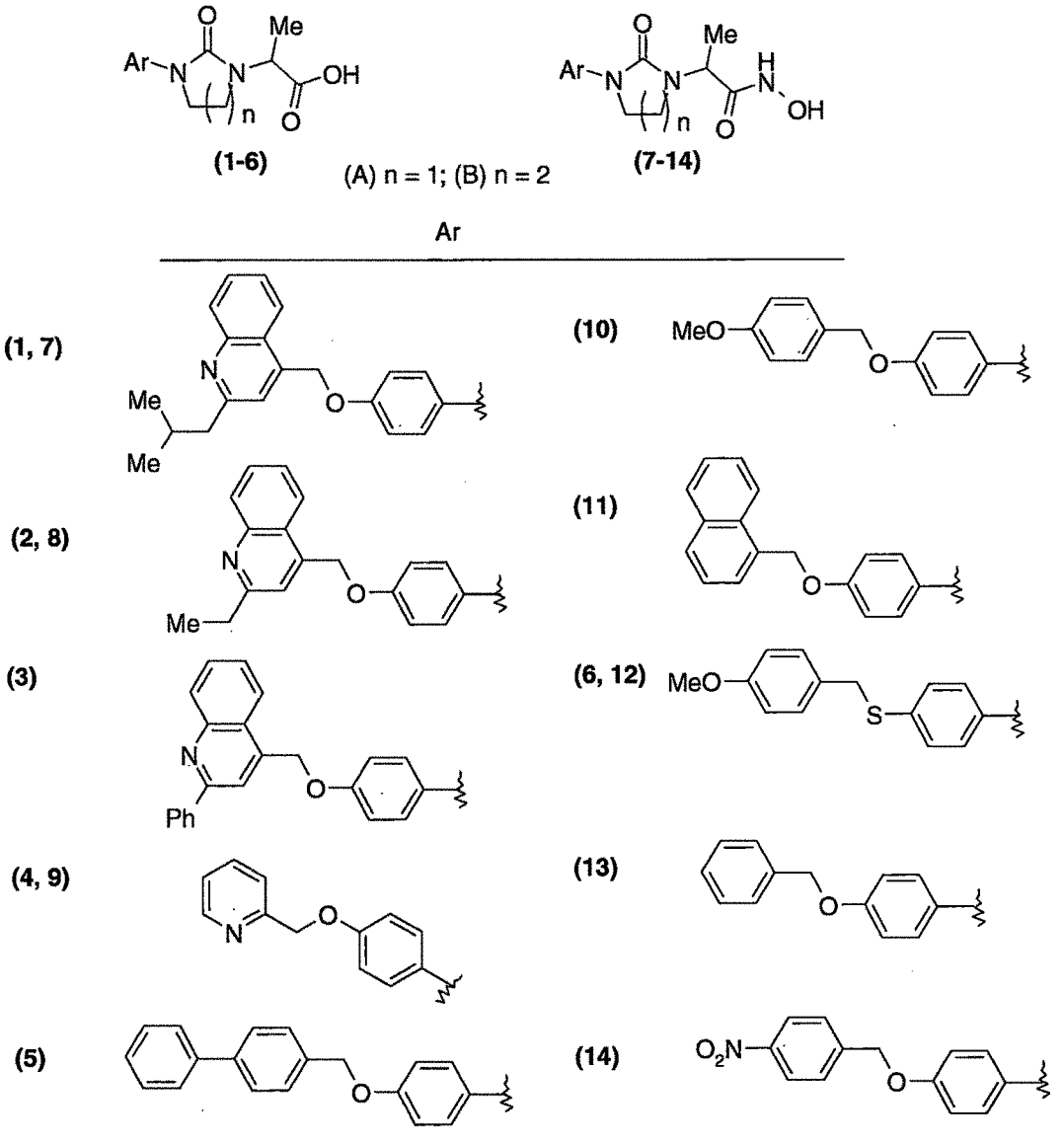

Figure 4.4.1 Compounds used for modeling study

In order to see the effect of ring size, six-membered ring **(II; n = 2)** was also incorporated in place of five-membered imidazolidinone ring. For binding to the S2' site of TACE, methyl group of IK-682 was retained in the designed compounds. A zinc binding motif was required in the designed molecules as group 'X'. The most effective zinc binding motif known till date is hydroxamate. Hence, it was envisaged to incorporate

hydroxamic acid in the designed molecules. In some of the compounds hydroxamic acid was replaced with thiol as thiol is also a strong ligand for zinc ions and hydroxamates have reports of poor bioavailability of the molecules. Hydroxamates have also been reported to pose toxicity problems due to their conversion to toxic hydroxylamine [295]. Thiol grouping can offer an additional advantage of higher selectivity for the enzyme, TACE [307, 308]. Although carboxylate is not that good a ligand for zinc ions but due to its non-controversial nature it was thought of retaining this grouping in some of the molecules.

It was envisaged to carry out the molecular modeling studies of the designed compounds. The structures of the designed compounds are shown in **Figure 4.4.1.** All the designed compounds were energy minimized and docked in the active site of human TACE. Binding interactions of only a few of them are discussed here. Docking study was carried out for both the isomers. Binding score differences between *R* and *S* isomers were found to be marginal for majority of the docked compounds. However, most of the compounds having *R*-configuration showed better G-score than *S*-isomers (**Table 4.4.1**).

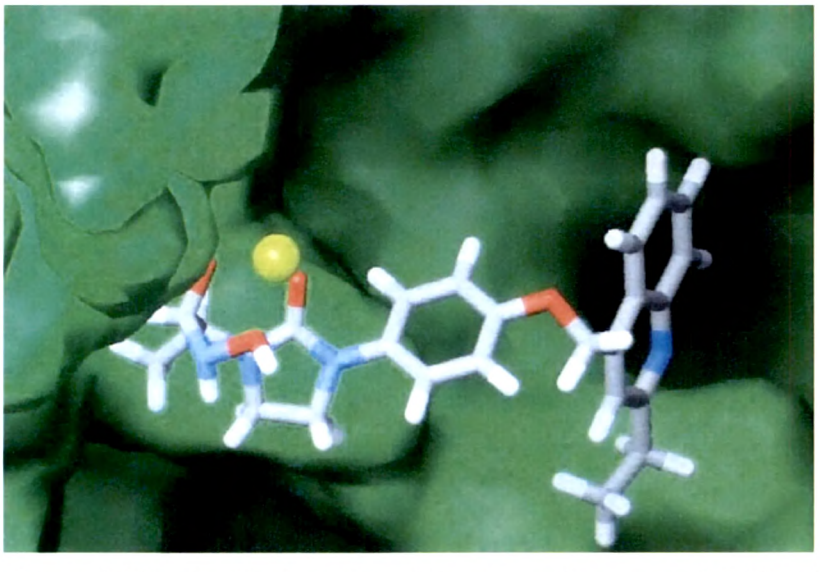

Figure 4.4.2 Positioning of the P1' group of compound (ball and stick) 2-{3-[4-(2-ethyl-4-quinolinylmethoxy)phenyl]-2-oxo-1-imidazolidinyl}-N-hydroxy propionamide (**8A**) in the active site of TACE.

In compound IK-682, *R* isomer is also the active form. Compound **9A** is the highest ranked compound with *R*-isomer, whereas compound **8A** with *S*-isomer showed higher binding score (G-score: -12.51) (**Table 4.4.1**). During the modeling studies it was observed that the conformation of methyl group in the side chain in the molecules of

both the series changes as the aryl/heteroaryl substituents are varied. The binding interaction of 2-{3-[4-(2-ethyl-4-quinolinylmethoxy)phenyl]-2-oxo-1-imidazolidinyl}-N-hydroxypropionamide **8A**, 62% TACE inhibitory activity) was studied within the TACE binding site by docking studies. P1' group of **8A** (2-ethyl-4-quinolinyl)methoxy is oriented toward larger S1' pocket of the TACE (**Figure 4.4.2**) interacting with active site (Glu398, Leu348, Leu350, Ala439, Val440, Lys432 and Leu401). Central phenyl ring interacts with His405 and Tyr436 as shown in **Figure 4.4.3A**. Catalytic zinc bonds with oxygen of NHOH group along with carbonyl group of imidazolidine ring. Glu406 and Leu348 residues interact with methylene group of imidazolidine ring. Carbonyl group of CONHOH bonds with the His405 and Leu350. This interaction study clearly reveals that compound **8A** interacts perfectly with the catalytic active site and also P1' group orients toward S1' pocket giving excellent TACE inhibitory activity along with best docking score (**G-score: -12.51**) (**Table 4.4. 1**).

Table 4.4.1 G-Score of designed compounds and experimentally determined % Inhibition of TACE by the compounds

Compound	G-Score		% Inhibition
	***R*-isomer**	***S*-Isomer**	**at 0.1 μM/L**
1A	-7.75	-7.79	47
1B	-8.98	-7.67	20
2A	-8.48	-8.13	49
3A	-6.67	-6.83	30
3B	-5.43	-5.72	31
4A	-7.08	-7.08	28
4B	-8.53	-8.52	35
5A	-7.84	-7.52	30
5B	-7.25	-7.41	28
6A	-7.36	-9.97	40
7A	-10.01	-8.35	60
8A	-10.83	-12.51	62
8B	-7.56	-9.54	34
9A	-12.65	-11.85	50
9B	-10.47	-8.28	37
10A	-11.10	-12.31	38
10B	-8.76	-8.27	18
11A	-8.64	-7.99	36
11B	-11.13	-8.82	40
12A	-9.29	-9.97	42
13A	-9.49	-9.26	39
13B	-10.35	-8.42	28
14A	-12.04	-9.32	40
TAPI	-8.89		28
IK 682	-9.39		-

Binding mode of N-hydroxy-2-{2-oxo-3-[4-(2-pyridinylmethoxy)phenyl]-1-imidazolidinyl}propionamide (**9A**, 50% TACE inhibitory activity) was also examined (**Figure 4.4.3b**). Leu401, Lys432 and Tyr433 residues interact with pyridinylmethoxy as shown in **Figure 4.4.3b**. Central phenyl ring interacts with Leu348 and Val402 residues.

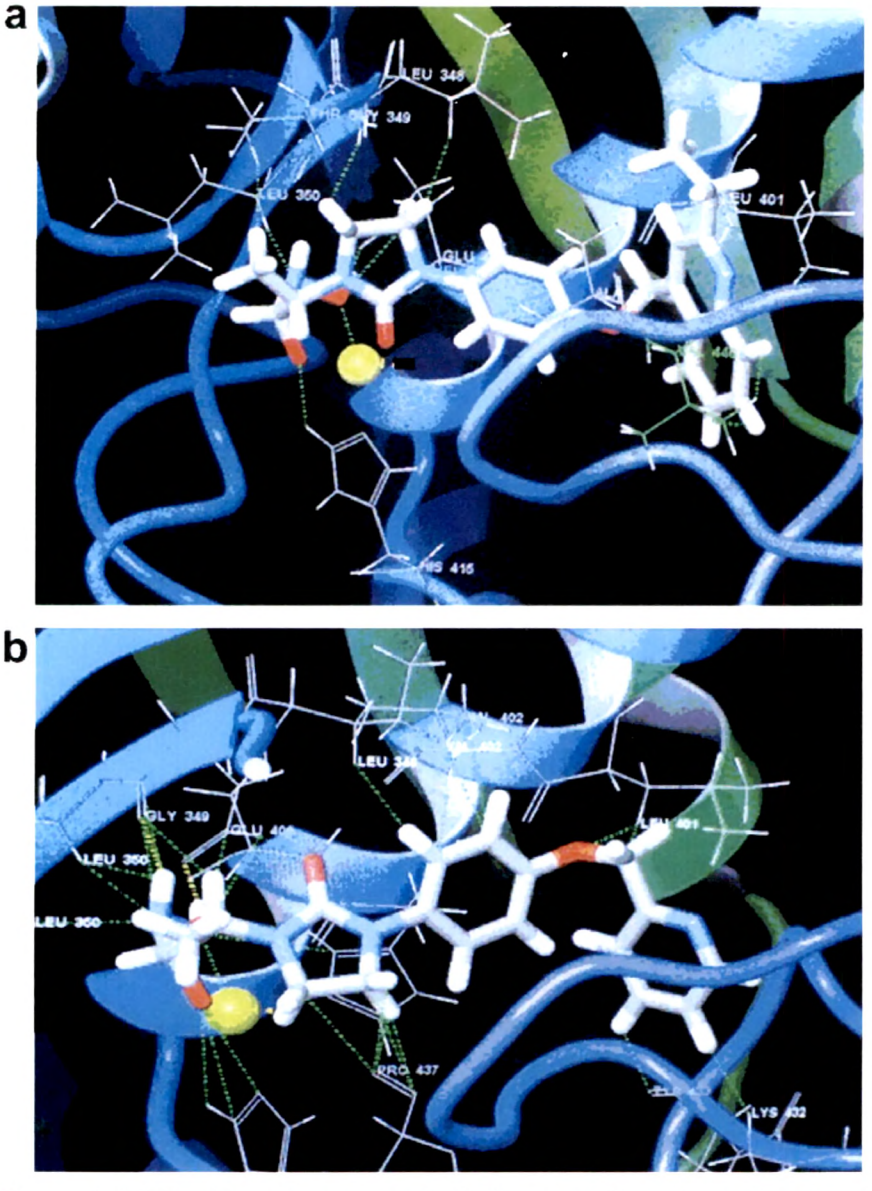

Figure 4.4.3 Docking of compounds (ball and stick) in the active site of TACE (**a**) 2-{3-[4-(2-ethyl-4-quinolinylmethoxy)phenyl]-2-oxo-1-imidazolidinyl}-N-hydroxy- propionamide (**8A**) and (**b**) N-hydroxy-2-{2-oxo-3-[4-(2-pyridinylmethoxy) phenyl]-1-imidazolidinyl}propionamide(**9A**). Interactions are shown as dashed lines and zinc is shown in yellow color.

Imidazolidine ring is engaged with Glu406 residue through interaction with oxygen of carbonyl group and both the methylene groups interact with Pro437 residue. Oxygen of the NHOH group interacts with His405 and Glu406 residues along with the zinc.

Nitrogen of NHOH is engaged with His415, Gly349 and Leu350 residues as shown in **Figure 4.4.3b**. Thus, compound **9A** interacts with all the amino acid residues which are part of the active site such as Zn, Glu406, Leu350, Gly439, His405, His415, Leu348 and Lys432. This might be a reason for showing good inhibitory activity and having highest ranked Glide score (-12.65) (**Table 4.4.1**).

From the interaction study of compound (**4A**) (**Figure 4.4.4**), it is observed that the carboxylate end of the compound interacts with TACE almost in a similar manner as the hydroxamate group of compounds (**8A, 9A**). But the P1' group of the molecule interacts with Leu401 only. No other part of the compound interacts with the active site residues of S1' site of TACE, unlike compounds (**8A, 9A**). Moreover, the orientation of P1' group of (**4A**) is not aligned toward the S1' pocket of the enzyme (**Figure 4.4.4**). This might explain the poor docking score as well as biological activity of compound (**4A**). This proves that the orientation of the P1' group is one of the most important factors for the biological activity of TACE inhibitors, particularly in imidazolidin-2-one and tetrahydropyrimidin-2(1*H*)-one scaffold-containing compounds.

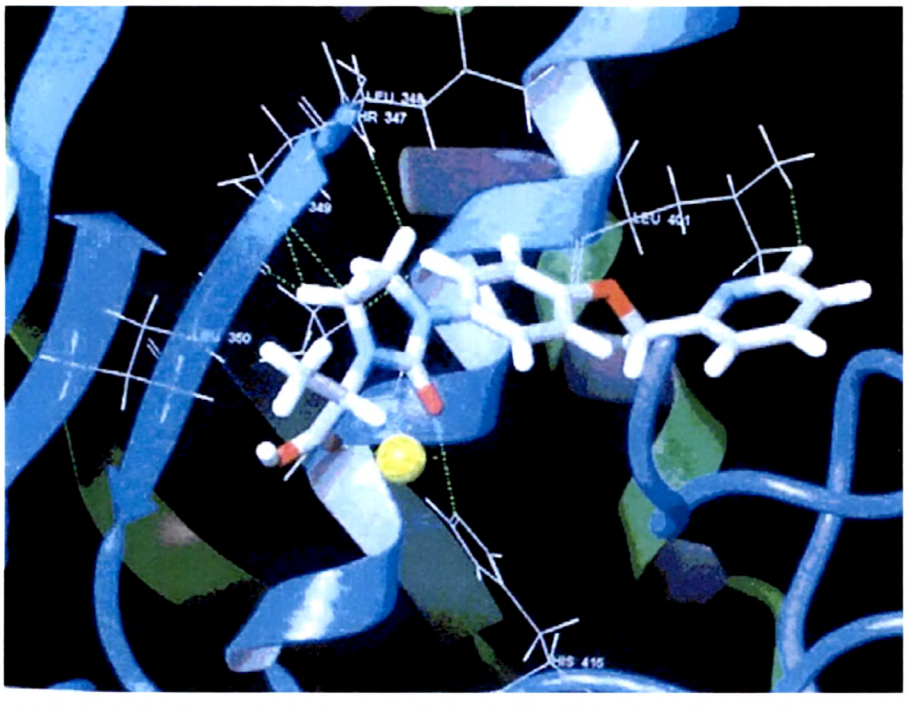

Figure 4.4.4 Docking of compound **4A** (ball and stick) in the active site of TACE.

The designed compounds (**1-14**) were synthesized in the laboratory by other researchers followed by *in vitro* biological evaluation for the binding affinity for TACE

enzyme. Since it was a preliminary work, no efforts were made to prepare optically pure isomers. All the synthesized compounds were recemic mixtures and they were evaluated biologically as such. Broadly, a good match was observed between the G-scores and % inhibition of the TACE inhibitory activity (**Table 4.4.1**). This work proves that these two classes of molecules could be used as potential leads for further development of newer TACE inhibitors.

4.5 Molecular Modeling Studies of Some New Heterocyclic Inhibitors of TACE

Researchers from BMS have reported a series of orally bioavailable β-benzamidohydroxamates amongst which BMS-566394 demonstrated exceptionally high potency for the suppression of LPS induced TNF-α in human whole blood, with high selectivity over MMP's and ADAM proteases. While the hydroxamic acid part of these molecules attached to the central phenyl ring was considered to be responsible for inter-

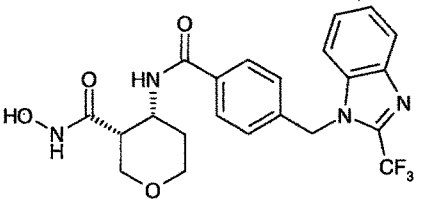

BMS-566394

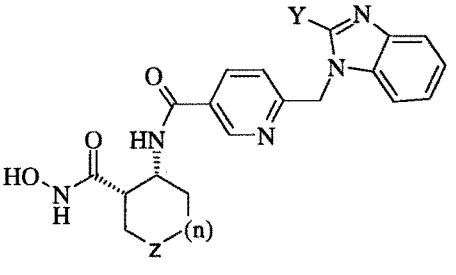

(1) Y = CH_3, Z = O, n = 1
(2) Y = CF_3, Z = O, n = 1
(3) Y = CH_3, Z = CH_2, n = 1
(4) Y = CF_3, Z = CH_2, n = 1
(5) Y = CH_3, Z = CH_2, n = 0
(6) Y = CF_3, Z = CH_2, n = 0

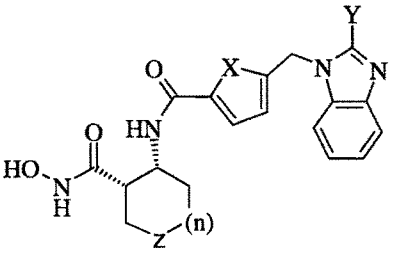

(7) X = S, Y = CH_3, Z =O, n = 1
(8) X = S, Y = CF_3, Z = O, n = 1
(9) X = S, Y = CH_3, Z = CH_2, n = 0
(10) X = S, Y = CF_3, Z = CH_2, n = 0
(11) X = O, Y = CH_3, Z = CH_2, n = 0
(12) X = O, Y = CF_3, Z = CH_2, n = 0
(13) X = S, Y = CH_3, Z = CH_2, n = 1
(14) X = O, Y = CH_3, Z = CH_2, n = 1

action with the zinc binding site of TACE, the group in the para position of the central phenyl ring imparted selectivity as well as cellular potency. It appeared that the central phenyl ring remained dormant and did not contribute to any binding interaction with the

active site of TACE [309, 310]. Considering it to be a benign component of the molecule for the purpose of molecular modifications of BMS-566394, it was thought logical by one of our collaborating groups to replace the central phenyl ring hitherto with 5/6-membered heterocyclic rings. This modification was expected to improve the overall pharmacokinetic profile of the molecule without compromising the binding affinity to the enzyme. Hence, it was thought to design compounds wherein the central phenyl ring was replaced with pyridine, thiophene and furan rings.

Compounds (**1-14**) were synthesized by one of our collaborating groups and the prepared compounds were evaluated in whole blood assay for inhibition of TACE enzyme activity (**Table 4.5.1**). The outcome of the study was quite surprising. Substitution of phenyl with pyridyl group afforded potent compounds (**1-6**) while its substitution with five-membered heterocyclic rings like thiophenyl or furyl afforded almost inactive derivatives (**7-14**).

An alteration in the presumed dormant central ring system of the molecule leading to significant changes in the inhibitory activity was quite unexpected. We therefore undertook molecular modeling studies on the designed compounds (**1-14**) so as to gather insight into their binding affinity. The IC_{50} values of the potent compounds and their corresponding Glide scores are summarized in **Table 4.5.1.**

The molecular modeling studies reported herein have been performed on a Silicon Graphics Fuel Workstation running on the IRIX 6.5 operating system using SYBYL 7.0 molecular modeling software from Tripos, Inc., USA [311] and GLIDE from Schrödinger Inc., USA [102,103] All compounds used for docking studies were built using the 'Sketch Molecule' function within SYBYL. Initial optimization of the structures was carried out using TRIPOS force fields with Gasteiger–Huckel charges and repeated minimization was performed using steepest descent and conjugated gradient methods till the root mean square deviation (RMSD) of 0.001 kcal/mol Å was achieved. Conformational energies were computed with electrostatic terms; the lowest energy structures finally minimized were used subsequently for docking. The crystal structure of human TACE (pdb code: 1ZXC) obtained from the Protein Data Bank (USA) was refined to remove water molecules. The bond orders and formal charges of the ligands were adjusted prior to docking. Docking was performed using GLIDE software according to the previously reported protocol [102,312].

The compounds were energy minimized and docked in the active site of human TACE. The docking score (G-score) for the designed compounds is shown in **Table 4.5.1.** Since compound **5** shows the highest binding score (G score -6.51) and is the most active compound in the series, the binding interactions of compound **5** were extensively studied within the binding site of the enzyme (**Figure 4.5.1**). The docking study for compound **5** suggested that the P1' group of compound **5** (i.e. 2-methylbenzoimidazol-1-ylmethyl) is oriented towards the larger S1' pocket of TACE (**Figure 4.5.2**) and it interacts with the active site residues (Gly346, Ala349, Tyr390, Ile438 and Thr347).

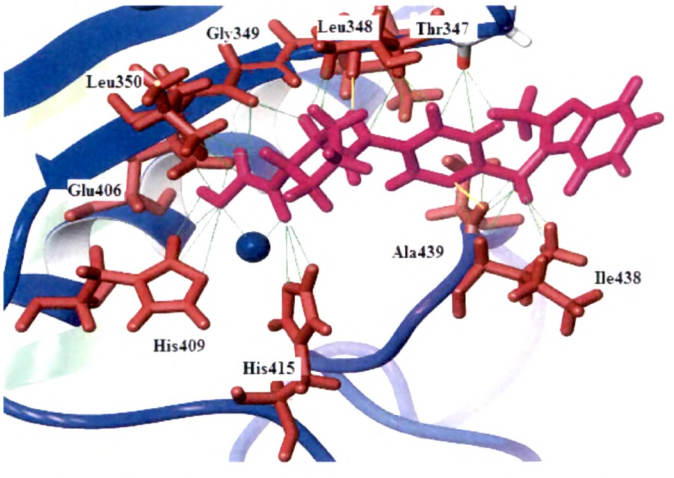

Figure 4.5.1: Docking of compound **5** (shown in violet color) in the active site of TACE. Interactions are shown in green lines, zinc is shown in blue color and active site residues are shown in brown color (for the sake of clarity only important amino acid residues are given).

Hydroxamic acid moiety of compound **5** binds with the zinc ion in the active site. Catalytic zinc binds with oxygen atom of NHOH group of compound **5**. Carbonyl group of hydroxamate interacts with the His415 and Leu348 whereas NH group of hydroxamate interacts with Gly349, Leu350 and Glu406 active site residues (nitrogen of the hydroxamate is interacting with oxygen of carbonyl group of Glu406 and Gly349, and also have interaction with α-hydrogen and hydrogen of methyl group of Leu350). Oxygen of the carbonyl group adjacent to the central pyridine ring of compound **5** interacts with the hydrogen of NH group present on Gly349 and Leu348. The same oxygen also interacts with His415 and Thr347. γ-Carbon and hydrogen present on Thr347 are interacting with oxygen as well as carbon of the carbonyl group. The nitrogen atom of the central pyridine ring (compound **5)** makes hydrogen bonding with the Ala439 of the active site residue having bond distance of 2.33 Å (**Figure 4.5.2**). Thr347 interacts with

Table 4.5.1 G-score and *in vitro* biological activity of the compounds for TACE inhibition

Compound	Glide Score (G-score)	% inhibition of TACE at		IC_{50} (μM)
		1μM	0.3μM	
BMS-566394	-5.03	77.78	66.26	0.130
1	-641	80.09	72.45	0.080
2	-6.04	83.07	66.40	0.160
3	-6.37	78.10	66.48	0.126
4	-5.53	64.23	40.61	0.280
5	-6.51	84.90	80.53	0.070
6	-5.58	81.20	77.98	0.074
7	-5.31	58.50	24.90	-
8	-4.83	3.98	0.00	-
9	-5.05	0.00	0.00	-
10	-4.94	55.80	29.20	-
11	-6.08	3.26	9.57	-
12	-5.32	3.50	7.06	-
13	-6.14	0.00	0.00	-
14	-6.35	6.40	13.20	-

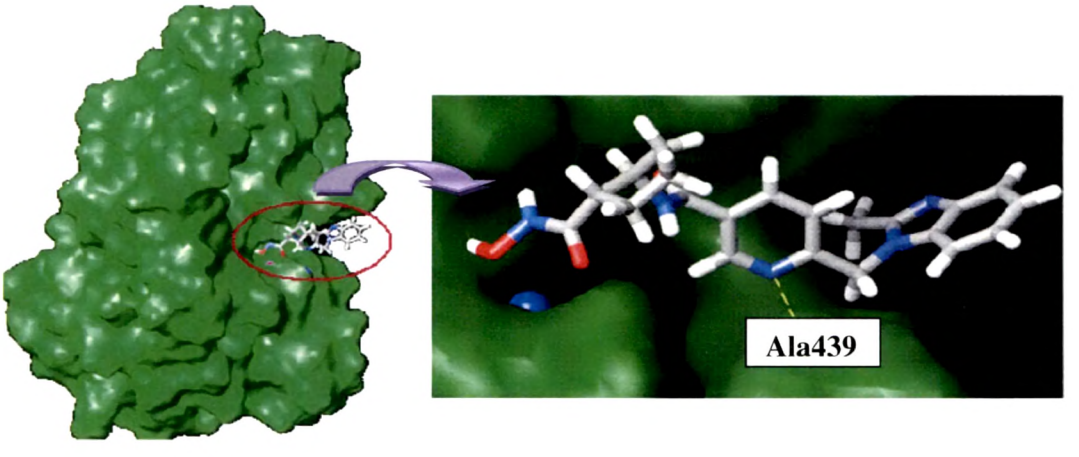

Figure 4.5.2 Hydrogen bonding of the compound **5** with Ala439 active site

the cyclopentane ring and central pyridine ring of compound **5**. The carbonyl oxygen of Gly346 interacts with the central pyridine ring and methyl group present on benzimidazole ring. Ile438 interacts with nitrogen present on central pyridine ring and -CH_2 group present between pyridine ring and benzimidazole ring. There is a favorable bonding between the hydrogen of the spacer –CH_2 and carbon of the methyl group attached to β-carbon of Ile438. Ala439 interacts with the methyl group present on the benzimidazole ring as well as nitrogen of the central pyridine ring.

The most interesting outcome of the docking study is that compound **5** (highest ranked compound in the present series) is making four hydrogen bonds with the active site residue of the TACE enzyme. Nitrogen of the central pyridine ring interacts with the proton of the amide function of Ala439 through hydrogen bonding (2.33 Å) thereby affording an extra stabilization. Apart from this crucial hydrogen bonding, three other hydrogen bonds mentioned below were also observed:

- Hydroxyl group of hydroxamate with oxygen of the carbonyl group present on Glu406 (1.527 Å)
- Hydrogen attached to nitrogen of CONHOH with the oxygen of the carbonyl group of Gly349 (2.142 Å) and
- Oxygen of the carbonyl group attached to the pyridine ring with the NH group of Leu348 (2.041 Å).

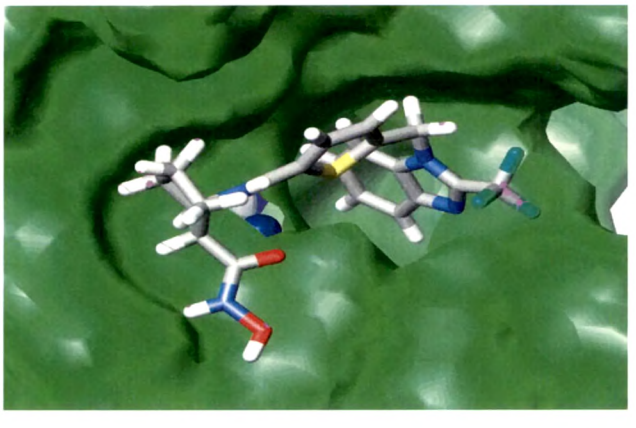

Figure 4.5.3 Docking of compound **10** in the active site of TACE.

Thus, the docking data suggests that the hydroxamic acid moiety of compound **5** binds with the zinc metal in the active site. Nitrogen present on the central pyridine ring interacts with the amide nitrogen proton of Ala439 (2.33 Å) through hydrogen bond, which could afford an extra stabilization to the compound **5**, making the compound sit comfortably in the active site. This interaction does not exist for compounds having central phenyl ring or five membered rings (furan and thiophene). In fact, docking studies revealed that those compounds having central five membered rings (compound **7-14**) adopted such a pose in the binding pocket in which the zinc binding group (hydroxamate) of these compounds oriented away from the catalytic zinc (**Figure 4.5.3**). Typically, as shown in **Figure 4.5.3**, the thiophene containing compound **10** does not fit properly into the active site of TACE; the P1' group is not being located in the S1' region

of the active site. Probably, this is the reason for poor TACE inhibitory activity of the compounds having five membered central rings.

In summary, compound **5** having the highest activity was found to have an extra binding to the active site in the form of hydrogen bond between the pyridine nitrogen and the Ala439. Compounds **7-14** possessing central five-membered heterocyclic rings were shown to have a "different pose" which disallowed interaction between the zinc-binding hydroxamate group and the catalytic zinc ion site, in these modeling studies. This study throws new light on the unexplored and unreported role played by the central aromatic ring in benzamidohydroxamate series of compounds belonging to BMS-566394.

The molecular modeling studies involving some new heterocyclic inhibitors with TACE enhances our understanding of the binding interactions of these inhibitors with the TACE active site. This could facilitate the designing of inhibitors with improved potency for the treatment of disorders mediated by TACE.

B. STUDIES ON INHIBITORS OF NEURAMINIDASE

4.6 Determining of Structural Requirements of Influenza Neuraminidase Type A Inhibitors and Binding Interaction Analysis with the Active Site of A/H1N1 by 3D-QSAR CoMFA and CoMSIA Modeling

4.6.1 Data set

As it is well known, the validity of 3D-QSAR analysis is strongly dependent upon the selected training data set. Therefore, the dataset of compounds with reported bioactivity need to be selected very judiciously. Sixty one molecules selected for the present study were taken from the published work by Wang *et al.* [313] Chand *et al* [186,314] and Kim *et al.* [315]. The structures of the training and test molecules are given in **Table 4.6.1-4.6.3**. The biological activity used in the present study was expressed as $pIC_{50} = -\log IC_{50}$ where, IC_{50} is the molar concentration of the inhibitor producing 50% inhibition of neuraminidase Type A.

4.6.2 Homology Modeling of A/H1N1 and Molecular Docking

An accurate 3D structure of the target enzyme is important for molecular docking and rational development of novel potential inhibitors. Since the three dimensional structure of A/H1N1 neuraminidase is not known currently, a homology model of A/H1N1 neuraminidase using H5N1 bound with Relenza as the starting point was used

for docking studies [251]. Molecular docking was carried out by using the Glide module of Schrodinger package according to the previously reported protocol [102,312].

4.6.3 Molecular alignment rules for CoMFA modeling

Two different methods were used for defining alignment rules in the CoMFA modeling study as described below:

Method 1: Atom and centroid/atom based alignment (Alignment IA-IE)

In this method five different alignments (A-E) were carried out as shown in **Figure 4.6.1.** Alignments A, D and E were based solely on the selection of ligand atoms i.e. only atoms were selected for superimposition on the template. In alignments B and C both atoms

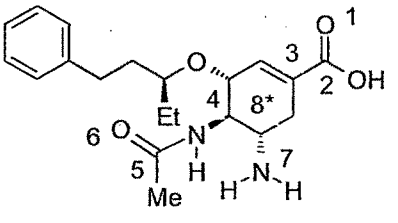

Template structure (45)

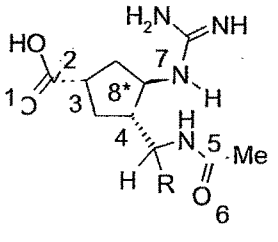

(Type 1)

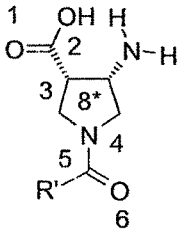

(Type 2)

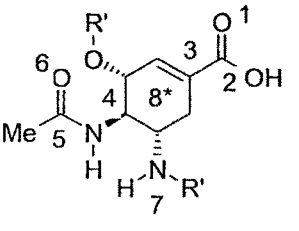

(Type 3)

Alignment I	Atoms/centroids			
	Template	Type 1	Type 2	Type 3
A	2,4,5,7	2,4,5,7	2,4,5	2,4,5,7
B	2,5,7,8*	2,5,7,8*	2,5,8*	2,5,7,8*
C	**1,6,7,8***	**1,6,7,8***	**1,6,8***	**1,6,7,8***
D	2,3,4,5,7	2,3,4,5,7	2,3,4,5	2,3,4,5,7
E	1,3,4,6,7	1,3,4,6,7	1,3,4,5	1,3,4,6,7

*Centroid

Figure 4.6.1 Designation of atoms for atom and atom-centroid based alignments for Method 1 (Alignments I A-E)

and centroid were selected for superimposition on the template. The SYBYL conventional fit-atom molecular alignment rule was applied by using the module of SYBYL/Analyze/Fit-atom. The Fit-atom module adjusted the geometry of the molecule

Table 4.6.1 Compounds used for CoMFA model development

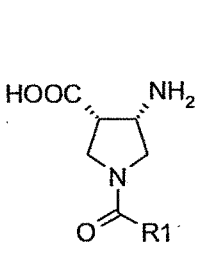

1-12

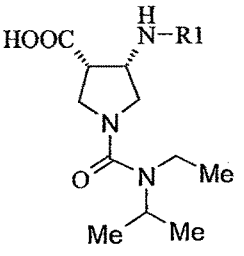

13

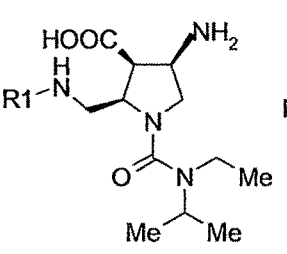

14-18

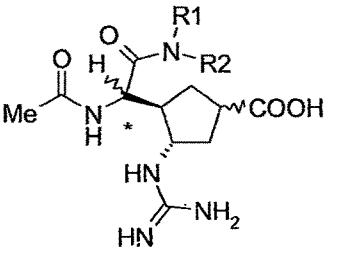

19-22 (19, 21-22: **S*; 20: **R*)

Comp.	R1	R2	Biological Activity		
			Observed		Predicted
			$IC_{50\,\mu M}$	pIC_{50}	pIC_{50}(CoMSIA)
1.	$-CH(C_2H_5)_2$	-	22	4.657	3.836
2. (T)	$-N(C_2H_5)_2$	-	25	4.602	5.318
3.	$-N(C_3H_7)_2$	-	32	4.494	4.064
4.	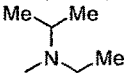	-	1.6	5.975	5.221
5.	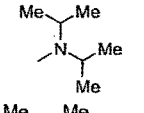	-	4	5.397	5.396
6. (T)	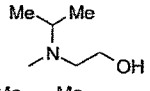	-	21	4.677	5.079
7.	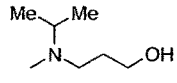	-	2.1	5.677	5.558
8.	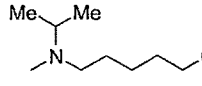	-	2.0	5.698	5.541
9. (T)	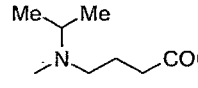	-	19	4.721	5.790
10.	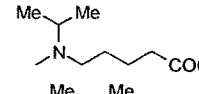	-	1.3	5.886	5.892
11.	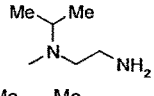	-	46	4.337	5.46
12.	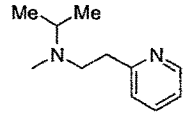	-	1.3	5.886	5.891
13. (T)	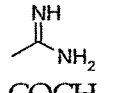	-	13	4.886	5.229
14. (T)	$-COCH_3$	-	7.5	5.124	5.099
15.	$-COC_2H_5$	-	16	4.795	5.016
16.	$-COCH=CH_2$	-	96	4.017	5.005
17.	$-COCF_3$	-	0.28	6.552	5.587
18. (T)	$-SO_2CH_3$	-	130	3.886	5.750
19.	H	$CH(C_2H_5)$	0.06	7.221	7.595
20.	H	$CH(C_2H_5)$	25.0	4.602	4.478
21.	$-C_2H_5$	C_2H_5	0.07	8.154	7.670
22.	$-C_3H_7$	C_3H_7	0.043	7.366	7.516

Table 4.2.2 Compounds used for CoMFA model development

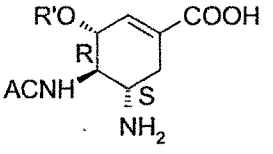

23-47

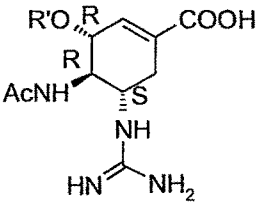

48-53

Comp.	R'	Biological Activity		
		Observed		Predicted
		IC_{50} (nM)	pIC_{50}	pIC_{50} (CoMSIA)
23.	H	6300	5.200	5.408
24.	CH_3-	3700	5.431	5.755
25. (T)	CH_3CH_2-	2000	5.698	6.049
26.	$CH_3(CH_2)_2$-	180	6.744	6.349
27.	$CH_3(CH_2)_3$-	300	6.522	6.537
28. (T)	$CH_3(CH_2)_4$-	200	6.698	6.598
29.	$CH_3(CH_2)_5$-	150	6.823	6.618
30.	$CH_3(CH_2)_6$-	270	6.568	6.602
31. (T)	$CH_3(CH_2)_7$-	180	6.744	6.576
32.	$CH_3(CH_2)_8$-	210	6.677	6.550
33.	$CH_3(CH_2)_9$-	600	6.221	6.525
34.	$(CH3)_2CHCH_2$-	200	6.698	7.682
35. (T)	$CH_3CH_2(CH_3)CH$-	10	8.00	7.280
36.	(s) $CH_3CH_2(CH_3)CH$-	9	8.045	8.055
37.	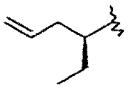	1	9.000	8.821
38.	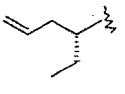	3	8.522	7.866
39. (T)	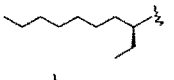	1	9.000	7.372
40.		60	7.221	7.523
41.	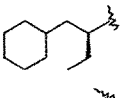	16	7.795	8.387
42.	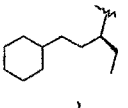	1	9.000	8.590
43. (T)	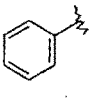	530	6.275	7.152
44.	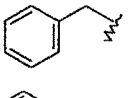	620	6.207	5.941
45.	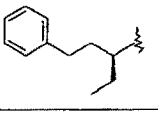	0.3	9.522	9.535

46.	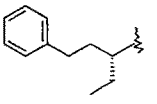	12	7.920	8.485
47.	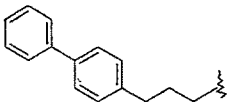	90	7.045	6.397
48.	H	100	7.000	7.585
49.	$CH_3(CH_2)_2$-	2	8.698	8.681
50.	$CH_3(CH_2)_3$-	3	8.522	8.855
51.	(R) $CH_3CH_2(CH_3)CH$-	0.5	9.301	8.971
52. (T)	(S) $CH_3CH_2(CH_3)CH$-	0.5	9.301	8.922
53.	$(CH_3CH_2)_2CH$-	0.5	9.301	9.224

Table 4.6.3 Compounds used for CoMFA model development

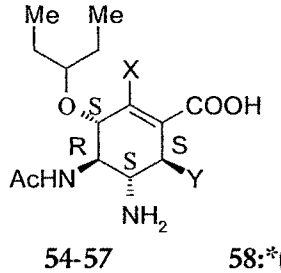

54-57

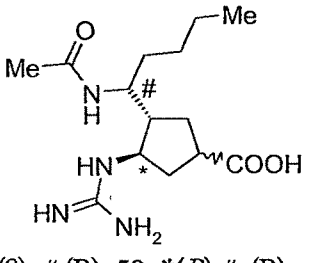

58:*(S), # (R) ;59; *(*R*) # (R)

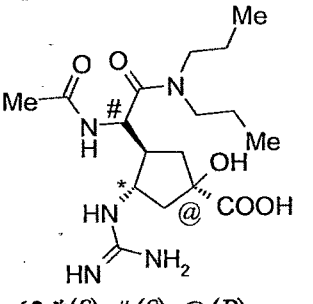

60:*(*S*), # (*S*), @(*R*)
61:*(*S*), # (*S*), @(*S*)

Comp.	X	Y	Biological activity		
			Observed		Predicted
			IC_{50} (μM)	pIC_{50}	pIC_{50}(CoMFA)
54.	H	H	1 (nM)	9.000	8.551
55.	CH_3	H	2300 (nM)	5.638	5.643
56.	F	H	3 (nM)	8.522	7.417
57.	H	CH_3	1500 (nM)	5.823	6.552
58.	-	-	0.013	7.886	7.730
59	-	-	14.6	4.835	5.078
60 (T)			4.9	5.309	5.130
61			2300	2.638	3.284

in such a way that its steric and electrostatic fields matched the template molecule. The template molecule chosen in the present study was compound **45**, which was the most potent inhibitor in the series. A set of low energy conformations for template molecule under study were generated by dynamics using simulated annealing technique with Tripos force fields in SYBYL. The template molecule was heated to 700 K followed by cooling to 300 K. Time spent for annealing was 1000 fs. Time increment for dynamics computations was 0.5 fs and coupling time for temperature regulation was 2.0 fs. Ten

consecutive cycles were calculated. Repeating the cycle many times and collecting the low energy structures resulted in a set of low energy conformations. The lowest energy conformers thus, obtained were further minimized using the conjugate gradient method in SYBYL 7.0 using Tripos force fields and atomic charges assigned by the MMFF94 method with a distance dependent dielectric function until a root mean square deviation (rms) of 0.001 kcal/mol Å was achieved. The lowest energy conformer thus obtained was subsequently used for alignment purpose. The atoms used as fitting scaffold were marked with numbers [(1,2,..7 and 8* (centroid)] in the representative structures I-III of the series under study for 3D-QSAR analysis as shown in **Figure 4.6.1.**

Method 2: Docking Based alignment

The docked conformations of the compounds in the active site of A/H1N1 homology model structure was used in two different ways in this method as mentioned below:

a. Alignment II: Docked conformations were aligned on one another and the same were used for the CoMFA model development
b. Alignment III: The lowest energy conformer of compound (45) obtained through dynamics using simulated annealing technique (explained in Method 1) was submitted for docking and this docked conformer was used for alignment. After docking all the conformations in the active site, all the compounds were aligned on the above obtained conformation of compound (45) as per the procedure adopted in Method 1.

4.6.4 CoMFA analysis

The negative logarithm of the IC_{50} (pIC_{50}) was used as dependent variable in the 3D-QSAR study (**Table 4.6.1-4.6.3**). The PLS analysis results for all the three types of 3D-QSAR CoMFA modeling are summarized in **Table 4.6.4.** The CoMFA models were built using a training set of 47 compounds and tested using a test set of 14 compounds. Selection of the training set and test set molecules was done by considering the fact that test set molecules represented a range of biological activity similar to that of the training set. To diversify the training set and test set, they were grouped manually so that molecules possessing diverse functionalities and biological activity of wide range were included in both sets. The lower energy conformers obtained from the MULTISEARCH option in SYBYL were used in the study. All the molecules were aligned employing three different types of alignments. Various 3D-QSAR models were generated and based on the statistically significant parameters obtained, the best model was chosen.

Table 4.6.4 Summary of CoMFA statistics

Parameters	Alignment-Ic	Alignment-II	Alignment-III
R^2_{cv}	0.415	0.483	0.519
NC	6	8	6
R^2_{ncv}	0.909	0.921	0.914
SEE	0.532	0.363	0.521
F-value	48.231	128.312	59.265
R^2_{Pred}	0.354	0.358	0.605
Contribution (S, E)	56.3; 44.7	59.6; 40.4	53.1; 46.9

A preliminary study was performed to study the importance of each field individually. All further analyses were performed with steric and electrostatic fields calculated at each grid point simultaneously. Partial least square (PLS) analysis was performed using varying column filtering values. Finally, column filtering was set to 2.0 kcal/mol. Different alignments such as Alignments I to III were carried out.

Alignment I was carried out in five different ways (A-E) and various 3D-QSAR models were generated for all of them. Alignemnt Ic afforded the best statistical model hence only Alignment Ic based model is discussed below. Alignment-Ic showed cross-validated r^2 = 0.415 with six components, non cross-validated r^2 = 0.909, F-value 48.231, predictive r^2 = 0.358; the steric and electrostatic contributions were 56.3 and 44.7%, respectively.

The CoMFA model generated from Alignment-II i.e. docking-based alignment showed cross-validated r^2 = 0.483 with eight components, non cross-validated r^2 = 0.921, F-value 128.312, predictive r^2 = 0.358 with 59.6 steric and 40.4% electrostatic contributions. Alignment-III (**Table 4.6.4**) yielded the highest cross-validated r^2 of 0.519 with six components, non cross-validated r^2 of 0.914, F-value 59.26 and predictive r^2 of 0.605 with 53.1% steric and 46.9% electrostatic contributions. The statistics in **Table 4.6.4** shows that out of the three different CoMFA models developed on the basis of different alignments, the model developed with Alignment-III has highest predictive power lending credit to the reliability of the active conformations obtained by Glide. The predicted pIC_{50} values are in good agreement with the experimental data with small residuals.

Quantitatively, the steric and electrostatic fields derived from the conventional atom-centroid fit molecular alignment (Alignment-Ic) is only ligand-centeric; whereas, the

one derived from the docking-based active conformation alignment (Alignment-III) is a combined product of the minimized conformations of the ligands and the active site structure. This innovative approach used in Alignment-III, is predominantly responsible for the differences in the results of the two sets of CoMFA modeling. In the following discussion on CoMFA and CoMSIA analyses, Alignment-III only has been considered.

4.6.5 CoMSIA analysis

The CoMSIA analysis was performed using steric, electrostatic, hydrophobic, and hydrogen bond donor and acceptor fields as CoMSIA offers five different fields. 3D-QSAR models can be generated using the above fields in different combinations. Alignment-III used in CoMFA studies was used as the alignment for CoMSIA studies and the results of these studies are summarized in **Table 4.6.5.** The CoMSIA model showed considerable correlative and predictive properties. The CoMSIA model with combination of all the fields yielded a crossvalidated r^2 = 0.446 with five components, non-crossvalidated r^2 = 0.913, F-value 64.035 and predictive r^2 = 0.623. The contributions of steric, electrostatic, hydrophobic, hydrogen bond donor and acceptor fields of this model were 13.6, 19.7, 20.6, 21.5 and 24.5% respectively. Combination of steric, electrostatic and hydrogen bond donor fields yielded a CoMSIA model with a cross-validated r^2 = 0.454 with four components, non-crossvalidated r^2 = 0.834, F-value 51.601 and predicted r^2 = 0.619. The steric, electrostatic and hydrogen bond donor field contributions were 25.1, 35.5 and 39.3%, respectively.

Table 4.6.5 Summary of CoMSIA results

Parameters	SE	SEH	SED	SEA	SEDA	SEHD	SEHDA
R^2_{cv}	0.487	0.433	0.454	**0.526**	0.423	0.474	0.446
N	4	5	4	**6**	3	3	5
R^2_{ncv}	0.838	0.890	0.834	**0.915**	0.788	0.828	0.913
SEE	0.699	0.582	0.704	**0.517**	0.789	0.711	0.517
F-value	52.836	64.795	51.601	**70.215**	51.990	69.674	64.035
R^2_{Pred}	0.617	0.589	0.619	**0.641**	0.628	0.618	0.623
Contributions	39.2;	22.4	25.1;	**25.1;**	17.5;	16.6;	13.6;
	60.8	38.4;	35.5;	**35.8;**	25.3;	26.3;	19.7;
		39.2	39.3	**39.1**	27.6;	29.6;	20.6;
					29.6	27.5	21.5;
							24.5

Combination of steric, electrostatic and hydrophobic fields yielded a CoMSIA model with a crossvalidated r^2 = 0.433 with five components, non-cross-validated r^2 = 0.890, F-value 64.795 and predicted r^2 = 0.589. The steric, electrostatic and

hydrophobic field contributions were 22.4, 38.4 and 39.2%, respectively. Combination of steric, electrostatic hydrogen bond donor and hydrogen bond acceptor fields yielded a CoMSIA model with a crossvalidated r^2 = 0.423 with three components, non-cross-validated r^2 = 0.788, F-value 51.990 and predicted r^2 = 0.628. The steric, electrostatic and hydrogen bond donor and hydrogen bond acceptor field contributions were 17.5, 25.3, 27.6 and 29.6%, respectively. Combination of steric, electrostatic, hydrophobic and hydrogen bond donor fields yielded a CoMSIA model with a crossvalidated r^2 = 0.474 with three components, non-crossvalidated r^2 = 0.828, F-value 69.674 and predicted r^2 = 0.618. The steric, electrostatic, hydrophobic and hydrogen bond donor fields contributions were 16.6, 26.3, 29.6 and 27.5%, respectively.

The CoMSIA model with a combination of steric, electrostatic and acceptor fields yielded the highest cross-validated r^2 = 0.526 with six components, non-cross-validated r^2 = 0.915, F-value 70.215 and highest predictive r^2 of 0.641.

The models generated by various combinations of CoMSIA fields (**Table 4.6.5**) showed moderate to high, internal and external predictions, in which the acceptor fields were dominant over the hydrogen bond donor and hydrophobic fields. The CoMSIA steric and electrostatic contours (not shown) were positioned similarly to those of the CoMFA model as shown in **Figures 4.6.2** and **4.6.3**, hence are not discussed. The hydrogen bond acceptor contour maps of CoMSIA (STDDEV*COEFF) are displayed in **Figure 4.6.4.**

4.6.6 CoMFA versus CoMSIA

In CoMFA, only one model having the two fields, the steric and the electrostatic fields was possible whereas in CoMSIA seven models were constructed with different combinations of the available fields. The CoMFA model that takes into account steric and electrostatic interactions gave an acceptable r^2_{cv} value of 0.519 and r^2_{pred} value of 0.605 (**Table 4.6.4**; Alignment III). If identical interactions were assumed for CoMSIA, then a smaller value of r^2_{cv} 0.487 and r^2_{pred} 0.617 were observed. The best CoMSIA model showed slightly better r^2_{cv} value i.e. 0.526 and $r^2_{predictive}$ value i.e. 0.641 than the best CoMFA model. Hence, as for as predictive ability of the model is considered, CoMSIA model is better than the COMFA model.

4.6.7 Graphical interpretation of the CoMFA and CoMSIA models

To visualize the information contents of the derived 3D-QSAR models, CoMFA contour maps were generated by interpolating the products between the 3D-QSAR coefficients and their associated standard deviations. The field values generated at each grid point were calculated as the scalar product of the associated QSAR coefficient and the standard deviation of all values in the corresponding column of the data table (STD*COEFF) plotted as the percentage contributions to QSAR equation. The CoMFA steric and electrostatic contour maps shown in **Figures 4.6.2** and **4.6.3**, respectively are derived from the CoMFA model using docking-based (Alignment-III) active conformation alignment. The 3D contour maps show that the changes in molecular fields are associated with the differences in biological activity. **Figure 4.6.2A** indicates the CoMFA steric maps obtained from the best model (Alignment-III) using most active compound **45** (shown in magenta color) and least active compound **61** (shown in red color), as reference structures. In this figure, the green contours represent regions of high steric tolerance (80% contribution), while the yellow contours represent regions of low steric tolerance (20% contribution). The green colored regions indicate areas where steric bulk enhances biological activity, while the yellow contours indicate regions where steric bulk is detrimental for biological activity. Blue colored regions show areas where electropositively charged groups enhance activity, while red regions represent regions where electronegatively charged groups improve the activity.

Figure 4.6.3A indicates the CoMFA electrostatic contour maps obtained from the best model (Alignment III) using the most active compound **45** (shown in magenta color) and the least active compound **61** (shown in yellow color) as reference structures. In this figure increase in positive charge is favored in blue regions while increase in negative charge is favored in red regions.

The steric contour map of CoMFA (**Figure 4.6.2A**) shows a green contour observed near 3-substituted phenylpentan-3-yloxy group of cyclohexene of compound **45** and another small green counter to the left side i.e. in the vicinity of carboxylic acid suggesting that steric substituents in these regions may favor activity. Good inhibitory potency of compounds **39** (IC_{50} = 1.00 nM), **42** (IC_{50} = 1.00 nM) and **51-54** is due to orientation of bulkier groups towards sterically favored green contours. While the disfavored yellow contours surrounding the cyclohexene ring restrict the steric substitution indicating decrease in biological activity. Compound **61** is the least active

compound (shown in red color) since 4-guanidino group and acetamido-2-[butyl(propyl)amino]-2-oxoethyl group present on cyclopentane ring are directed completely towards the disfavored yellow region. Same is the case with other compounds having less or moderate activities. Compound **18** (IC_{50} = 130 μM) is having poor activity since 5-methylsulfonamido group present on pyrrolidine ring is directed towards the yellow contour. Compound **16** is having poor activity (IC_{50} = 96 μM) since 5-acrylamidomethyl and 1-ethyl(isopropyl)carbamoyl groups present on pyrrolidine ring are directed towards the yellow contour. For compound **11** (IC_{50} = 46 μM) the 2-aminoethyl side chain present on pyrrolidine is completely embedded in the yellow contour present on the upper side i.e. 1-substituted region of the pyrrolidine ring and this could be one of the reasons for compound **11** to have poor biological activity. Compound **2** having IC_{50} value of 25 μM is having poor activity since the 3-carboxylic acid group is completely embedded and diethylcarbamoyl group is directed towards the yellow region.

CoMFA electrostatic contour plots displayed a positively charged favored prominent large blue contour near methyl group of 4-acetamido of compound **45** and two other blue contours, one surrounding the 5-amino group and other in the vicinity of 2nd substituted region of the cyclohexene ring of compound **45**. A small red contour is also observed near the carboxyl group, suggesting that the increase in activity may be due to the presence of an electron rich subtitutent group (compounds **51-53**). For compounds **49-53,** C-5 guinidino moiety is completely embedded in the large and prominent blue contour and the carboxyl group is pointing towards the red contour justifying good inhibitory activity for these compounds. C-4 guanidino group of compound **20** is pointed away from the prominent blue contour and this could be the reason for it having lower biological activity (pIC_{50} = 4.60).

Two big sized negatively charged favored red contours were observed, one pointing towards the oxygen of the acetamido group and another one in the viscinity of ethyl group of 3-phenylpropoxy of cyclohexene group of compound **45** (**Figure 4.6.3A**). A small red contour was also observed near the oxygen of the 1-ethyl-3-phenylpropoxy side chain present on cyclohexene of compound **45**. Another red contour is present in the vicinity of carboxylic acid region of compound **45**. Close observation for compounds **1-12** suggested that the R1 substitution is pointing away from the blue contour and the

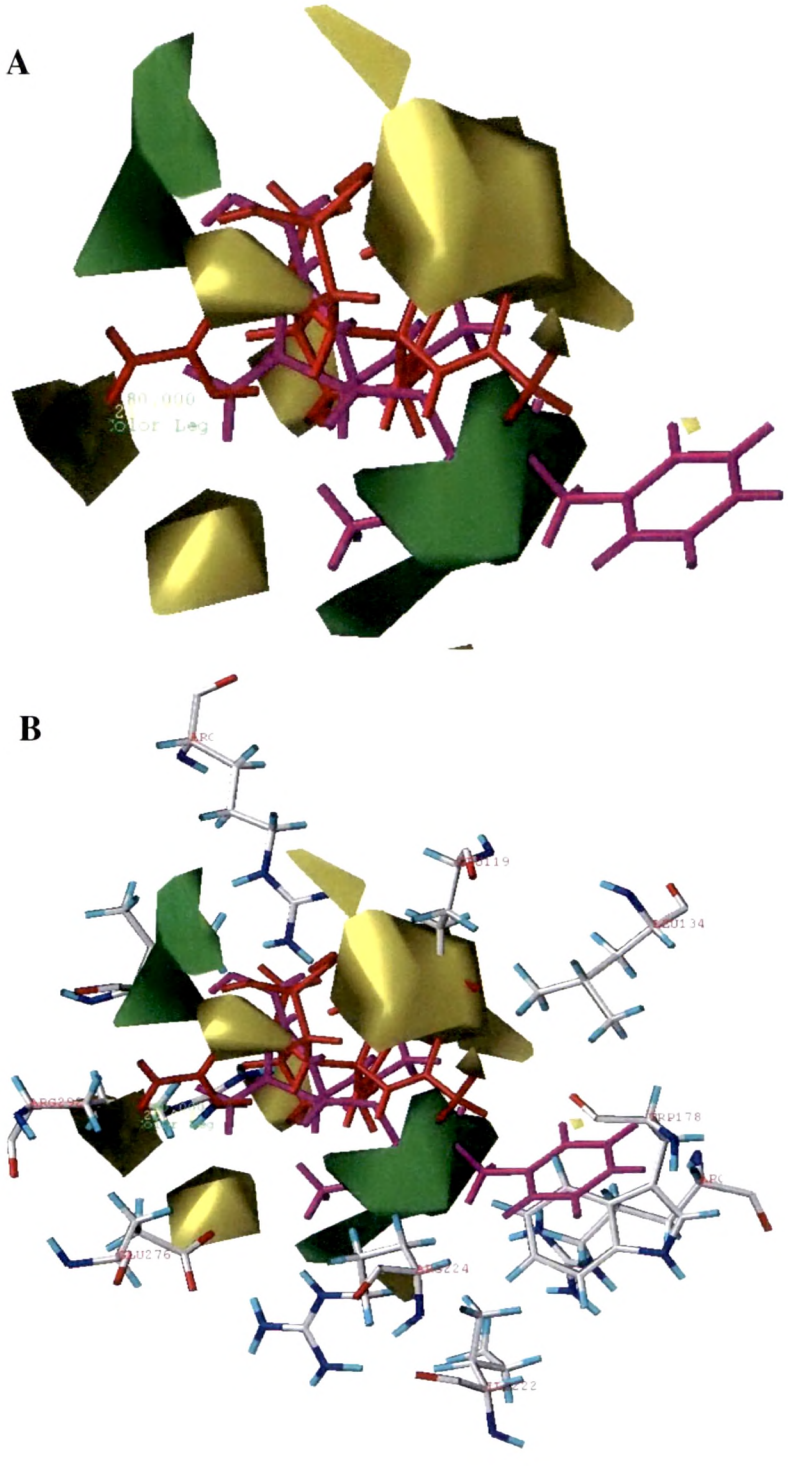

Figure 4.6.2. The steric contour map of CoMFA. (**A**) Compound **45** (shown in magenta color) occupies the green colored contour in the region whereas inactive compound **61** (shown in red color) occupies a section of the yellow colored contour in the region. (**B**) Superimposition of steric contours on A/H1N1 active site

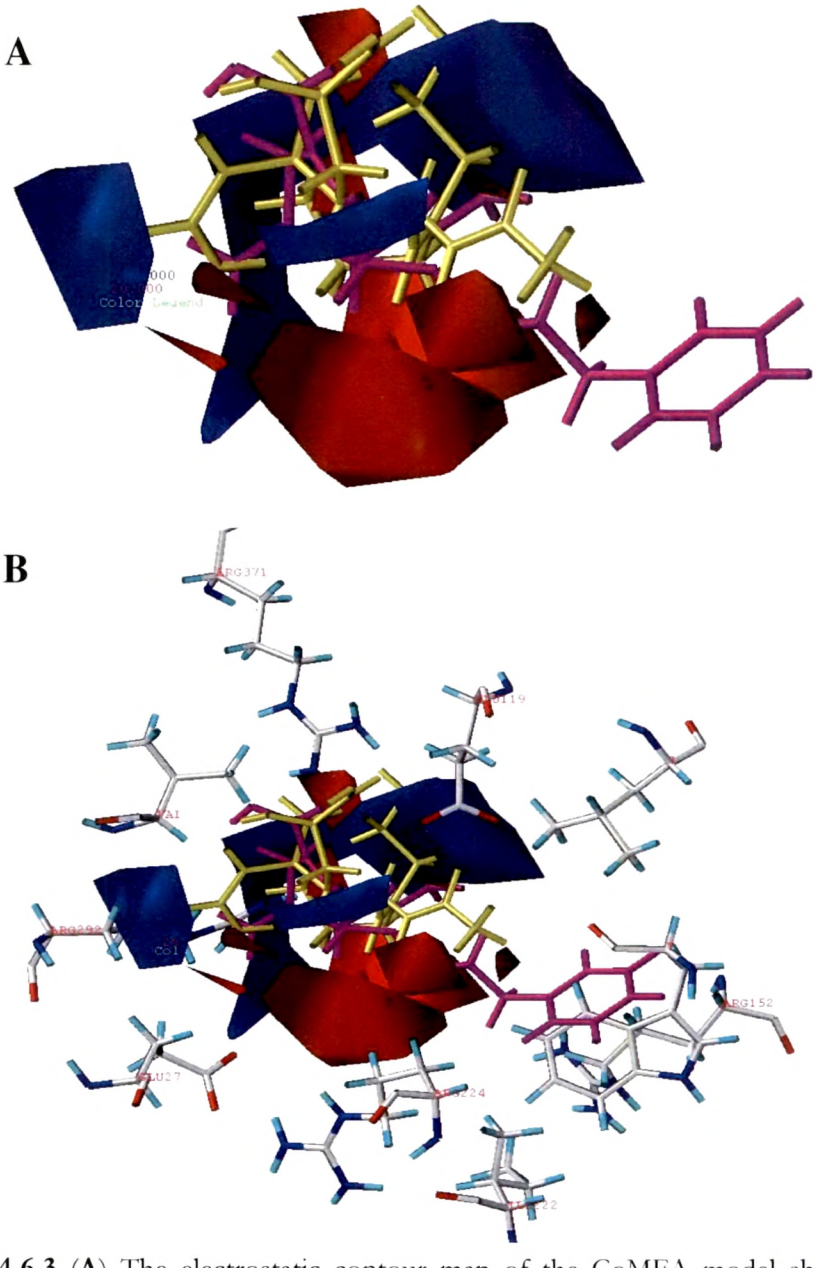

Figure 4.6.3 (**A**) The electrostatic contour map of the CoMFA model shown together with the conformations for the most active derivative **45**. (**B**) Superimposition of electrostatic contours on A/H1N1 active site.

carboxyl group away from the red contour, suggesting lower degree of activity for these compounds. In compound **28,** methyl group of acetamide is pointing towards the red contour and the carbonyl group is placed towards the blue contour, both of which are unfavorable and thus causing decrease in biological activity.

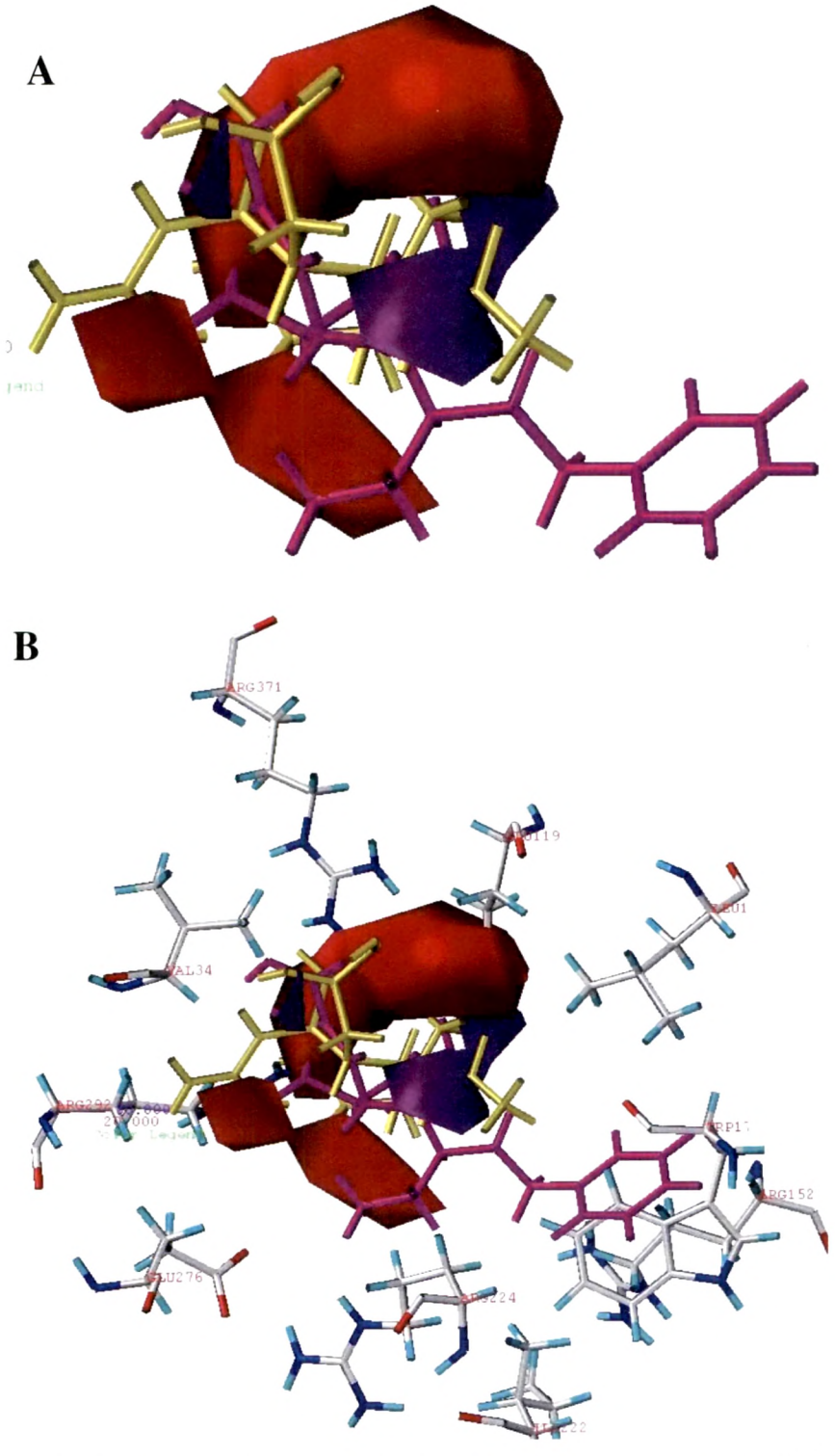

Figure 4.6.4. (**A**) The hydrogen bond acceptor contour maps of the CoMSIA model are shown together with the conformations for the most active derivative **45** (shown in magenta color) and the inactive derivative **61** (shown in yellow color). (**B**) Superimposition of hydrogen bond acceptor contours on A/H1N1 active site. Cyan polyhedron shows the hydrogen bond favorable region and violet colored polyhedron disfavors the hydrogen bond donor group.

The CoMSIA steric and electrostatic contours (not shown) were positioned similarly to those of the CoMFA model, hence are not discussed. The hydrogen bond acceptor contour maps of CoMSIA ((STDDEV*COEFF) is displayed in **Figure 4.6.4A**. In this figure, it is observed that in the highly active template molecule **45** (shown in magenta color), the violet colored contour is in the region of oxygen of the 1-ethyl-3-phenylpropoxy side chain present on cyclohexene. On the contrary, in the inactive compound **61** (shown in yellow color) there is no hydrogen-bond acceptor group in that region and this could be one of the reasons for poor activity of compound **61**. CoMSIA model generated from steric and electrostatic fields did not vary both in terms of statistical values and positions of contours as compared to its CoMFA model, hence are not discussed.

4.6.8 Superimposition of CoMFA and CoMSIA maps on the active site of A/H1N1

Interaction of relenza with the active site of A/H1N1 (homology modelled) is shown in **Figure 4.6.5**. COMFA steric and electrostatic contour plots mapped on the

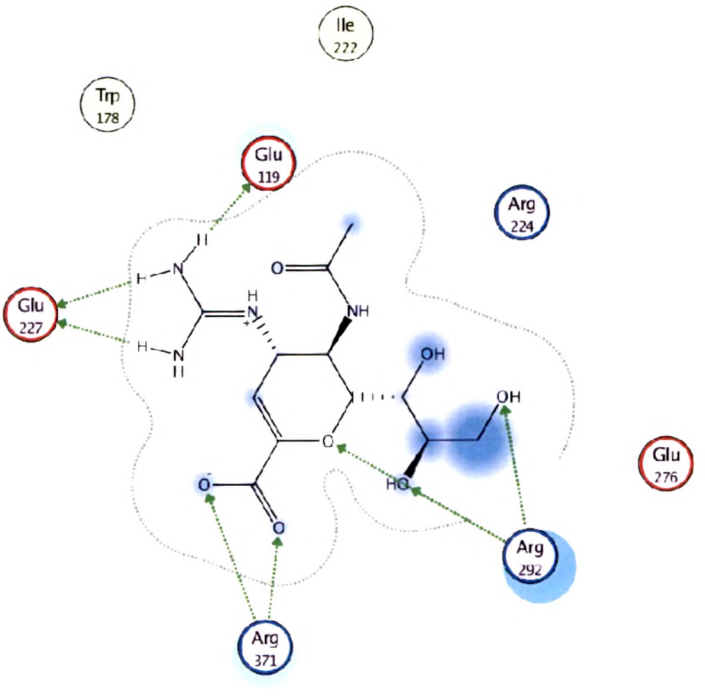

Figure 4.6.5. Interaction of Relenza with the active site of A/H1N1

active site of A/H1N1 are depicted in **Figures 4.6.2B** and **4.6.3B** respectively, with highest active compound **45** (magenta) and lowest active compound **61** (shown in red color in steric and yellow colored in electrostatic contour maps). For better perception, only active site residues and nearby residues of the active site i.e. Trp178, Glu119, Ile222,

Arg224, Glu227, Glu276, Arg292 and Arg371 were retained for the superimposition of the contour maps on the active site of A/H1N1. The sterically favored big green contour was placed in between Arg224, Arg152 and Leu134 and the other one was placed in the vicinity of Val349, while disfavored yellow contours were observed at the periphery of Glu119, Glu276 and Arg292. The positively charged favored blue contour near the NH_2 and acetamido (NHAc) substituent was placed close to Glu276 and Glu119 indicating ionic interactions.

Figure 4.6.4B displays the CoMSIA acceptor contour maps and their overlapping on the A/H1N1 active site with the most active compound **45** (shown in magenta color) and the least active compound **61** (shown in yellow color). Magenta contour was observed in the viscinity of Arg292 suggesting hydrogen bond acceptor group in the viscinity would increase the activity. While mapping the contours on the active site an interesting observation was made that aromatic ring present in compound **45** is making hydrophobic interaction with Trp178. This could be one of the reasons for the good activity of compound **45**.

C. STUDIES ON POTENTIAL AROMATASE INHIBITORS

4.7 Molecular Modeling Studies of Some Novel Androstanes as Potential Aromatase Inhibitors

Mechanism-based inhibitors have distinct advantages in drug design strategy because these inhibitors are highly enzyme specific, produce prolonged inhibition and often exhibit minimum toxicitiy [316]. Exemestane (**1**), a third generation steroidal mechanism-based aromatase inhibitor has been found not to affect cortisol or aldosterone secretion at baseline or in response to adrenocorticotropic hormone at any dose [317]. The apparent lack of cross-resistance between exemestane (**1**) and other aromatase inhibitors is a major benefit of the drug [318]. Exemestane (**1**) is the most recently FDA approved drug as steroidal aromatase inhibitor. It may differ from others as the steroidal structure potentially protects bone and lipid metabolism from estrogen ablation [319].

In the steroidal moieties effective aromatase enzyme inhibition is observed with an androstane skeleton possessing an A/B trans ring junction, a ketone functionality at the C-3 position, unsaturation in the steroid nucleus (4-ene, 4,6-diene or 1,4,6-triene functions) and either a 17-ketone or 17β-hydroxyl group [316].

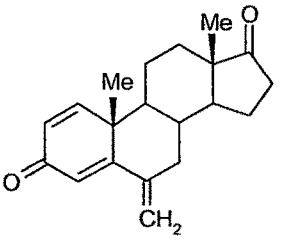

(1)

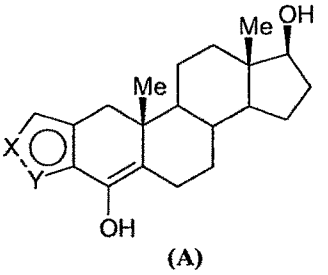

(A)

In light of the above discussion it was thought logical to design some novel steroidal derivatives (2-5) with the given structure (A) wherein the 2,3 position of the ring-A is fused to five-membered heterocyclic rings like isoxazole (X=O/N and Y= N/O) and pyrazole (X=Y=N) and to perform modeling studies.

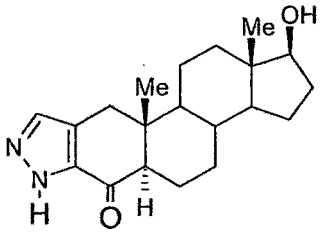

(2)

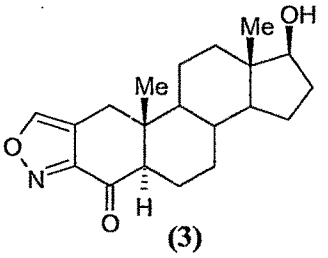

(3)

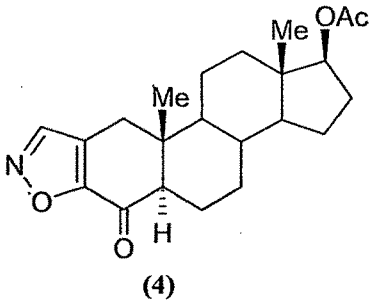

(4)

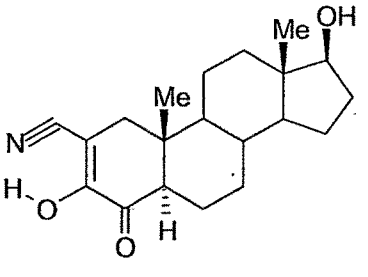

(5)

4.7.1 Molecular modeling studies

Molecular modeling studies were performed on a Silicon Graphics Fuel Workstation running on the IRIX 6.5 operating system using SYBYL 7.0 molecular modeling software from Tripos, Inc., [311] and GLIDE from Schrodinger Inc., USA [102]

installed on Microsoft Windows XP Professonal (version 2002) based Intel core2 Duo 2.53 GHz PC (with 4.0 GB memory).

4.7.2 Molecular structure generation

All compounds were built from the fragments in the SYBYL database. A set of low energy conformations for each molecule under study were generated by dynamics using simulated annealing technique with Tripos force fields in SYBYL. The molecules were heated to 700 K followed by cooling to 300 K. Time spent for annealing was 1000 fs. Time increment for dynamics computations was 0.5 fs and coupling time for temperature regulation was 2.0 fs. Ten consecutive cycles were calculated. Repeating the cycle many times and collecting the low energy structures resulted in a set of low energy conformations. The lowest energy conformers thus obtained were further minimized using the conjugate gradient method in SYBYL 7.0 using Tripos force field, atomic charges assigned by the Gasteiger-Huckel method with a distance dependent dielectric function until a root mean square deviation (rms) of 0.001 kcal/mol Å was achieved. The lowest energy conformer thus obtained was subsequently used for docking studies.

4.7.3 Docking studies

The crystal structure of human placental aromatase (pdb code: 3EQM) [222] obtained from the Protein Data bank (USA) was refined to remove water molecules. The bond orders and formal charges were adjusted prior to docking. Docking was performed using GLIDE software according to the previously reported protocol except for scaling of van der Waals radii which was modified (Scaling factor 0.60).

It was envisaged to perform molecular docking studies on the designed compounds (**2-5**). Structures of these compounds were minimized as per the protocol given in the experimental section. The energy minimized structures were docked independently into the active site of the aromatase enzyme. Similarly, the two known inhibitors exemestane (**1**) and formestane (**6**), and the substrate androstenedione (**7**) were also docked. Glide scores for the enzyme-drug complexes for all of them were calculated (**Table 4.7.1**). It is evident from the data that the best score was obtained for compound (**5**) followed by compound (**2**) while compound (**4**) afforded poorest of the score (-4.44).

The crystal structure of human placental aromatase shows that the bound androgen ligand makes a hydrogen bond with the backbone amide of $Met374^{320}$. Similar

hydrogen bonding was observed with oxygen of 17-hydroxyl group for compounds (**2**) and (**5**) (**Figure 4.7.1**), which indicates that both the compounds bind with the active site in similar way as that of natural substrate (**1**). Moreover, compounds (**2**) and (**5**) showed

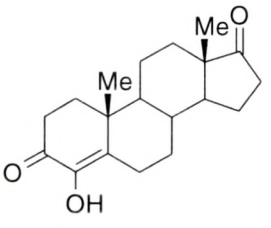

(6)

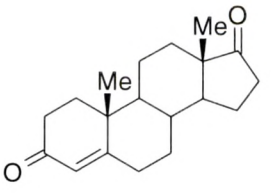

(7)

additional hydrogen bonding of C-4 carbonyl group with amino acid residue Thr310 (**Figure 4.7.1**). Compound (**4**) did not show the hydrogen bonding with Met374 or Thr310. This could be one of the probable reasons for poor docking score for compound (**4**). Compound (**3**) showed hydrogen bonding of Met374 with oxygen of C-4 hydroxyl group (instead of C-17) which is contrary to the hydrogen bonding of the natural substr-

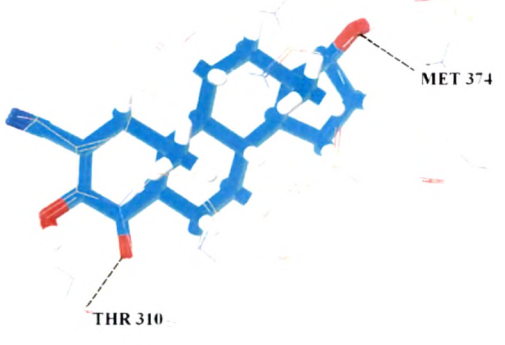

(A)

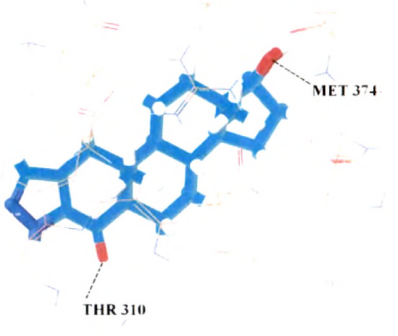

(B)

Figure 4.7.1 Docked conformations of (**A**) compound **2** and (**B**) compound **5** along with the important amino acid residues of human placental aromatase. Both the compounds are forming two hydrogen bonds.

ate, flipping the conformer in opposite direction. Thus, poor binding score of compound (**3**) could be because of its unfavorable positioning in contrast to the natural substrate in the active site. Compounds (**2**) and (**5**) showed good contacts with Ala306, The310, Trp224, IIe133, Phe134, Val370, Leu372, Val373, Met374 and Ser478 active site residues of aromatase.

Takahashi *et al.* have reported that hydrophobic amino acids such as Ile132, Ile133, Ile305, Phe148, Met303 and Ala306 might play a critical role in the binding to the

active site [320]. Similar type of observation was made with compound (**2**) and compound (**5**) as shown in **Figure 4.7.2a** and **4.7.2b** respectively. Both of the compounds are having good contacts with β-carbon of Ala306 through the hydrogen attached to position-3 of the A-ring while, this feature is missing in compounds (**3**) and (**4**) (**Figure 4.7.2c**). This could be one of the reasons for good binding score of both of the compounds (**2** and **5**).

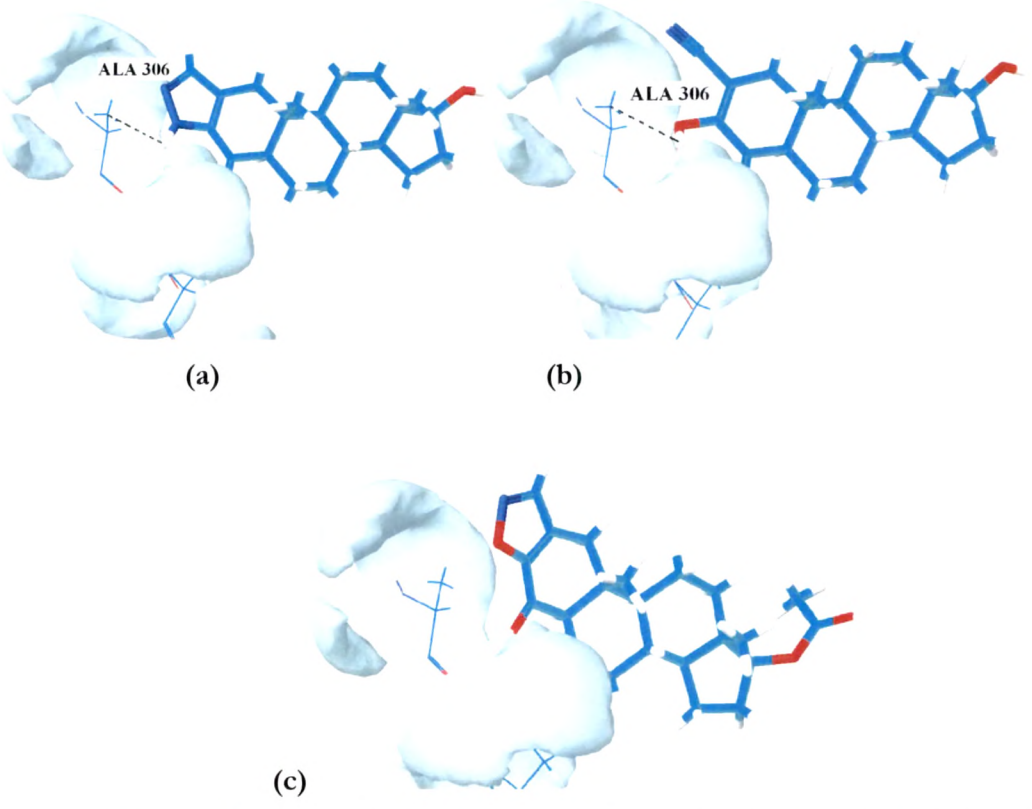

Figure 4.7.2 Interaction of (**a**) compound (**2**) and (**b**) compound (**5**) with β-carbon of Ala306. NH of compound (**2**) and OH of compound (**5**) orients to the hydrophilic pocket whereas (**c**) compound (**4**) dislocates from the hydrophilic pocket.

All of the designed compounds were synthesized **(2-5)** and were evaluated for their aromatase inhibiting activity by another researcher in the laboratory. The assay was performed by monitoring the enzyme activity by measuring the ^3H_2O formed from [1β-^{3}H]androstenedione during aromatization [321]. The activity profile of the compounds is indicated in **Table 4.7.1**. IC_{50} values of aminoglutethimide and fadrozole were determined to be 30 μM and 30 nM in the test system utilized for the evaluation of the test compounds. It is ample clear from the **Table 4.7.1** that the pyrazole derivative **(2)** showed the highest activity followed by nitrile derivative **(5)**. Both of the isomeric isoxazoles were found to be inactive. It is worth noting that both of the active

compounds (2 and 5) have hydrogen bond donating groups attached to position 3 of the A-ring while, this feature is missing in the two inactive derivatives (3 and 4). There is a high probability that these compounds are binding to a site in the aromatase enzyme which acts as a hydrogen bond acceptor thereby increasing the stability of the enzyme-inhibitor complex. Exemestane (1) does not have hydrogen bond donor group in ring A or B. As discussed earlier, Exemestane (1) is a mechanism-based inhibitor as it has electrophilic sites in ring A and B which can lead to covalent bond formation between the enzyme and the drug. Compounds (2 and 5) do not have such active sites indicating that these compounds might be acting as reversible competitive inhibitors. Studies have shown now that these compounds are reversible competitive inhibitors of aromatase.

Table 4.7.1 Biological activity and docking score of the compounds

Compd.	G-Score	% Inhibition of Aromatase[a]			IC_{50} (nM)
		In normal test procedure at		After irreversible binding at	
		0.5 μM[b]	2.0 μM[b]	2.0 μM[b]	
1 (Exemestane)	-6.99	-	88.9±0.8	66.3±0.6	153.9±14.7
2	-7.77	46.1± 11.8	78.7±2.6	12.3±2.1	512.0±93.3
3	-6.90	1.3±2.2	-	-	-
4	-4.44	0.0± 0.0	-	-	-
5	-7.90	37.0±10.3	53.6±5.0	2.0±3.5	1019.8±157.5
6 (Formestane)	-6.96	-	-	-	-
7 (Androstenedione)	-7.13	-	-		

[a] The given values are mean values of at least three experiments; [b]Inhibitor concentration

In conclusion, novel pyrazole (2), isoxazole (3 and 4) and nitrile (5) derivatives were designed. Molecular docking studies were carried out for the designed compounds show good docking scores for compound (5) followed by compound (2) while, compound (4) afforded poorest of the score. Aromatase inhibitory activity for compound (2) having pyrazole ring at 2,3-position was found to be the highest followed by the nitrile derivative (5). Isomeric forms of isoxazole (3 and 4) showed very poor activity compared to fadrozole and aminoglutethimide. The modeling studies showed that compounds (2 and 5) have slightly acidic protons attached to position 3 of the A-ring which binds to a site in the aromatase enzyme that acts as a hydrogen bond acceptor thereby increasing the stability of the enzyme-inhibitor complex, whereas this feature lacked in compounds (3 and 4) showing poor binding with the active site of the enzyme. Thus, docking study was found to be in consonance with the biological data for the designed compounds.